
# INS AIDING BY TRACKING AN UNKNOWN GROUND OBJECT

THESIS

MURAT POLAT, 1LT, TUAF

AFIT/GE/ENG/02M-20

**DEPARTMENT OF THE AIR FORCE**
**AIR UNIVERSITY**

## AIR FORCE INSTITUTE OF TECHNOLOGY

**Wright-Patterson Air Force Base, Ohio**

# Report Documentation Page

| Report Date | Report Type | Dates Covered (from... to) |
|---|---|---|
| 4 Mar 02 | Final | Jun 2001 - Mar 2002 |

| | |
|---|---|
| **Title and Subtitle**<br>INS Aiding by Tracking an Unknown Ground Object | **Contract Number** |
| | **Grant Number** |
| | **Program Element Number** |
| **Author(s)**<br>Lt Murat Polat, TUAF | **Project Number** |
| | **Task Number** |
| | **Work Unit Number** |
| **Performing Organization Name(s) and Address(es)**<br>Air Force Institute of Technology Graduate School of Engineering and Management (AFIT/EN) 2950 P Street, Bldg 640 WPAFB, OH 45433-7765 | **Performing Organization Report Number**<br>AFIT/GE/ENG/02M-20 |
| **Sponsoring/Monitoring Agency Name(s) and Address(es)**<br>AFRL/SNAT ATTN: Dr. Devert Wicker Bldg 621 WPAFB OH 45433-7765 | **Sponsor/Monitor's Acronym(s)** |
| | **Sponsor/Monitor's Report Number(s)** |

**Distribution/Availability Statement**
Approved for public release, distribution unlimited

**Supplementary Notes**
The original document contains color images.

**Abstract**
The reduction of the navigation error in an inertial navigation system by optically tracking a ground object is investigated. Multiple observations of the ground object are used. The location of the ground object is assumed unknown. A careful analysis of the measurement situation at hand reveals that by optically tracking an unknown ground object using passive, bearings-only measurements, the aircraft's angle of attack and sideslip angle can be measured. Thus, two new independent measurement equations featuring the aircraft's angular navigation variables are obtained. Hence, by optically tracking over time an unknown ground object, inertial navigation system aiding is in fact possible. Moreover, the estimation algorithm, which operates on the bearing measurements record, simultaneously, and in parallel, produces corrections required for both inertial navigation system aiding and geo-location of the ground object. The theory presented in this paper is sufficiently general to encompass the conventional methods of inertial navigation system updating where both bearing and range measurements are used and the coordinates of the ground object are known. In all cases where additional independent measurements and/or prior information are used, the accuracy of both the navigation solution and the geo-location are enhanced.

| | |
|---|---|
| **Subject Terms**<br>Inertial Navigation Aiding, Passive Tracking, Estimation | |
| **Report Classification**<br>unclassified | **Classification of this page**<br>unclassified |
| **Classification of Abstract**<br>unclassified | **Limitation of Abstract**<br>UU |
| **Number of Pages**<br>162 | |

AFIT/GE/ENG/02M-20

# INS AIDING BY TRACKING AN UNKNOWN GROUND OBJECT

MURAT POLAT

1LT, TUAF

Approved:

| | |
|---|---|
| M. Pachter | March 4, 2002 |
| Dr. Meir Pachter<br>Professor - Committee Chairman | Date |
| Peter S. Maybeck | 4 March 2002 |
| Dr. Peter S Maybeck<br>Professor - Committee Member | Date |
| | 4 March 02 |
| Lieutenant Colonel Mikel M. Miller - PhD<br>Assistant Professor - Committee Member | Date |
| | 4 MAR 02 |
| Major John F Raquet - PhD<br>Assistant Professor - Committee Member | Date |

AFIT/GE/ENG/02M-20

# INS AIDING BY TRACKING AN UNKNOWN GROUND OBJECT

THESIS

Presented to the Faculty of the Graduate School of Engineering and Management

of the Air Force Institute of Technology

Air University

In Partial Fulfillment of the

Requirements for the Degree of

Master of Science in Electrical Engineering

MURAT POLAT

1LT, TUAF

March, 2002

# *Preface*

I thankfully acknowledge the contribution of Dr. Pachter who has helped me by providing great initiative, insight, and encouragement for producing this thesis.

I express my heartfelt thanks to Dr. Maybeck for his comments and inputs on the draft which led me have more improved final draft.

I appreciate the hard work of Colonel Miller and Major Raquet for their comments on my thesis and for teaching us invaluable classes. Besides, I also thank all my friends in the Navigation and Control class for their help and friendship.

Last but not the least, I greatly acknowledge the endless support and patience of my wife, Ruya, for giving of herself to myself and our son, Sarp Bora. I also owe my wife and my son an apology since I obliged them to share their father with AFIT.

MURAT POLAT

# *Table of Contents*

# *List of Figures*

# *List of Tables*

# *Abstract*

The reduction of the navigation error in an inertial navigation system by optically tracking a ground object is investigated. Multiple observations of the ground object are used. The location of the ground object is assumed unknown. A careful analysis of the measurement situation at hand reveals that by optically tracking an unknown ground object using passive, *bearings-only* measurements, the aircraft's angle of attack and sideslip angle can be measured. Thus, two new independent measurement equations featuring the aircraft's angular navigation variables roll, pitch, yaw angles, $\psi, \theta, \phi$, and flight path angle $\gamma$ and heading $H$ are obtained. Hence, by optically tracking over time an unknown ground object, inertial navigation system aiding is in fact possible. Moreover, the estimation algorithm, which operates on the bearing measurements record, simultaneously, and in parallel, produces corrections required for both inertial navigation system aiding and geo-location of the ground object. Furthermore, the theory developed in this paper is easily adapted to accommodate additional measurements and/or prior information. The former entail range measurements, and prior information entails some, or all, position coordinates of the ground object. These enhancements reflect the current operational practice. Thus, the theory presented in this paper is sufficiently general to encompass the conventional methods of inertial navigation system updating in which both bearing and range measurements are used and the coordinates of the ground object are known. In all cases in which additional independent measurements and/or prior information are used, the accuracy of both the navigation solution and the geo-location are enhanced.

# INS AIDING BY TRACKING AN UNKNOWN GROUND OBJECT

# *I. Introduction*

## *1.1 Introduction*

Determining a vehicle's position and velocity by measuring its acceleration and processing the acceleration information in a computer is one of the many definitions for *inertial navigation* [4]. An *Inertial Navigation System*(INS) is a self-contained and autonomous method of navigation. It is self-contained because acceleration and angular rate information necessary for navigation are measured by built-in accelerometers and gyroscopes, which are non-radiating and non-jammable. It is autonomous, because all the required information is obtainable at all latitudes, in all weather and even without the aid of any external source. From this point of view, INS is the most favorable means of navigation. Unfortunately, INS suffers from *drift*, the degradation of accuracy in position, velocity and attitude information. As a result, the accuracy of the INS deteriorates over time; therefore, it needs to be updated periodically.

In a simple way, position errors caused by drift can be corrected by resetting the position to the coordinates of a point which is observable by the pilot on the surface of the earth. These corrections either require the use of *active systems* which transmit electromagnetic signals causing the presence of the aircraft to be revealed, or on enemy territory, the coordinates of the point required for correction may not be available - or may be inaccurate[4].

> An inertial system periodically corrected with external position measurements will have bounded errors in all the navigation variables. But, such a system is obviously not autonomous and is subjected to intentional or unintentional denial, which is unattractive in military applications[4]

## 1.2 Problem

In this research, the possible reduction of the navigation error in an inertial system by tracking a ground object is addressed. Particularly, in an environment a GPS outage is expected, by optically tracking an unknown ground object, INS is tried to be updated. Tracking will be provided by passive, *bearing-only* measurements.

## 1.3 Summary of Current Knowledge

**1.3.1 Inertial Navigation System.** The operation of inertial navigation systems depend on the laws of classical mechanics as formulated by Newton. Newton's laws can be described as follows. "The motion of a body is maintained unless disturbed by an other force". This force produces a proportional acceleration of the body. Measuring that acceleration, it is possible to calculate the change in velocity and position of the body by successive integration of the acceleration with respect to time. Acceleration is measured by the accelerometers. Each for obtaining acceleration measurement in a single direction, an inertial system contains three such devices whose sensitive axes are constructed perpendicular each other.

Gyroscopes are used to determine the orientation of accelerometers in the inertial reference frame. Measured inertial acceleration is resolved into the local reference frame by using the orientation information. By so doing, the direction of which the accelerometers are pointing is determined.

Inertial navigation system combines the two sets of measurements provided by the accelerometers and gyroscopes to determine the velocity and position of the vehicle within the inertial reference frame. Unlike many others types of navigation system, inertial systems are self-contained. Required measurements for the navigation are obtained without use of any external source. Nevertheless, inertial systems rely on the availability of the accurate knowledge of the vehicle position at the start of navigation [8].

**1.3.2 Aided INS Concept.** Aided inertial navigation is a method to reduce the INS errors, in particular the position error drift, and to align the INS or improve its

alignment while moving. Other navigation sensors that measures the position, velocity and orientation provide the INS aiding data. A Kalman filter performs the integration of the INS and aiding navigation data. The Kalman filter estimates the INS and aiding sensor errors based on the navigation data presented, and then corrects the INS navigation errors based on the estimated errors. This closed loop INS error reduction algorithm is known as INS aiding [2].

***1.3.3 Position Updates by INS Fix-Taking.*** The INS estimate of present position can be updated either via use of a radar or by overflying a known point. INS in-flight updating in third generation fighter aircraft is currently performed by using the following fix modes [6]:

1. Radar fix update
2. Head Up Display (HUD) fix update
3. Overfly (OFLY) fix update
4. Targeting pod fix updates

In all the modes above, the position of the ground object is assumed to be known, and to have been stored in the on-board computer before the flight. Inertial positioning errors of the master navigation filter result in an initial mis-location; to correct the error, the radar ground map or radar air-to-ground ranging (Head Up Display (HUD) sighting) sensor modes can be used [6].

***1.3.4 Position Updates by Passive Measurements.*** Currently, there is not any applications or research focused on INS aiding by using passive measurements on *an unknown ground object*. Some ideas had been produced, but have not been implemented.

One of the related ideas was the INS aiding by using bearings' measurements from an unknown (lunar) landmark. The idea was first suggested for [7] space navigation research of *Apollo Mission*. "During the orbital and mid-course phase of a space mission, inertial measurements no longer provide information about the position of the vehicle due to the lack of force [7]". Therefore, the navigation system needs external sensors and

measurements to update the position information within the vehicle. Optical bearing measurements by tracking an unknown landmark is one of the possible measurements that have been considered.

### *1.3.5 Optical Flow.*

The formulation of the *tracking problem* is driven by the need to maintain the non-radiating capability of the INS when tracking an unknown ground object. Thus, passive, *bearing-only* measurements of the ground object should be used. These measurements can be provided by an optical tracker or an electo-optical tracker. The assumption *the position of the ground object is not known* will essentially introduce the measurements of *optical flow*.

In this research, we confine our attention to the optical measurements obtained from tracking of a ground object. We assume that there are low intensity variations in the observed scene. In this case a human operator is needed to close the optical tracking loop, similar to the use of a *driftmeter*[9]. Furthermore, INS-aiding using measurements on a ground object is intimately related to the problem of geo-location. The latter entails the estimation of the a priori information for the unknown position of the ground object from measurements taken by the aircraft. In this case, the estimation of the ground object's position relies on the accuracy of aircraft current position and attitude knowledge. It is obvious that these navigational errors are reflected in the ground object's position estimate. Conversely, in conventional INS-aiding, it is usually assumed that the position of the ground object is known, and range and bearing measurements are used to obtain an independent position estimate of the aircraft. Hence, INS-aiding and geo-location appear to be on the opposite sides of the same situations.

## *1.4 Scope*

In this research we assume that the position of the ground object is not known. Also, we initially remove the requirement of range measurements and we exclusively rely on *bearings-only* measurements, however, we use multiple observations of the ground object. Hence, we consider an austere geo-location type scenario and we will show that INS-aiding

is, in fact, possible. In addition, and as expected, we will show that geo-location is also possible.

## *1.5 Approach/Methodology*

The research presented herein starts by the careful analysis of the measurement situation at hand. In the analysis, we develop two hypotheses: while the first hypothesis claims that the aircraft angle of attack (AOA) and drift angle could be obtained by optically tracking an unknown object, the second claims that the AOA and drift angle yield two new independent measurement equations featuring the aircraft's navigation variables roll, pitch, yaw angles, $\psi, \theta, \phi$, and flight path angle $\gamma$ and the heading $H$. Modelling of the measurement situation follows the validation of these two hypotheses.

Next, we develop the Minimum Variance Estimation formulae based on the suggested measurement situation model. By incorporating bearing-only measurements, INS-aiding is mathematically discussed. Investigating different scenarios, it is shown that one can perform INS aiding by tracking an unknown object by means of LOS measurements only. The theoretical framework developed in this research, however, can be easily adapted to accommodate additional measurements and/or *a priori* information. Additional measurements would entail range measurements and/or range rate measurements; and prior information would entail some, or all, position coordinates of the ground object. These enhancements would reflect the current operational practice. Thus, the theory presented in this research is sufficiently general to encompass the conventional methods of INS updating in which both bearing and range measurements are used and the coordinates of the ground object are known. In all cases where additional independent measurements and/or prior information are used, the accuracy of the navigation solution is enhanced.

Furthermore, we show that the geo-location is possible, too. Using a ground object for INS aiding to improve one's position estimate and then performing a geo-location of the same ground object by using just aided INS information is an illusion. This is not the case, and in fact, the algorithm which operates on the bearing measurements simultaneously, and in parallel, produces corrections required for both INS update and geo-location.

Based on the physical insight gained from the theory, the estimation algorithms are developed. In the algorithms, bearing-only measurements and INS provided inertial measurements are optimally weighted in a *Bayesian formulation*, using their respective parameter estimation error covariances.

Finally, simulation experiments are performed to validate the novel navigation concept. Concluding remarks are made at the end of the research, including that INS error reduction by tracking an unknown ground object via bearing-only measurements is partly possible.

## *1.6 Summary*

In this section, we presented an introduction for the research about INS aiding by tracking an unknown ground object. After a brief summary of the current knowledge, we defined the scope of the research. Next, approach and methodology were explained shortly.

# II. Literature Review

## 2.1 Introduction

"*INS is the King!*" says a leading professor from the AFIT Guidance, Navigation & Control research group. Surely, you are asking yourselves *why is this so?*

Determining a vehicle's position and velocity by measuring its acceleration and processing the acceleration information in a computer is one of the many definitions for *inertial navigation*[4]. Among the several methods of navigation, the inertial navigator, namely the *Inertial Navigation System* (INS), is a self-contained and autonomous one. It is self-contained because acceleration and angular rate information necessary for navigation are measured by built-in accelerometers and gyroscopes, which are non-radiating and non-jammable. It is autonomous, because all the required information is obtainable at all latitudes, in all weather and even without the aid of any external source. Thus, the claim that "INS is the King!" is not a poor analogy.

Unfortunately, *the King* suffers from *drift*, degradation of accuracy in position and velocity information obtained autonomously and inclusively. As a result, the accuracy of the INS deteriorates over time; therefore, it needs to be updated periodically; that is, the King asks for an *advisor* occasionally.

Much research on the INS aiding concept exists in the literature. It includes not only inventions of practical solutions but also considerable research aiming to enhance degraded INS accuracy. *INS aiding by tracking ground objects* is among the most popular areas studied. However, little research into INS aiding by tracking *an unknown* ground object exists. A few suggestions have been made on this but they have not gone beyond theory. In this thesis, we will investigate the possible reduction of the navigation error of an inertial system by tracking a ground object. In particular, the ground object will be assumed unknown and tracking will be provided by passive, *bearing-only* measurements. Although not exactly related to unknown ground object tracking, various basic research publications on INS aiding are available in the open literature. Thus, the basic objective of

this review is to comb the literature for background information clarifying the problem at hand and providing information that might help produce a related theory for the solution.

Appropriate for this problem, eight articles have been covered in this literature review, and it is organized into three sections. In the first section, background information is presented. Definition of the inertial system and the concept introducing INS aiding are the first two topics in the background. The next two topics describe the methods used in aiding. In the second section, four topics are reviewed. *Optical Measurements and Navigation Phenomena* is particularly relevant to the problem. Here, a theory suggested for the *Apollo Mission* is studied explicitly. The following three topics cover *autonomy of the INS* that motivates the research, *optical flow* and *driftmeter*. The last two are the significant tools for the research validity. A conclusion in the third section summarizes the problem and concludes that a solution is achievable.

This literature review gives only a glimpse into the problem at hand. The most significant work will be to produce the theory for the solution of the problem and to validate it.

## *2.2 Background*

***2.2.1 Inertial Navigation System.*** Inertial navigation systems use measurements obtained from the accelerometers and gyroscopes mounted on a platform whose angular velocity either is controlled (as with gyro stabilized gimballed platforms) or is measured (as with strapdown systems) to provide position, velocity, and attitude information of the aircraft. In all INS implementations, it is an unavoidable fact that altitude and vertical velocity computation is unstable (assuming gravity magnitude is computed as a function of the indicated altitude). The time constant of the exponential instability is about 10 minutes. Some external altitude reference must be incorporated into the vertical channel measurements for typical navigation durations (an hour or more) to alleviate the errors caused by this instability [10].

Other than the vertical channel instabilities, however, there are additional errors inherent to the design of inertial navigation systems that cause a drift in INS position,

velocity, and attitude outputs. These errors result from the imperfection of the inertial sensors which contain built-in errors. A medium quality INS contains ring-laser-gyros (RLG) with less than 0.01 degrees/hour bias and pendulous servo accelerometers with less than 50 micro-g's bias, and exhibits a typical position error rate of 1 nm/hour [2]. Although these inertial drift rate errors are small and acceptable for A/C navigation initially, they become larger and larger with time unless they are corrected by more accurate and independent measurements [11]. This phenomenon also introduces the aided INS concept.

***2.2.2 Aided INS Concept.*** The performance of an inertial system is characterized by a time dependent drift in the accuracy of the position estimates it provides. The rate of the growing error depends basically on the accuracy of the initial alignment, inertial sensor imperfections, and the dynamics of the trajectory of the host vehicle. While improvements in accuracy can be obtained through the use of more accurate and higher quality sensors, there are limits to the performance which can reasonably be achieved before the cost of the inertial system becomes too great to be affordable.

An alternative approach, suitable for many implementations, can be devising some additional navigation sources different than those the inertial system provides, to improve the accuracy: in other words, *an aided inertial system.* In an aided inertial system, one or more of the inertial measurements is compared to the identical measurements obtained from the external sources. The corrections are applied to the system based on these differences. The optimal combination of these differences and inertial measurements yields more accurate navigation solutions than the inertial system would provide alone.

Basically, the various types of navigation aids may be introduced in two classes: *External measurements* are acquired by receiving signals outside the vehicle. The required data can be transmitted to the vehicle during the navigation or there will be a receiver onboard to acquire the observations. This class of navigation aids usually provide a position fix which may be expressed as co-ordinates with respect to local reference frame. Radio navigation aids such as Tactical Air Navigation System (TACAN), Very high frequency Omni-directional radio Range (VOR), Distance Measuring Equipment (DME), and Global Positioning System (GPS), star-trackers or a ground based radar trackers are examples of

this class of navigation aid.

*Onboard measurements* are obtained, as the name indicates, by using onboard sensors such as the altimeter, aircraft's radar, airspeed indicator, magnetic sensors, and infra-red or electro-optical imaging systems. Such sensors can be used to provide attitude, velocity or position updates [8].

***2.2.3 Position Updates Of An Inertial System.*** In a simple way, position errors caused by drift can be corrected by resetting the position to the coordinates of a point which is observable by the pilot on the surface of the earth. Designing fixed gain mechanizations to feed back the observed position differences between the INS and the reference measurements to correct the sources of these errors has been inconvenient due to time-varying error dynamics associated with the inertial system. However, this problem was diminished with the development of recursive filtering by R. E. Kalman in 1960, and the powerful digital computers made possible algorithm mechanizations. With Kalman filtering theory, gains are weighted based on the error covariance instead of fixed gains. Error corrections through the use of such gains provide optimal minimization of the existing errors [4].

***2.2.4 INS Position Updates by Fix-Taking.*** INS position updates by fix-taking subject addressed below is based on my knowledge as a pilot and the reference [6]. The INS estimate of present position can be updated either via use of the radar or by overflying a known point. The radar ground map or radar air-to-ground ranging (HUD sighting) sensor modes can be used to update position. The basic geometry of these fix modes is depicted as follows.

1. Radar fix update: The multifunctional display provides a radar image of the ground. System solution indicates the ground object based on the pre-determined and stored coordinates. The pilot makes a manual correction by slewing and placing the big cross on the true aim-point location. This registers the range to the ground object and depressions and bearing angles of the ground object with central navigation Kalman filter.

2. Head Up Display (HUD) fix update: HUD, located on the center of the glare shield at the eye-level of the pilot, provides a visual reference by locating a diamond on the ground object based on the pre-determined and stored coordinates. The pilot indicates the true aim-point location by slewing the diamond onto target location. An air-to-ground ranging mechanism provides range information and the bearing and depression angles are registered with the central navigation Kalman filter.

3. Overfly (OFLY) fix update: The pilot overflies a pre-determined landmark for which coordinates have been stored as a steering point (STPT) or an Initial Point (IP) and, at the pilot's cue, its observed position is sent to the central navigation Kalman filter to provide correction.

4. Targeting pod fix updates: The pilot updates the master navigation filter by using Forward Looking Infra Red (FLIR) or Down Looking Infra Red (DLIR) video for sightings on known ground object. The pod cursor is initially pointed at the estimated position of the ground object, based on the stored coordinates of the ground object, its elevation, and the navigation system's estimation of present position, altitude, and attitude of the aircraft. The pilot manually applies the correction by moving the cursor to the ground object, thus nullifying the pointing error. By pulling the trigger on the stick, a laser range measurement can be obtained as well. Moreover, the pilot can get a laser lock to ground object, provided the contrast is sufficiently high.

In all scenarios above, the position of the ground object is assumed to be known, and to have been stored in the on-board computer before the flight. Inertial positioning errors of the master navigation filter result in an initial mis-location of the big cross in (1), the diamond in (2), or the cursor in (4) by the amount of error. This initial placement error is displayed in Data Entry Device (DED) and the pilot manually applies the correction.

## *2.3 The Possible Solution*

***2.3.1 Optical Measurements and Navigation Phenomena.*** The idea of INS aiding by using bearings measurements on unknown (lunar) landmark was

first suggested in [7] space navigation research associated with the *Apollo Mission*. Optical bearing measurements by tracking an unknown landmark was considered to aid the inertial system. Different from the conventional means of obtaining inertial measurements, the navigational system is obliged to use the changes in the tracking angle as the vehicle passes over a landmark, especially when the landmark has *unknown coordinates*.

Let's assume that the astronaut is able to lock onto an identifiable but unknown point on the earth's surface. Figure 2.1 describes the measurement geometry. The problem here

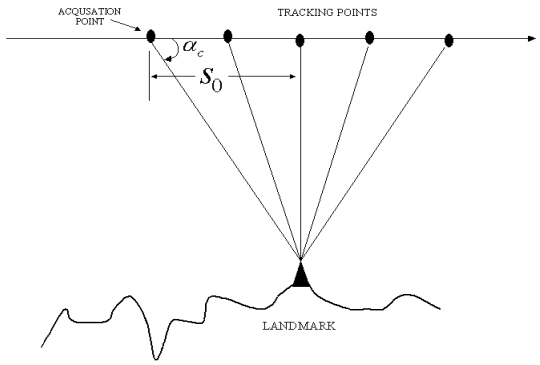


Figure 2.1 Nominal tracking sequence.

is to determine the errors at the acquisition point. Also assume that $H_0$ is the height of the velocity vector, $r_0$ is the distance travelled for some time $\tau$, and $\omega_0$ is the angular velocity of the vehicle (see Figure 2.1). In this situation, the computed bearing measurements is given by:

$$\cot \alpha_c = \frac{S_0 - r_0 \omega_0 \tau}{H_0} \tag{2.1}$$

The suggested idea is investigated in Appendix A in detail. The measurement situation is very similar to our problem, and can be used as a point of departure for the development of algorithm concerning optical tracking of a ground object.

***2.3.2 About The Autonomy of INS.*** Autonomy represents the ability of a system to determine its position and velocity on by own, without external navigation aids. Autonomy has a great significance for military vehicles operating on the enemy territories

or in the areas of inadequate radio-navigation coverage. Autonomy can be examined in five classes [4]:

1. *Passive self-contained systems*: This class of autonomy is the most desired one since it neither receives nor transmits any electro-magnetic signals which would reveal its presence, and it does not require any external navigation aid that may not be available on the enemy territories. Dead reckoning systems like inertial navigation systems (INS) are presented in this class.
2. *Active self-contained systems*: These systems do not receive any signals, but unfortunately they do transmit electro-magnetic signals. Since the transmitted signals are easily detectable by the enemy radar warning receivers (RWR) or threat warning systems (TWS), they are less desirable than the passive self-contained systems.
3. *Receivers of natural radiation*: Magnetic compasses, star-trackers and passive map correlators are able to receive naturally transmitted electro-magnetic radiation. As in the passive self-contained systems, they are also independent from any external navigation aid and they do not expose their presence.
4. *Receivers of artificial radiation*: These systems completely depend on external navigation aids. Even if they do not transmit any electro-magnetic signal to reveal their presence, they measure the electro-magnetic radiation sent out by the external navigation sources. Loran, Omega, VOR and GPS can be treated in this class.
5. *Active radio nav-aids*: The least autonomous ones are the active radio nav-aids, such as Distance Measuring Equipment (DME), Joint Tactical Information Distribution System (JTIDS), Position Location Reporting System (PLRS), and collision avoidance systems because of their signal exchange requirements with external sources. It is obvious that emitting and transmitting electro-magnetic signals betray their presence.

If INS is aided in a way mentioned in Sect. 2.2.4, transmitting electro-magnetic signals becomes unavoidable. Trade-off between INS aiding and presence giveaway brings another motivation behind this research: while aiding, also keep the silence of INS.

### *2.3.3 Optical Flow.*

One of the motivations behind the formulation of the *tracking problem* is the desire to maintain non-radiating capability of the INS. Thus, passive, *bearing-only* measurements of the ground object should be used. These measurements can be provided by an optical tracker or an electo-optical tracker. The assumption that *the position of the ground object is not known* will essentially introduce the measurements of *optical flow*. Basically, four different scenarios are possible when a ground object is being tracked:

1. The ground object is a high intensity point source compared to the surroundings. In this case, one could use a point source Infra Red (IR) tracker, as used in the IR seekers of the guided missiles. The tracking function can be easily automated.
2. There is an intermediate level of intensity variation in the scene of being viewed. In this case, one would use an *optical flow* sensor[3].
3. There are low intensity variations in the observed scene. This is the case a human operator is needed to close the optical tracking loop, similar to the use of a *driftmeter* [9].
4. In a very low signal-to-noise ratio (SNR) condition as in night flight, or when flying over cloud cover or water, one is denied use of optical sightings of the ground objects for navigation.

In this research, we confine our attention to scenario 3. However, the theory concerning the use of optical and inertial measurements together is similar in scenarios 1 to 3. Furthermore, INS-aiding using measurements on a ground object is intimately related to the problem of geo-location. The latter entails the estimation of the a priori information for the unknown position of the ground object from measurements taken by the aircraft. In this case, the estimation of the ground object's position relies on the accuracy of aircraft current position and attitude knowledge. It is obvious that these navigational errors are reflected in the ground object's position estimate. Conversely, in conventional INS-aiding, it is usually assumed that the position of the ground object is known, and range and bearing measurements are used to obtain an independent position estimate of

the aircraft. Hence, INS-aiding and geo-location appear to be on the opposite sides of the same situation. Schematically;

$$\text{own ship position known} \overset{Geo-Loc}{\longrightarrow} \text{ground object not known}$$
$$\text{own ship position not known} \overset{INS-aiding}{\longleftarrow} \text{ground object known}$$
$$\text{own ship position} \overset{Geo-loc\ v.s.\ aiding}{\longleftrightarrow} \text{ground object}$$

Using a ground object for INS aiding to improve one's position estimate and then performing a geo-location of the same ground object by using just aided INS information is an illusion. This is not the case, and in fact, the algorithm which operates on the bearing measurements simultaneously, and in parallel, produces corrections required for both INS update and geo-location.

***2.3.4 Driftmeter.*** The driftmeter is a simple device to measure drift and ground speed. It makes the comparison possible between true course and true heading by rotating a transparent plate until lines etched on its surface match the track of objects passing on the ground below. The measured angle of rotation from a reference line gives the drift. Its gyroscopically stabilized structure makes it reliable to use in rough air and its optical system can be rotated forward and backward in the aircraft to provide a means of taking *bearing measurements*. Figure 2.2 presents a B-3 Driftmeter. The driftmeter is also used to measure the ground speed by timing the passage of an object from one line to the other and using the aircraft altitude information. For better accuracy several measurements are taken and averaged. It is also possible to determine the wind vector from the drift and ground speed by solving the wind triangle[9].

## *2.4 Conclusion*

The inertial system and its time exponential drift error are presented in this chapter. This chapter also includes the methodology for eliminating system errors. By the current technology, this can be easily performed by aiding the INS with external sources. At this point, the trade-off between aiding INS for a better accuracy and keeping the silence for the sake of a successful intruding into the enemy depths is worth-considering. The significance

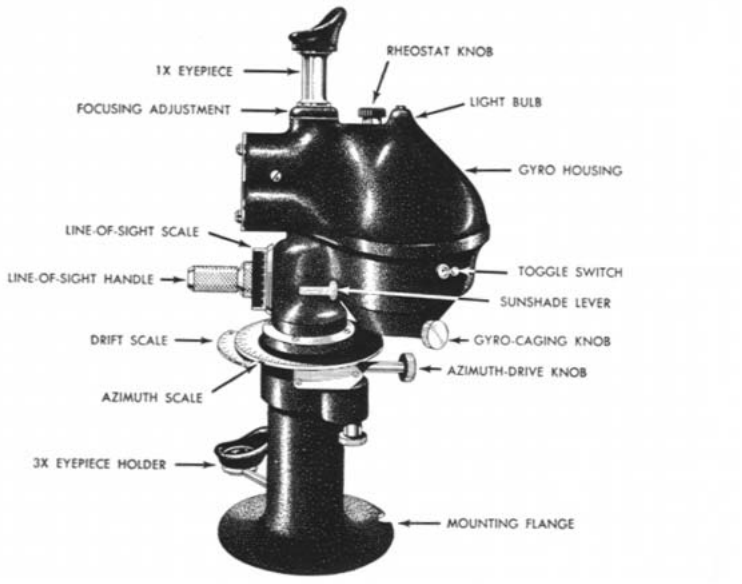


Figure 2.2 B-3 Driftmeter [9].

of the INS autonomy is inevitable in this situation. Although no research exists on aiding the INS by tracking unknown objects, presented theoretical computation [7] can be detailed and applied for ground object tracking formulation.

# III. Methodology

## 3.1 Introduction

In this chapter, we develop the methodology for INS aiding by tracking an unknown ground object. The first objective in the development is to determine the equations which will make the INS aiding possible. Based on a proposed measurement scenario, we first present the theory and than we develop the methodology to calculate the variables of the INS aiding equations.

## 3.2 Analysis

In the development we consider the plane **P** formed by the aircraft's velocity vector **V** and the point $P$ on the ground - see Fig 3.1. The inertial reference frame is X, Y, Z. A local frame of reference $x, y, z$ is also introduced. Its origin is collocated with the aircraft's initial position $X_0, Y_0, Z_0$, the x-axis is aligned with the aircraft's inertial velocity vector **V**, the y-axis is in the plane **P**, normal to the x-axis, and points in the direction of the point $P$, and the z-axis complements the right handed axes system. The aircraft's body axes are $x_b$, $y_b$, and $z_b$. The bearings-only kinematic measurement scenario is illustrated in Fig 3.1. The measurements are

1. Time $t$.
2. The LOS in inertial space:
   (a) The LOS angle $\sigma_N$ in the $(x, y)$ plane **P**, or the angular rate $\dot{\sigma}_N$ of the LOS in the plane **P**, and,
   (b) The unit vector $\vec{\omega}_1$ normal to the plane **P**, obtained from the measurement of the inertial LOS rate vector $\vec{\omega}$; $\vec{\omega}_1 = \frac{\vec{\omega}}{|\vec{\omega}|}$.
3. The LOS relative to the aircraft: The direction cosines of the telescope's LOS vector relative to the aircraft's body axes.

The tracker envisioned herein consists of a precision telescope mounted on a gimbal system. This allows the telescope to remain pointed to the ground object independent of vehicle motion. The direction of the Line of Sight (LOS) relative to the aircraft body axes is measured by pickups attached to the gimbals. In addition, the inertial angular rate $\vec{\omega}$ of the LOS is measured. Specifically, the following efficient mechanization of the optical tracker is proposed: The inertial angular rate $\vec{\omega}$ of the LOS is measured using a 2 Degree-of-Freedom (DOF) rate gyro whose spin axis is aligned with the optical axis of the telescope. The gyros' input axes and the telescope's optical axis ($\equiv$ LOS in the absence of tracking errors) form a triad of orthogonal axes. The telescope mounted 2 DOF gyro directly measures the angular rate $\vec{\omega}$ of the LOS with respect to an inertial reference frame. The gyro should be of medium quality, so as not to pick up the earth rate. Since the gimballed tracker's azimuth and elevation angles relative to the aircraft body axes are measured, $\vec{\omega}$ is resolved in the aircraft body axes. The proposed arrangement is akin to the seeker of the Sidewinder air-to-air missile.

Concerning the state of the art of optical tracking of ground objects/targets from aircraft: Pilots of F-16 class fighter aircraft equipped with Forward Looking Infra Red (FLIR) targeting pods and pilots of FLIR and Down Looking Infra Red (DLIR) equipped

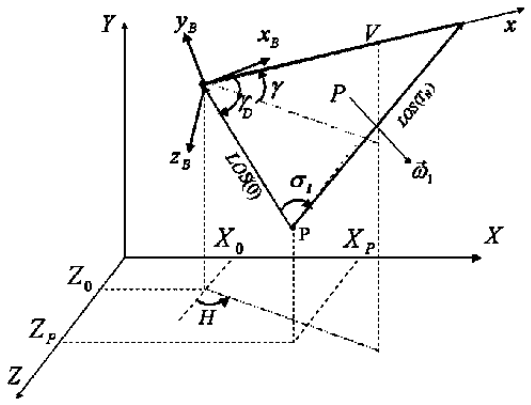


Figure 3.1 The measurement situation in the 3-D case

F-117 attack aircraft currently have the capability to designate and track ground targets manually from high altitudes (20,000').

We shall show that the following holds.

**Theorem 1** Consider the kinematic measurement scenario shown in Fig 3.1 where bearing measurements on a ground object, whose position is not known, are taken over time. Assuming a constant aircraft speed V during the (short) measurement interval, it is then possible to estimate the angles which specify the direction of the aircraft's inertial velocity vector **V** relative to the aircraft's body axes, viz., $\alpha'$ and $\beta'$, where

$$\alpha' = \arctan(\frac{w}{u}) \ , \qquad \beta' = \arctan(\frac{v}{u}) \ ,$$

and where $u,\ v$, and $w$ are the components of the inertial velocity vector **V** resolved in the body axes.

The proof of Theorem 1 is given in Sect. 3.3 in the sequel.

Thus, we realize that:

**Corollary 2** An optical flow sensor measures the angles $\alpha'$ and $\beta'$ which specify the direction of the aircraft's inertial velocity vector relative to the aircraft's body axes.

□

**Corollary 3** The kinematic measurement scenario which entails bearing measurements over time on a ground object whose position is not known, affords the estimation of the aircraft's aerodynamic angles $\alpha$ and $\beta$, provided that the air mass is stationary, viz., there is no wind.

Proof The no wind/stationary air mass hypothesis implies that the aircraft's inertial velocity is the airspeed. Hence, by definition, the aerodynamic angles $\alpha$ and $\beta$ satisfy

$$\begin{aligned} \alpha &= \alpha' \\ \beta &= \beta' \end{aligned}$$

□

We also realize that - see Sect. 3.3.3:

**Proposition 4** The angles $\alpha'$ and $\beta'$ are related to the aircraft's angular navigation variables roll, pitch, yaw angles, $\psi, \theta, \phi$, and flight path angle $\gamma$ and heading $H$.

□

Theorem 1 and Proposition 4 are exploited in Sect. 4.2 in the sequel to lay the foundation for INS-aiding using bearings-only measurements, as stated in:

**Theorem 5** The kinematic measurement scenario which entails bearing measurements over time on a ground object whose position is not known, yields two new independent measurement equations featuring the aircraft's angular navigation variables roll, pitch, yaw angles, $\psi, \theta, \phi$, and flight path angle $\gamma$ and heading $H$.

□

Hence, a careful analysis of the proposed unknown landmark bearing measurement scheme using an optical or electro-optical device and summarized in Theorem 1 and Corollary 2, reveals the following: A stand-alone measurement of the angles $\alpha'$ and $\beta'$ included between the aircraft's inertial velocity vector $\mathbf{V}$ and the aircraft body axes is obtained. According to Corollary 3, in the absence of wind, an estimate of the aircraft's aerodynamic angles $\alpha$ and $\beta$ is obtained. More importantly, and irrespective of the presence of wind, the said optical flow measurement can be used for INS aiding. Indeed, according to Proposition 4, the optical sensor provided angles $\alpha'$ and $\beta'$ can also be expressed as a function of the INS provided aircraft's Euler angles $\psi, \theta, \phi$, and the inertial aircraft velocity vector angles $\gamma$ and $H$; and this in turn, allows the development of an estimation algorithm for improving these variables' estimates, as stated in Theorem 5. This should come as no surprise - indeed, the proposed INS aiding concept is a modern mechanization of a *driftmeter* [9] . In other words, the gist of the research is an investigation into INS aiding using a modern *driftmeter*, a.k.a., optical flow.

## *3.3 Estimation*

In this section, Theorem 1 is proven.

### *3.3.1 Development of the Regressor H.*

In the sequel we'll assume that the aircraft overflies the ground object $P$ - see Fig 3.2 . Thus we'll confine our attention to flight in the vertical plane $(X, Y)$ ($\equiv \mathbf{P}$). In other words, we do not allow for an offset flight path and the course in Fig 3.1 $H = \frac{\pi}{2}$, however the aircraft could be climbing or diving ($\gamma \neq 0$). This considerably simplifies the development without impacting the proof of concept. Moreover, we then obtain the following reduced set of variables relevant to the solution of the navigation problem: The navigation variables are $X_0, Y_0, V, \gamma, \theta$, and the ground object coordinates are $X_P, Y_P$. The ground object, referred to as the point $P$, has the coordinates $(x, y)$ in the local frame in the plane $\mathbf{P}$. Since the aircraft overflies the reference point $P$, the following coordinate transformation applies.

$$\begin{aligned} X_P - X_0 &= x\cos\gamma + y\sin\gamma \\ Y_P - Y_0 &= x\sin\gamma - y\cos\gamma \end{aligned} \tag{3.1}$$

The bearings measurements' time is $t$ and the LOS angle $\sigma(t)$ is in the $(x, y)$ plane $\mathbf{P}$.

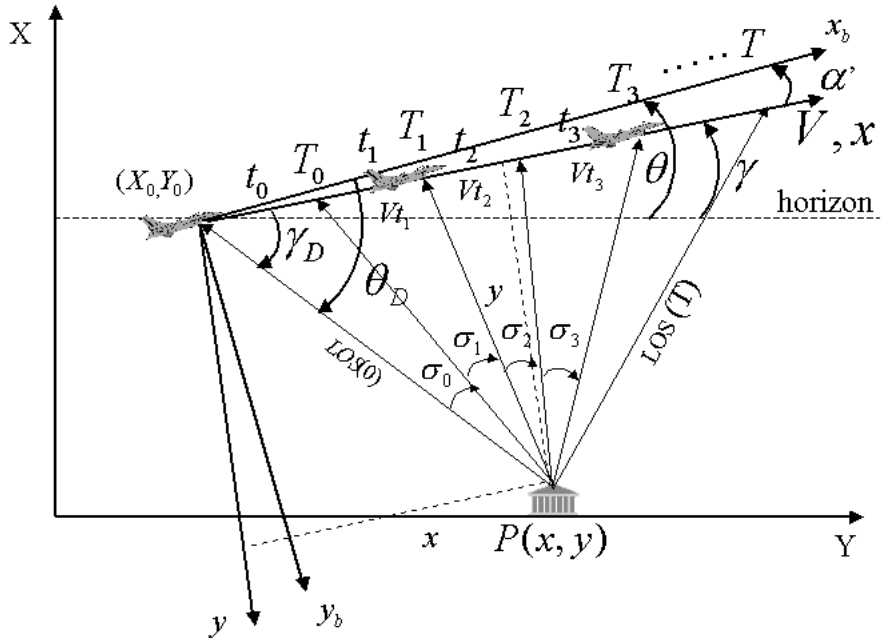


Figure 3.2 The measurement situation in the 2-D case - the plane $\mathbf{P}$

Measurements of the LOS angles $\sigma_k$ are taken at the time instants $T_k$, $k = 0, 1, ..., N$. The time intervals between measurements are denoted by $t_k$. Thus,

$$T_k = \sum_{i=0}^{k} t_i \tag{3.2}$$

As shown in Fig 3.3 a), the point $P$ is evidently located on the circumference of the circle $C_k$, $k = 0, 1, ..., N$; the circle $C_k$ is the locus of points where from the angle of visibility of the segment $Vt_k$ is $\sigma_k$. Moreover, the point $P$ is located at the intersection of the $N + 1$ circles $C_k$ - see Fig 3.3b).
The radius of the circle $C_k$,

$$R_k = \frac{Vt_k}{2\sin\sigma_k} \ , \quad k = 0, 1, ..., N \tag{3.3}$$

and the center of the circle $C_k$ in the local $(x, y)$ frame is at

$$\begin{aligned} x_{C_k} &= \sum_{i=0}^{k-1} Vt_i + \frac{1}{2}Vt_k \\ y_{C_k} &= \frac{Vt_k}{2\tan\sigma_k} \ , \quad k = 1, ..., N, \end{aligned} \tag{3.4}$$

and the center of the circle $C_0$ is at

$$\begin{aligned} x_{C_0} &= \frac{1}{2}Vt_0 \\ y_{C_0} &= \frac{Vt_0}{2\tan\sigma_0} \end{aligned} \tag{3.5}$$

$C_0$ is referred to as the "prime" circle. The equations of the circles are

$$(x - \frac{1}{2}Vt_0)^2 + (y - \frac{Vt_0}{2\tan\sigma_0})^2 = \frac{V^2t_0^2}{4\sin^2\sigma_0} \tag{3.6}$$

and

$$(x - \sum_{i=0}^{k-1} Vt_i \ - \ \frac{1}{2}Vt_k)^2 + (y - \frac{Vt_k}{2\tan\sigma_k})^2 = \frac{V^2t_k^2}{4\sin^2\sigma_k} \ , \quad k = 1, ..., N \tag{3.7}$$

Eqs. (3.6) and (3.7) yield a set of $N+1$ quadratic equations in $x$ and $y$,

$$x^2 + y^2 - Vt_0 x - \frac{Vt_0}{\tan\sigma_0} y = 0 \tag{3.8}$$

and

$$x^2 + y^2 - (2\sum_{i=0}^{k-1} Vt_i + Vt_k)x - \frac{Vt_k}{\tan\sigma_k} y = -(\sum_{i=0}^{k-1} Vt_i)^2 - Vt_k \sum_{i=0}^{k-1} Vt_i \ , \quad k = 1, ..., N \tag{3.9}$$

Subtracting eq. (3.8) from eq. (3.9), and dividing both sides of the resultant equation by $V$ and using the definition (3.2) for $k = 1, ..., N$, yields the linear homogeneous system of $N$ equations in $x, y$, and $V$:

$$(2T_k - t_k - t_0)x + (t_k \cot\sigma_k - t_0 \cot\sigma_0)y - T_k(T_k - t_k)V = 0 \tag{3.10}$$

The linear homogeneous system (3.10) can be compactly written in matrix form as

$$H\theta = 0 \tag{3.11}$$

where the parameter vector

$$\theta = \begin{bmatrix} x & y & V \end{bmatrix}^T$$

and the $N \times 3$ regressor matrix $H$

$$H = \begin{bmatrix} 2T_1 - t_1 - t_0 & t_1 \cot\sigma_1 - t_0 \cot\sigma_0 & -T_1(T_1 - t_1) \\ \cdot & \cdot & \cdot \\ \cdot & \cdot & \cdot \\ 2T_k - t_k - t_0 & t_k \cot\sigma_k - t_0 \cot\sigma_0 & -T_k(T_k - t_k) \\ \cdot & \cdot & \cdot \\ \cdot & \cdot & \cdot \\ 2T_N - t_N - t_0 & t_N \cot\sigma_N - t_0 \cot\sigma_0 & -T_N(T_N - t_N) \end{bmatrix}_{N\times 3}$$

Remark The time measurements are accurate and therefore only the second column of the regressor $H$, where the LOS angles feature, is noise corrupted.

The following holds.

**Theorem 6** The true rank of the $N \times 3$ regressor $H$ is 2.

Proof

When $V$ is considered a parameter, the solution $x$ and $y$ of Eq. (3.10) is homogenous in $V$. Hence, the "prime" nonlinear Equation (3.8) is homogeneous in $V$ and therefore, upon inserting the solution $x$ and $y$ of the linear system (3.10) into Eq. (3.8), it is impossible to calculate $V$. Furthermore, when one inserts the above solution for $x$ and $y$ into the quadratic equation of the "prime" circle (3.6), the latter becomes an identity.

□

Concerning the meaning of the "true" rank of $H$: This is the rank of a "clean" $H$, and not the numerical rank of the actual, experimentally obtained and noise corrupted, regressor. The deleterious effect of measurement noise is to increase the apparent rank of the regressor $H$ so that the latter masquerades as a full rank, and therefore, invertible matrix (in which case the parameter would be $\theta = 0$).

In conclusion: Our regressor $H$ is an $N \times 3$ matrix. The true rank of $H$ is 2, whereas a noise corrupted regressor matrix $H$ will boast a rank of 3. In the deterministic case one could pick any two equations from the linear system (3.10) and express $x$ and $y$ as a linear (in fact, homogeneous) function of $V$. In the noiseless case, the same solution will be obtained irrespective of which two equations one uses. In the stochastic case, the following course of action is taken.

***3.3.2 Development of the $\gamma_D$ Formula.*** As shown in Fig 3.2 in the simplified planar case, the navigation variables consist of 3 "positional" variables and 2 angular variables. They are $X_0$, $Y_0$, $V$, and $\gamma$, $\theta$, respectively.

The navigation variables are assumed constant during the (short) measurement interval.

The raw measurements are

1. The time instants $t_k$, $k = 0, 1, ..., N$.

2. The LOS rate with respect to inertial space, i.e., $\sigma_k$, $k = 0, 1, ..., N$.

3. The angle of depression of the initial LOS, $\theta_D$; it is the angle included between the aircraft's x-body axis and the initial LOS to the ground object P.

The raw measurements are pre-processed and the regressor $H$ is formed according to the development in Section 3.3.1. The angle $\gamma_D$ included between the velocity vector $\mathbf{V}$ and the initial LOS is computed as follows.

Performing a Singular Value Decomposition (SVD) of the noise corrupted regressor $H$ yields [1]

$$H = U\Sigma V^T$$

where $U$ and $V$ are $N \times 3$ and $3 \times N$ matrices, respectively. The $3 \times 3$ diagonal matrix $\Sigma$ has 3 singular values. The third singular value is much smaller than the first two singular values. Set the third singular value to 0 and only the nonzero elements of $\Sigma$ are preserved in a reduced $2 \times 2$ matrix $\underline{\Sigma}$. Furthermore, the last column of $U$ and, similarly, the last row of $V^T$, are removed, forming the reduced matrices $\underline{U}$ and $\underline{V}$, respectively. Take the square root of the $\underline{\Sigma}$ matrix and form the matrices

$$\underline{H} = \underline{U\Sigma}^{\frac{1}{2}} \tag{3.12}$$

and

$$K = \underline{\Sigma}^{\frac{1}{2}}\underline{V}^T \tag{3.13}$$

$\underline{H}$ is a full rank ($\equiv 2$) $N \times 2$ matrix and $K$ is a $2 \times 3$ matrix of rank 2. Hence, we have performed a full rank factorization of the regressor $H$,

$$H = \underline{H}K$$

Define the reduced parameter

$$\underline{\theta} = K\theta \tag{3.14}$$

Thus,

$$\underline{H\theta} = 0 \tag{3.15}$$

which yields

$$\underline{\theta} = 0 \tag{3.16}$$

Combining Eqs. (3.14) and (3.16) allows us to replace the original linear homogeneous system of $N$ equations with the reduced linear homogeneous system of 2 independent equations in 3 unknowns

$$K\theta = 0 \tag{3.17}$$

where the full rank matrix $K$ is constructed according to Eq. (3.13). Thus, Eq. (3.17) is a set of 2 linear equations in the 3 unknowns $x$, $y$ and $V$, viz.,

$$\begin{aligned} K_{1,1}x + K_{1,2}y + K_{1,3}V &= 0 \\ K_{2,1}x + K_{2,2}y + K_{2,3}V &= 0 \end{aligned} \tag{3.18}$$

This yields the solution

$$\begin{aligned} x &= K_x V \\ y &= K_y V \end{aligned} \tag{3.19}$$

where the "gains" are given by

$$\begin{aligned} K_x &= \frac{K_{1,2}K_{2,3} - K_{2,2}K_{1,3}}{K_{1,1}K_{2,2} - K_{1,2}K_{2,2}} \\ K_y &= \frac{K_{2,1}K_{1,3} - K_{1,1}K_{2,3}}{K_{1,1}K_{2,2} - K_{1,2}K_{2,2}} \end{aligned} \tag{3.20}$$

Evidently, $x$ and $y$ are homogeneous in $V$.
Now, the angle

$$\gamma_D = \arctan(\frac{y}{x})$$

The SVD yields the "gains" $K_x$ and $K_y$ and, in view of Eqs. (3.19), we calculate

$$\gamma_D = \arctan(\frac{K_y}{K_x})$$

where the "clean" $K_x$ and $K_y$ parameters are the result of the SVD. The above calculated angle $\gamma_D$ included between the A/C velocity vector and the initial LOS to P is referred to as $\gamma_{D_{meas}}$.

***3.3.3 The Angle $\theta_D$.*** In the simulation we generate the angle included between the A/C body axis and the initial LOS to P,

$$\theta_D = \gamma_D + \alpha \tag{3.21}$$

where $\alpha$ is the aircraft's Angle Of Attack, AOA. It is the angle included between the aircraft body axis $x_b$ and flight path axis $x$. The measurement is then generated as

$$\theta_{D_{meas}} = \theta_D + v_2, \tag{3.22}$$

where $v_2$ is white Gaussian measurement noise with the statistics below. Half a radian is assumed a reasonable $\sigma$ value for an optical tracker.

$$\begin{aligned} v_2 &= \mathcal{N}(0, \sigma^2_{\theta_D}) \\ \sigma_{\theta_D} &= 5 \times 10^{-4}[rad.] \end{aligned} \tag{3.23}$$

At the same time, $\alpha$ is the difference between $\theta$ and $\gamma$, which are the INS measured pitch angle and flight path angle, respectively:

$$\theta = \gamma + \alpha \tag{3.24}$$

The difference between $\gamma_D$ and $\theta_D$ is also equal to $\alpha$ - see Eq.(3.21). The $\gamma_D$ and $\theta_D$ measurements are provided by the optical arrangement described above. Thus, subtracting Eq. (3.21) from Eq. (3.24) yields the equation which relates the optical bearing measurements to the angular navigation variables, as stated in Proposition 4,

$$\theta_D - \gamma_D = \theta - \gamma \tag{3.25}$$

Eq. (3.25) makes INS-aiding using bearings-only measurements of a ground object, possible. The development in this section constitutes the proofs of Theorem 1 and Proposition 4 for the simplified two dimensional case.

□

For the INS-aiding analysis in this research, we synthetically generate a measurement which is formed based on the two dimensional measurement geometry shown in Fig 3.2. The plane **P** is a vertical plane and we are exclusively concerned with the measurement of $\alpha'$. In the general three dimensional case, the two angles which define the optical tracker's initial LOS relative to the aircraft body axes are available. Moreover, a stand-alone estimate of the direction cosines of the angles included between the aircraft's velocity vector and the LOS to the point $P$, viz., an estimate of $\gamma_D$, and an estimate of $\vec{\omega}_1$, which yields the tilt angle of the plane **P**, are obtained. This then allows us to calculate the two "aero-

dynamic" angles of the aircraft, $\alpha'$ and $\beta'$. Thus, in the general three dimensional case, the two independent and stand alone estimates obtainable from the optical tracker are the aircraft's aerodynamic angles $\alpha'$ and $\beta'$, i.e., two new measurement equations are obtained. However, a cautionary note is in order: The said angles are the aircraft aerodynamic angles provided the air mass is stationary, i.e., there is no wind. At the same time, an independent aerodynamic measurement of the aerodynamic angles $\alpha$ and $\beta$ provided by the Air Data Computer could be used in conjunction with the optical tracker - provided measurements $\alpha'$ and $\beta'$, to estimate the prevailing wind vector.

More importantly, the measurements $\alpha'$ and $\beta'$ are related to the aircraft's angular navigation variables $\theta$, $\psi$, $\phi$, $\gamma$ and $H$, which afford INS aiding. Evidently, the instrument cannot be used during flight at night, over water, and flight over cloud cover.

## *3.4 Summary*

Based on two dimensional measurement scenario given by Fig 3.2, we produce the methodology to be used in INS aiding by optically tracking an unknown ground object. In particular, by taking a number of LOS angle measurements, we derive a linear regression in A/C position in local reference frame $x$ and $y$, and the inertial velocity vector $V$. This linear regression yields two homogeneous equation in $V$ so that we can calculate the estimation of two angles: the angle between A/C flight path and initial LOS vector, $\gamma_D$; and the angle between A/C body axis $x_b$ and initial LOS vector, $\theta_D$. Finally, we drive the INS aiding equation including $\gamma_D$ and $\theta_D$ estimates.

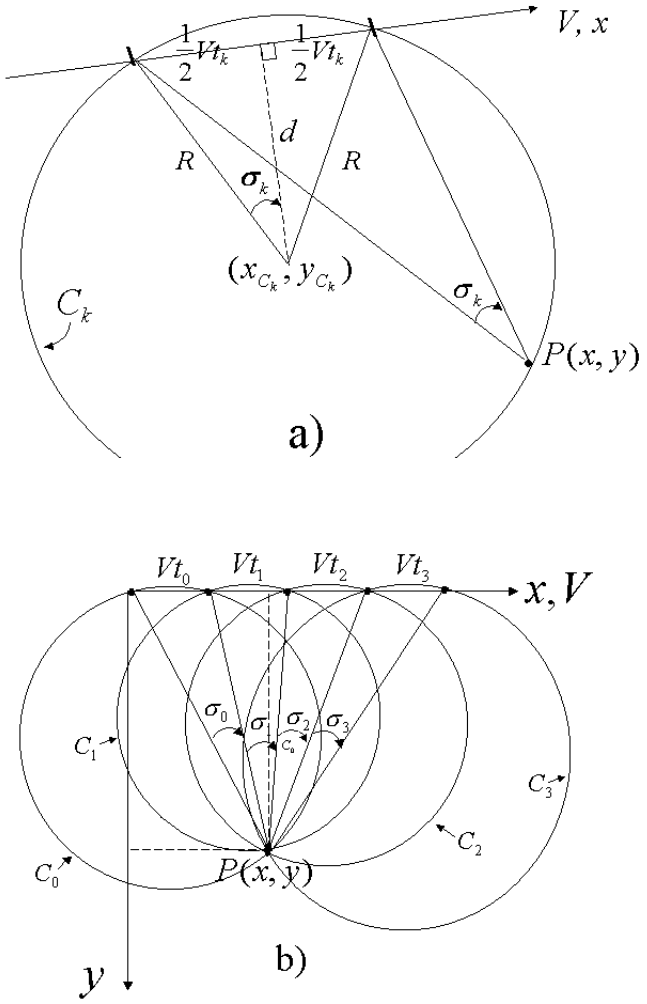


Figure 3.3 Geometry of bearings-only measurements - a) k th circle, b) Four circles (N=3)

# IV. Results and Analysis

## 4.1 Development of Optimal Measurement Geometry

The objective here is to find the optimal geometry for the estimation of $\gamma_D$ using noise corrupted LOS measurements. The measurement equation is given by

$$\sigma_{i_m} = \sigma_i + v_{1_i}, \qquad i = 0, 1, ..., N-1 \tag{4.1}$$

where $\sigma_i$ is the i th relative bearing measurement taken at time $T_i$, and $v_{1_i}$ is white Gaussian noise with the statistics

$$v_{1_i} = \mathcal{N}(0, \sigma_{v_1}^2), \qquad \sigma_{v_1} = 5 \times 10^{-4} \ [rad.] \tag{4.2}$$

The noise corrupted bearing measurements are used in the regressor H in Eq. (3.11), and the SVD of the regressor H provides the optimal "gains" $K_x$ and $K_y$ which yield $\gamma_D$, the angle included between the first LOS vector and the aircraft velocity vector. All computational details are presented in Equations (3.2) through (3.20).

Based on the measurement arrangement shown in Fig 3.2, numerical experiments are performed and the optimal measurement geometry, which yields the smallest estimation error, is obtained.

### 4.1.1 Optimal Geometry Experiments.

The optimal measurement geometry is attained when the estimation error is small, i.e., the difference between the true (no-noise) and the estimated $\gamma_D$ is minimal. Although, in reality, the position of the ground object is not known, we create a synthetic simulation scenario in which the position of the ground object is known, and generate the bearing measurements. The latter are corrupted by measurement noise according to Eq. (4.1). The accuracy of the derived geo-location of the ground object, and the $\gamma_D$ estimation error, are indicative of the quality of the achievable estimation performance. The number of measurements, N, and the total tracking time T, are also considered since the pilot may not be able, in a high risk and

dynamic environment, to keep the aforementioned navigation variables constant for long during the "navigation run". The results of the experiments are based on 1000 Monte Carlo runs and the statistics are summarized in Table 4.1.

Table 4.1 Measurement geometry summary.

| | SCENARIOS | | | | | | | |
|---|---|---|---|---|---|---|---|---|
| | 1 | 2 | 3 | 4 | 5 | 6 | 7 | 8 |
| alt [m] | 7000 | 3300 | 1000 | 300 | 300 | 300 | 300 | 300 |
| $\gamma$ [!deg] | -20 | -10 | -5 | 0 | 0 | 0 | 0 | 0 |
| $\gamma_D$ [rad] | 0.7024 | 0.5151 | 0.2798 | 0.1746 | 0.6423 | 0.3490 | 0.3490 | 0.3490 |
| $t_i$ [sec] | 1 | 1 | 1 | 1 | 0.5 | 0.5 | 0.5 | 0.5 |
| N | 10 | 10 | 10 | 10 | 5 | 5 | 10 | 5 |
| $T_N$ | 11 | 11 | 11 | 11 | 3 | 3 | 5.5 | 4.9 |
| $\hat{e}_{X_p}$ [m] | 2741.25 | 895.11 | 18.57 | 0.56 | 0.03 | 1.97 | 0.125 | 0.008 |
| $\hat{e}_{Y_p}$ [m] | -5798.1 | -898.9 | -9.93 | -0.209 | -0.06 | -1.02 | -1.03 | -0.017 |
| $\hat{\sigma}_{X_p}$ [m] | 390.16 | 442.16 | 50.18 | 4.24 | 0.47 | 18.66 | 1.28 | 0.74 |
| $\hat{\sigma}_{Y_p}$ [m] | 819.98 | 448.4 | 28.0 | 1.7 | 0.93 | 10.22 | 1.1 | 0.94 |
| $\bar{e}_{\gamma_D}$ [rad] | 3.14e-2 | 4.595e-3 | 2.928e-4 | 5.771e-5 | 3.210e-5 | 1.188e-4 | 4.298e-5 | 1.397e-5 |
| $\sigma_{\gamma_D}$ [rad] | 6.120e-2 | 1.889e-2 | 2.932e-3 | 5.474e-4 | 9.548e-4 | 3.720e-3 | 6.844e-4 | 7.21e-4 |

In the first scenario, Fig 4.1-1, the initial altitude is 7000 meters ($\approx$ 21000 feet) with a 20° angle of descent, and 10 bearing measurements are taken. The sampling interval is 1 sec. The velocity is 200 m/sec (0.6 M) and assumed constant. This entails a total tracking time of 11 sec. This initial scenario provides a poor geo-location solution, and an inaccurate $\gamma_D$ estimate. The uncertainty in the bearing measurements is half a milli-radian (mrad), however, the error in $\gamma_D$ is approximately 30 mrad.

To improve the estimation performance in the second scenario, the altitude is decreased to 3300 meters, as shown in Fig 4.1-2. Again, the number of measurements taken is 10. The results are poor.

In the third scenario, the altitude is 1000 meters ($\approx$ 3000 feet) with a 5° angle of descent. As shown in Fig 4.2-1, the values of the relative bearing measurements are larger than in the previous experiments, i.e., the Signal to Noise ratio (SNR) increased; thus, we expect to obtain better geo-location and estimation performance. The results in Table 4.1, however, are not as expected. A 30 mrad error in $\gamma_D$ is unacceptable for the $\frac{1}{2}$ mrad level

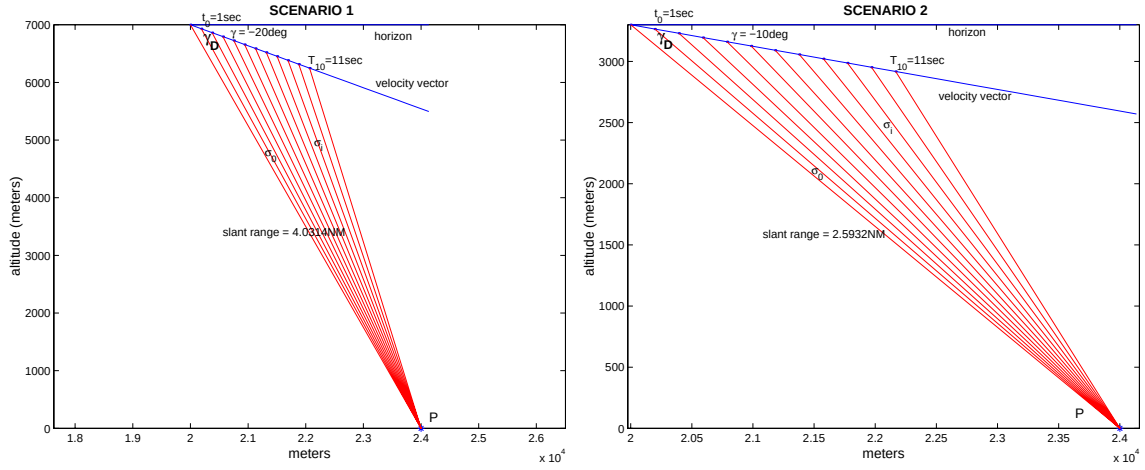


Figure 4.1 Measurement geometry for scenarios 1 and 2

of measurement noise. The basic reason for this error is slant range. 1.4 NM slant range results in a very small value of LOS angles in which measurement noise is high enough to corrupt this measurement and to decrease the SNR.

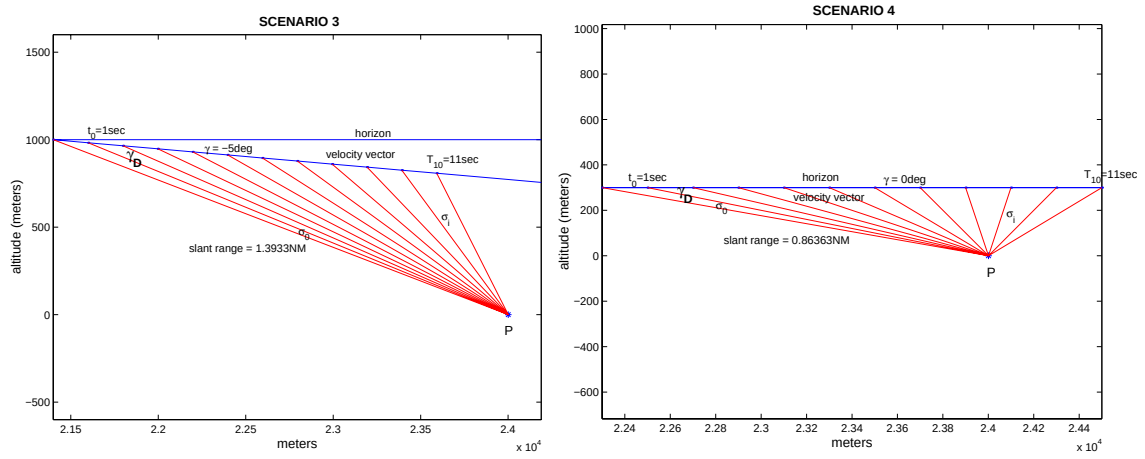


Figure 4.2 Measurement geometry for scenarios 3 and 4

The fourth scenario entails low altitude flight. In this scenario, $Y_0$, the initial altitude, is chosen 300 meters ($\approx$ 1000 feet). Fig 4.2-2 shows the geometry of this measurement situation. Actually, in this scenario, we conclude that the improvement in the estimations results from overflying the ground object; by so doing, we experience the largest rate of change of the LOS (the "$\sigma_i$'s" increase), which yields a higher SNR and, in return, better performance. However, the initial small values of $\sigma_i$ resulting from the long range tracking

geometry cause a higher error in the $\gamma_D$ estimate. Thus, taking the measurements at close range will improve the estimation accuracy, since the value of the experimental $\sigma_i$ will increase, and the measurement noise becomes less important. This geometry can be obtained in a low altitude scenario and when tracking close objects.

In the fifth scenario, the effect of tracking at close range with fewer measurements is addressed. The measurement geometry in Fig 4.3-1 provides the best performance for both geo-location and $\gamma_D$ estimation. Besides, a 3 seconds tracking time is the result of a faster sampling rate of $t_0 = 0.5$ sec., and is almost perfect for all tactical scenarios. The

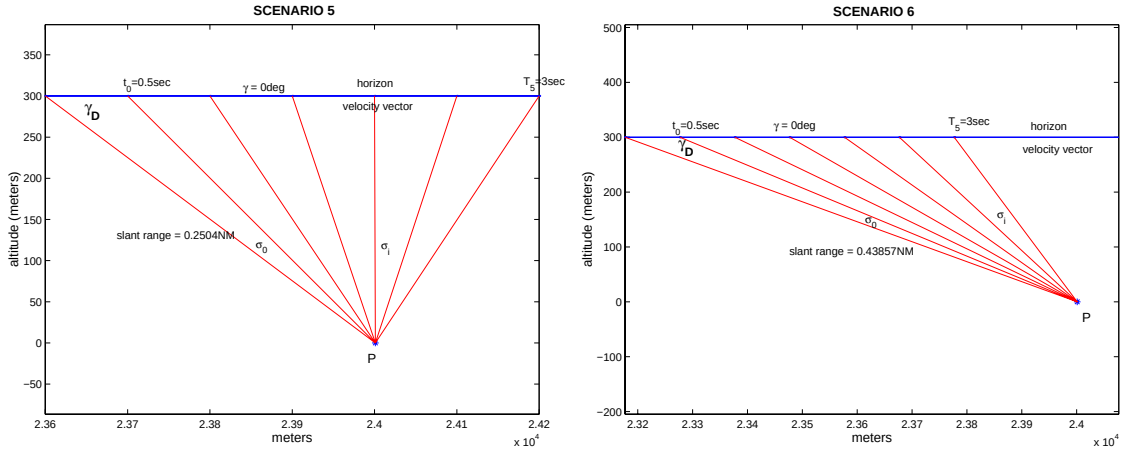


Figure 4.3 Measurement geometry for scenarios 5 and 6

experiments so far allow us to conclude that low altitude flight, below 1000 feet, 3 seconds of tracking time and, overflying the target, give the optimal measurement geometry. This is the theoretical solution to the problem at hand; however, practical considerations impose a constraint on the measurement situation. The constraint on the measurement geometry is shown in Fig 4.4. The LOS depression angle is limited in front of a fighter aircraft. For example, in an F-16 class A/C cockpit, the LOS angle of depression is limited to approximately 17°. Thus, since visual acquisition is needed, the pilot must initiate the measurement before the ground object disappears below the nose of the aircraft. This implies that $X_0$ is not chosen at will; its value varies based on the altitude according to

Eq. (4.3) and the last point to initiate a track is determined by this formula.

$$X_0 = X_P - \frac{Y_0 - Y_P}{tan(17° - \gamma)} \tag{4.3}$$

We also know that, for better accuracy in the $\gamma_D$ estimate, a minimal slant range is desired; and the lower the altitude, the lower the slant range to the object.

We handle this constraint in two ways: First, by using the FLIR in conjunction with the DLIR, as in F-117 A/C, the above discussed visibility constraint is removed , in which case the optimal measurement scenario 5 of Fig 4.3-1 is applicable. Second, the measurement scenario is accordingly revised taking this constraint into account, and a more robust technique is used as discussed in the following experiments.

In the sixth experiment, the scenario 5 is repeated, but this time, the range to the ground object when tracking is initiated is determined according to Eq. (4.3). In scenario 5, tracking has been initiated when the slant range to the ground object was approximately 0.25 NM; but this time, the 17° LOS depression constraint yields a slant range of approximately 0.44 NM. It means that now, the $\sigma_i$'s will have smaller values than in the previously investigated geometries, so that the SNR of the measurements is reduced.

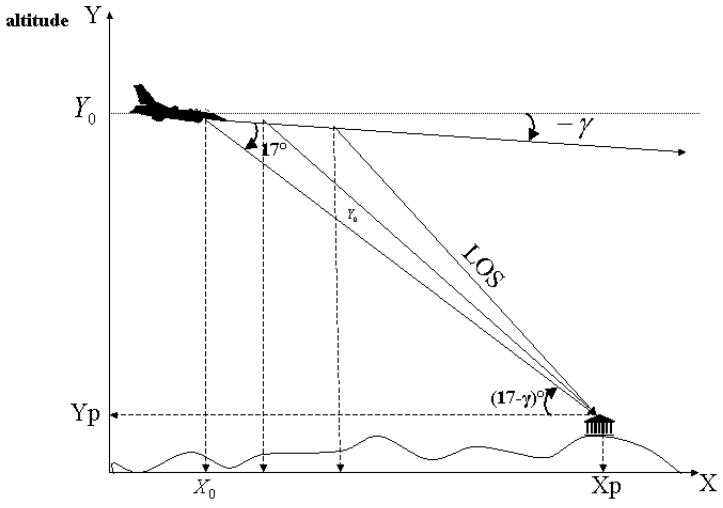


Figure 4.4 The pilot's LOS is 17° from the ±30° of a fighter aircraft (F-16).

The measurement noise $\sigma_v$, we recall, has a variance of 0.5 mrad. Due to the longer range to the ground object, 5 measurements in 3 seconds of tracking time will not be enough to overfly the object, as can be seen in Fig 4.3-2. The statistics given in Table 4.1 show the performance degradation. Two possible solutions to this problem are investigated in the following experiments.

By choosing a high enough number of measurements, the accuracy can be improved; but this geometry requires calculations with different numbers of measurements, based on the altitude and initial tracking distance. Scenario 7 in Fig 4.5-1 entails a measurement geometry with 10 bearing measurements during the 5.5 sec. tracking period. The statistics in Table 4.1 indicate an improvement, but it could have better accuracy. The other solution

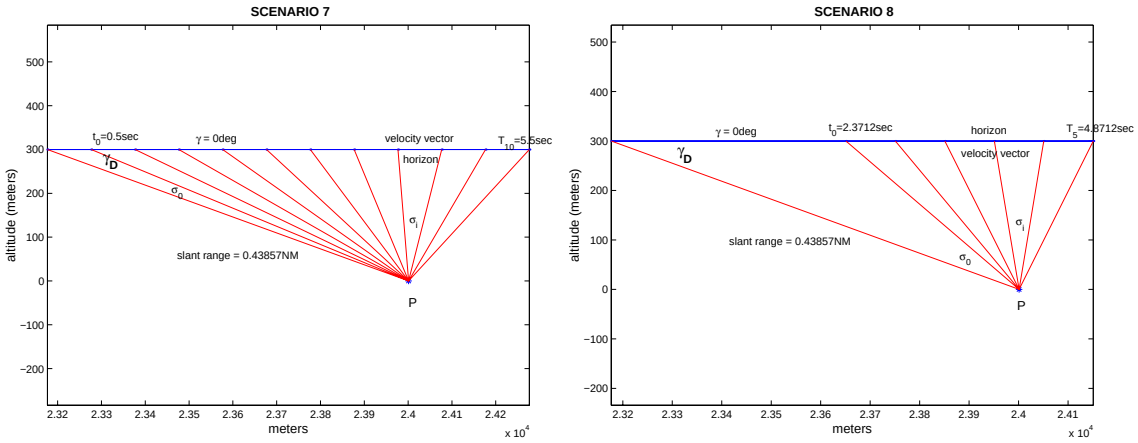


Figure 4.5 Measurement geometry for scenarios 7 and 8

to alleviate the visibility constraint's negative effect is to choose a longer $t_0$. This means that the pilot is going to initiate the tracking at long range, but the automated tracker is going to continue to take measurements when the aircraft is close enough to the ground object to overfly it. In the 8th experiment this measurement scenario is investigated. The statistical results of Scenario 8 show that the geometry in Fig 4.5-2 yields the minimum error and the best geo-location performance. Furthermore, the automated track initialization is not dependent on the pilot's track command whose timing may not be predicted, and it provides a robust way of obtaining the required measurements.

In conclusion, the low altitude and low slant range measurement geometries are desirable; however, depending on the altitude, the shortest slant range to the ground object

to be tracked is obtained as the altitude is lowered. To decrease the slant range further to the object, a 5° to 10° descent is suggested. On the other hand, the modified runs in which one waits until the range to the ground object becomes small are preferable. We examined two different geometries. The first one is the theoretically optimal geometry: low altitude (< 1000 feet), descending flight, with a reasonable number of measurements correlated with tracking time, as shown in scenario 5, Fig 4.3-1; the second geometry entails getting close enough to the object by using delayed tracking. In our work, we will use the latter scenario, which is illustrated in Fig 4.5-2. For a robust and more accurate measurement geometry synthesis, the scenario is modified according to the flight altitude and velocity. The modified geometry provides a good estimate of $\gamma_D$ for all reasonable altitudes and velocities; however, a 10° to 20° descent is recommended for high altitude runs. As a rule of thumb, the dive angle should be equal to the flight altitude approximately, e.g., for an initial altitude of 20,000 feet, a 20° dive angle is suggested. On the other hand, high altitude INS updates require long operation times to alleviate the deleterious effects of low SNR caused by long range tracking; at first sight, this may seem unacceptable, but this can be considered a peace-time mission.

## *4.2 Phase 1 - Angular Navigation Variables*

The measurement equation used for INS-aiding is based on the development leading to Eq. (3.25). We define the measurement

$$z = \theta_{D_{meas}} - \gamma_{D_{meas}} \tag{4.4}$$

where

$$\gamma_{D_{meas}} = \gamma_D + v_3, \qquad v_3 = \mathcal{N}(0, \sigma^2_{\gamma_D}) \tag{4.5}$$

Combining Eqs. (3.22), and (3.25)-(4.5) yields the measurement Equation for INS aiding:

$$\begin{aligned} z &= \theta_D + v_2 - \gamma_D - v_3 \\ &= \theta_D - \gamma_D + v_2 - v_3 \\ &= \theta - \gamma + v_6 \end{aligned} \tag{4.6}$$

where

$$v_6 = v_2 - v_3 \tag{4.7}$$

and thus, the measurement noise

$$v_6 = \mathcal{N}(0, \sigma_{\theta_D}^2 + \sigma_{\gamma_D}^2) \tag{4.8}$$

On the other hand, at the time instant of INS updating, the stand-alone INS provides the prior estimates of $\theta$ and $\gamma$, $\hat{\theta}^-$ and $\hat{\gamma}^-$, respectively:

$$\hat{\theta}^- = \theta + v_4 \tag{4.9}$$

$$\hat{\gamma}^- = \gamma + v_5 \tag{4.10}$$

where $v_4$ and $v_5$ are white Gaussian noise with the INS error statistics:

$$v_4 = \mathcal{N}(0, \sigma_\theta^2) \tag{4.11}$$

$$v_5 = \mathcal{N}(0, \sigma_\gamma^2) \tag{4.12}$$

Specifically, we will assume that $\theta$ and $\gamma$ measurement noises are independent so that they are uncorrelated (see Chapter 5, Recommendations) and the INS performance at the update moment to be specified by

$$\sigma_\theta = \frac{1}{8} \text{ deg.} \tag{4.13}$$

$$\sigma_\gamma = \frac{1}{8} \text{ deg.} \tag{4.14}$$

To Eqs. (4.9) and (4.10), one appends the measurement Equation (4.6), thus obtaining a linear regression in $\gamma$ and $\theta$. Hence, we can write the linear regression for INS aiding as follows:

$$\begin{array}{ccccccc} Z & = & H & & X & + & V \\ \begin{bmatrix} \theta^- \\ \gamma^- \\ z \end{bmatrix} & = & \begin{bmatrix} 1 & 0 \\ 0 & 1 \\ 1 & -1 \end{bmatrix} & \begin{bmatrix} \theta \\ \gamma \end{bmatrix} & + & \begin{bmatrix} v_4 \\ v_5 \\ v_6 \end{bmatrix} \end{array} \tag{4.15}$$

Since the value of $\sigma_{v_3}$ changes for each measurement geometry, varying with altitude, velocity, and flight path angle, the 1-$\sigma$ value of $v_3$ is determined using a look-up table whose entries are flight altitude, velocity, and flight path angle.

The linear regression (4.15) is solved using the Weighted Least Squares / Minimum Variance (MV) formulae [5]:

$$\hat{X}^+ = [H^T R^{-1} H]^{-1} H^T R^{-1} Z \tag{4.16}$$

$$P^+ = [H^T R^{-1} H]^{-1} \tag{4.17}$$

where $\hat{X}^+$ is the minimum variance parameter estimate, $P^+$ is the predicted parameter estimation error covariance matrix, and the weighting matrix R is the equation error covariance

$$R = \begin{bmatrix} \sigma_{v_4}^2 & 0 & 0 \\ 0 & \sigma_{v_5}^2 & 0 \\ 0 & 0 & (\sigma_{v_2}^2 + \sigma_{v_3}^2) \end{bmatrix} \tag{4.18}$$

The justification of the off-diagonal terms of the R matrix above being zeros can be shown as the following.

$$R = E\{VV^T\} = \begin{bmatrix} E\{v_4^2\} & E\{v_4 v_5\} & E\{v_4 v_6\} \\ E\{v_5 v_4\} & E\{v_5^2\} & E\{v_5 v_6\} \\ E\{v_6 v_4\} & E\{v_6 v_5\} & E\{v_6^2\} \end{bmatrix} \tag{4.19}$$

Diagonal terms here are equal to the $\sigma^2$ values of the variables. As given in the $R$ matrix however, the off-diagonal terms are zero because of the uncorrelatedness assumption of the white Gaussian noise samples.

$$E\{v_i vj\} = E\{v_i\}E\{v_j\} = 0 \tag{4.20}$$

The solution (4.16) and (4.17) of the linear regression (4.15) yields the improved angular navigational variables estimates $\hat{\theta}$ and $\hat{\gamma}$, thus accomplishing phase 1 of INS aiding.

***4.2.1 Simulation Results.*** After 1000 Monte Carlo (MC) runs and the solution of the linear regression in $\gamma$ and $\theta$, the statistics of the angular navigation variables $\gamma$ and $\theta$ are obtained and are documented in Table 4.2. The statistics given in Table 4.2 are:

The experimentally obtained mean estimation error (bias) in $\theta$ and $\gamma$ (after aiding),

$$\bar{e}_{\hat{\theta}^+} = \frac{1}{N_{MC}} \sum_{i=1}^{N_{MC}} (\hat{\theta}_i^+ - \theta) \tag{4.21}$$

$$\bar{e}_{\hat{\gamma}^+} = \frac{1}{N_{MC}} \sum_{i=1}^{N_{MC}} (\hat{\gamma}_i^+ - \gamma) \tag{4.22}$$

where $\hat{\theta}_i^+$ and $\hat{\gamma}_i^+$ are the respective MV estimates of $\theta$ and $\gamma$ obtained in the $i$-th MC experiment and $N_{MC} = 1000$ is the number of Monte Carlo experiments performed.

The estimation error statistics show the improvement in the angular variables' estimates resulting from INS aiding using bearing-only measurements on a ground object whose position is not known. The experimental validation of the predicted variances of the random estimation errors in $\hat{\theta}^+$ and $\hat{\gamma}^+$ is thoroughly pursued. The "relative errors" in the $\theta$ and $\gamma$ estimates (after aiding) are also recorded;

$$\bar{e}_{rel_{\theta^+}} = \frac{\sum_{i=1}^{N_{MC}} (\theta - \hat{\theta}_i^+)}{N_{MC} \times \hat{\sigma}_{\theta^+}} \tag{4.23}$$

$$\bar{e}_{rel_{\gamma^+}} = \frac{\sum_{i=1}^{N_{MC}} (\gamma - \hat{\gamma}_i^+)}{N_{MC} \times \hat{\sigma}_{\gamma^+}} \tag{4.24}$$

The experimentally obtained $\theta$ and $\gamma$ estimation error standard deviations (after aiding) are

$$\sigma^+_{E_\theta} = \sqrt{\frac{\sum_{i=1}^{1000}(\hat{\theta}^+_i - \theta)^2}{999}} \tag{4.25}$$

$$\sigma^+_{E_\gamma} = \sqrt{\frac{\sum_{i=1}^{1000}(\hat{\gamma}^+_i - \gamma)^2}{999}} \tag{4.26}$$

The predicted 1-$\sigma$ for $\theta$ and $\gamma$ after aiding are given by eq. (4.17), viz.,

$$\hat{\sigma}^+_\theta = \begin{bmatrix} \sqrt{P^+_{11}} & \cdot \\ \cdot & \cdot \end{bmatrix}, \tag{4.27}$$

$$\hat{\sigma}^+_\gamma = \begin{bmatrix} \cdot & \cdot \\ \cdot & \sqrt{P^+_{22}} \end{bmatrix} \tag{4.28}$$

We invariably obtained $\hat{\sigma}^+_\theta \approx \sigma^+_{E_\theta}$ and $\hat{\sigma}^+_\gamma \approx \sigma^+_{E_\gamma}$.

The measured probability of being within a 1-$\sigma$ of the true parameter vector, which is experimentally calculated as: "The number of times out of $N_{MC}$, the estimation error $\vec{x_i}$ satisfies $\vec{x_i}^T P^{-1} \vec{x_i} \leq$ [dimension of $\vec{x_i}$] divided by $N_{MC}$", and where

$$\vec{x_i} = \begin{bmatrix} \hat{\theta}^+_i - \theta \\ \hat{\gamma}^+_i - \gamma \end{bmatrix},$$

is also obtained. The theoretical probability of the two dimensional $\binom{\theta}{\gamma}$ parameter vector estimate being within a 1-$\sigma$ of the true parameter is $P_{1-\sigma} = 1 - \frac{1}{\sqrt{e}}$. The derivation is given in Appendix B.

It is surprising to learn that the 1-$\sigma$ probability for a bivariate Gaussian distribution in Euclidian space is calculated as $1 - \frac{1}{\sqrt{e}}$, and it is constant, and does not depend on the covariance matrix. Table 4.2 also includes the 1-$\sigma$ experimentally obtained probabilities for each flight condition. The experimentally obtained 1-$\sigma$ probabilities are only slightly higher than the predicted one. Hence, as shown in Table 4.2, the experimentally obtained values of the angular variables' estimation errors variances are very close to, or smaller

Table 4.2 Phase 1 - Statistics of $\gamma$ and $\theta$ estimates.

| h [ft] | 20,000 | | | 10,000 | | | 1000 | | |
|---|---|---|---|---|---|---|---|---|---|
| FC: Mach /$\gamma$ [deg] | 0.5/-20 | 0.8/-20 | 0.8/-10 | 0.5/-10 | 0.8/-10 | 0.8/-5 | 0.5/0 | 0.8/0 | 0.8/-5 |
| $\bar{e}_{\theta^+}$ [$\mu$ rad] | 24.4319 | 186.681 | 24.4338 | 49.7374 | 121.064 | 47.3571 | 11.3141 | 36.0262 | 108.620 |
| $\hat{\sigma}_{\theta^-}$ [mrad] | 2.19945 | 2.26192 | 2.17635 | 2.15509 | 2.15242 | 2.14091 | 2.26658 | 2.20672 | 2.11721 |
| $\hat{\sigma}^+_{E_\theta}$ [mrad] | 2.14255 | 2.08650 | 2.11096 | 1.96755 | 1.96388 | 2.05785 | 1.63193 | 1.70252 | 1.64816 |
| $\hat{\sigma}^+_{\theta}$ [mrad] | 2.12791 | 2.04848 | 2.12371 | 2.03033 | 2.03929 | 2.09850 | 1.62060 | 1.65673 | 1.62256 |
| $\bar{e}_{rel_{\hat{\theta}^+}}$ | 0.80159 | 0.82084 | 0.79620 | 0.78347 | 0.77100 | 0.77790 | 0.80937 | 0.82004 | 0.80369 |
| $\bar{e}_{\gamma^+}$ [$\mu$ rad] | 102.944 | 35.1121 | 16.7998 | 56.3497 | 19.5928 | 125.633 | 3.59614 | 51.4579 | 104.911 |
| $\hat{\sigma}_{\gamma^-}$ [mrad] | 2.16387 | 2.14477 | 2.12758 | 2.17085 | 2.23353 | 2.24532 | 2.13982 | 2.22110 | 2.17513 |
| $\hat{\sigma}^+_{E_\gamma}$[mrad] | 2.10306 | 1.95191 | 2.07291 | 2.01345 | 2.05224 | 2.13204 | 1.59245 | 1.67729 | 1.67214 |
| $\hat{\sigma}^+_{\gamma}$ [mrad] | 2.12791 | 2.04848 | 2.12371 | 2.03033 | 2.03929 | 2.09850 | 1.62060 | 1.65673 | 1.62256 |
| $\bar{e}_{rel_{\hat{\gamma}^+}}$ | 0.79234 | 0.74841 | 0.77592 | 0.80284 | 0.79595 | 0.80693 | 0.78604 | 0.80057 | 0.81873 |
| Experimental 1-$\sigma$ prob. | 39.6 | 41.4 | 40.4 | 39.2 | 41.3 | 39.4 | 39.0 | 36,9 | 36.3 |

| FC: Mach /$\gamma$ [deg] | 0.8 / -20 | | | 0.8 / -10 | | | 0.8 / -5 | | |
|---|---|---|---|---|---|---|---|---|---|
| $\sigma_{v_{\theta_{INS}}}$ & $\sigma_{v_{\gamma_{INS}}}$ [deg.] | 0.125 | 0.25 | 0.5 | 0.125 | 0.25 | 0.5 | 0.125 | 0.25 | 0.5 |
| $\bar{e}_{\theta^+}$ [$\mu$ rad] | 186.681 | 109.808 | 108.938 | 121.064 | 128.924 | 301.656 | 108.620 | 27.9252 | 90.7936 |
| $\hat{\sigma}_{\theta^-}$ [mrad] | 2.26192 | 4.14329 | 8.74514 | 2.15242 | 4.33003 | 8.78011 | 2.11721 | 4.37695 | 8.82962 |
| $\hat{\sigma}^+_{E_\theta}$ [mrad] | 2.08650 | 3.36806 | 6.55585 | 1.96388 | 3.64329 | 6.33120 | 1.64816 | 3.25077 | 6.19276 |
| $\hat{\sigma}^+_{\theta}$ [mrad] | 2.04848 | 3.56449 | 6.67755 | 2.03929 | 3.80758 | 6.81669 | 1.62256 | 3.12966 | 6.19370 |
| $\bar{e}_{rel_{\hat{\theta}^+}}$ | 0.82084 | 0.74977 | 0.78434 | 0.77100 | 0.76944 | 0.73714 | 0.80369 | 0.82219 | 0.79589 |
| $\bar{e}_{\gamma^+}$ [$\mu$ rad] | 35.1121 | 109.808 | 124.887 | 19.5928 | 112.694 | 363.925 | 104.911 | 2.22143 | 81.2309 |
| $\hat{\sigma}_{\gamma^-}$ [mrad] | 2.14477 | 4.14329 | 9.15095 | 2.23353 | 4.38194 | 8.49471 | 2.17513 | 4.56167 | 8.60954 |
| $\hat{\sigma}^+_{E_\gamma}$[mrad] | 1.95191 | 3.36806 | 6.64704 | 2.05224 | 3.65157 | 6.34829 | 1.67214 | 3.25519 | 6.26932 |
| $\hat{\sigma}^+_{\gamma}$ [mrad] | 2.04848 | 3.56449 | 6.67755 | 2.03929 | 3.80758 | 6.81669 | 1.62256 | 3.12966 | 6.19370 |
| $\bar{e}_{rel_{\hat{\gamma}^+}}$ | 0.74841 | 0.78784 | 0.79095 | 0.79595 | 0.76665 | 0.75319 | 0.81873 | 0.82987 | 0.80200 |
| Experimental 1-$\sigma$ prob. | 41.4 | 41.2 | 46.3 | 41.3 | 43.5 | 50.2 | 36.3 | 34.2 | 35.9 |

than the predicted variances. This means that the estimation algorithm works and filter divergence is avoided.

It is noteworthy that at the completion of Phase 1, the angular navigational variables are exclusively updated. While, at this point in time, the enhancement of the accuracy of the aircraft's attitude measurement does not directly translate into an improvement in the aircraft's position estimate, accurate attitude information is crucial in modern sensor-rich platforms for e.g., laser beam pointing.

## *4.3 Phase 2 - Positional Navigational Variables*

In Phase 1, we have exclusively addressed the angular navigation variables, and we updated the estimates of $\theta$ and $\gamma$ using optically acquired bearings-only measurements. We obtained the improved angular navigation variables' estimates $\hat{\theta}^+$ and $\hat{\gamma}^+$. In order to update the positional variables, we need to include additional measurements.

In Phase 2, we derive two different algorithms to update the INS positional variables. The first one derived in Sect. 4.3.1 is a standard linear regression using Phase 1 results and A/C position and velocity estimates from the INS. For the second algorithm given in Sect. 4.3.2, we use the A/C velocity information and the slant range to the ground object, which is obtained by using $x$ and $y$ estimates of Phase 1, to obtain a linear regression. The latter comes as a singular linear regression.

We simulate 6 different measurement scenarios for each algorithm to investigate the estimation performances. **Sit** represents the "measurement situations" for the scenarios simulated for standard linear regression. Similarly, **Scn** represents the "measurement scenarios" for the scenarios simulated for singular linear regression. Definition of each measurement situation and scenario is given in Table 4.3. This table explains the included measurements and the estimation variables in corresponding simulations. Derivation of the **Sit**s and **Scn**s are given in the Sects.4.3.1 and 4.3.2.

The statistics of the noise terms used in the measurement equations during the derivation of measurement situations and scenarios are chosen using the knowledge of myself as a pilot. Furthermore, the variable are assumed "uncorrelated"; thus, by a similar

calculation to Eq. (4.20), the off-diagonal terms for all the equation error covariance matrices become zeros.

Table 4.3 Definition of each measurement situation and scenario.

| $\hat{\theta}_{Sit}$ | Situations | Included Measurements | Scenarios | $\hat{\theta}_{Scn}$ |
|---|---|---|---|---|
| $\hat{x}, \hat{y}, \hat{V}$ | Sit 1 | $\sigma_i$ only | Scn 1 | $\hat{V}, \hat{R}, \hat{X}_0, \hat{Y}_0, \hat{X}_P, \hat{Y}_P$ |
| $\hat{x}, \hat{y}, \hat{V}, \hat{X}_0, \hat{Y}_0, \hat{X}_P$ | Sit 2 | $\sigma_i + Y_P^-$ | Scn 2 | $\hat{V}, \hat{R}, \hat{X}_0, \hat{Y}_0, \hat{X}_P, \hat{Y}_P$ |
| $\hat{x}, \hat{y}, \hat{V}$ | Sit 3 | $\sigma_i + R_m$ | Scn 3 | $\hat{V}, \hat{R}, \hat{X}_0, \hat{Y}_0, \hat{X}_P, \hat{Y}_P$ |
| $\hat{x}, \hat{y}, \hat{V}, \hat{X}_0, \hat{Y}_0, \hat{X}_P$ | Sit 4 | $\sigma_i + Y_P^- + R_m$ | Scn 4 | $\hat{V}, \hat{R}, \hat{X}_0, \hat{Y}_0, \hat{X}_P, \hat{Y}_P$ |
| $\hat{x}, \hat{y}, \hat{V}, \hat{X}_0, \hat{Y}_0, \hat{X}_P$ | Sit 5 | $\sigma_i + Y_P^- + X_P^-$ | Scn 5 | $\hat{V}, \hat{R}, \hat{X}_0, \hat{Y}_0, \hat{X}_P, \hat{Y}_P$ |
| $\hat{x}, \hat{y}, \hat{V}, \hat{X}_0, \hat{Y}_0, \hat{X}_P$ | Sit 6 | $\sigma_i + Y_P^- + X_P^- + R_m$ | Scn 6 | $\hat{V}, \hat{R}, \hat{X}_0, \hat{Y}_0, \hat{X}_P, \hat{Y}_P$ |

***4.3.1 Standard Linear Regression.*** First, we incorporate own-ship position and velocity measurements and solve a linear regression in $x$, $y$, $V$, $X_0$, $Y_0$: Our point of departure is Eq. (3.19), relating the principal variables $x$, $y$, *and* $V$:

$$x = K_x V$$

$$y = K_y V$$

where $K_x$ and $K_y$ are relatively "clean"; recall that they are the output of the SVD algorithm's application to the noise corrupted regressor H.

From the INS, we also have the own ship speed measurement $V_m$, i.e.,

$$V_m = V + v_V \tag{4.29}$$

where the measurement error

$$v_V = \mathcal{N}(0, \sigma_V^2)$$

Thus, we form the linear regression in the principal variables $x,\ y,\ and\ V$:

$$\begin{matrix} Z & = & H & & X & + & V \end{matrix}$$
$$\begin{bmatrix} 0 \\ 0 \\ V_m \end{bmatrix} = \begin{bmatrix} 1 & 0 & -K_x \\ 0 & 1 & -K_y \\ 0 & 0 & 1 \end{bmatrix} \begin{bmatrix} x \\ y \\ V \end{bmatrix} + \begin{bmatrix} v_x \\ v_y \\ v_V \end{bmatrix} \tag{4.30}$$

The equation error covariance matrix is

$$R_{3\times 3} = \begin{bmatrix} P_{x,y}(1,1) & P_{x,y}(1,2) & 0 \\ P_{x,y}(2,1) & P_{x,y}(2,2) & 0 \\ 0 & 0 & \sigma_V^2 \end{bmatrix} \tag{4.31}$$

where

$$E\{v_V^2\} = \sigma_V^2$$
$$\sigma_V = 2.5\ \ ft/sec. \tag{4.32}$$

and

$$P_{x,y} = E\left\{ \begin{bmatrix} v_x \\ v_y \end{bmatrix} \begin{bmatrix} v_x & v_y \end{bmatrix} \right\} \tag{4.33}$$

$P_{x,y}$ is synthetically obtained as follows.

For each specified scenario, in Phase 1, we perform a MC experiment to obtain the statistics of the errors in $x$ and $y$. Thus, assuming $V$ is known, we estimate $\hat{x}_i$ and $\hat{y}_i$, $i = 1, 2, ..., N$. $N = 1000$, and according to the Eq. (4.33), we experimentally obtain the $2 \times 2$ covariance matrix $P_{x,y}$ which renders the statistics of the $x$ and $y$ estimation errors.

Using the MV formulae, (4.16) and (4.17), we calculate the principal variables' statistics

$$\begin{bmatrix} x \\ y \\ V \end{bmatrix} = \mathcal{N}( \begin{bmatrix} \hat{x} \\ \hat{y} \\ \hat{V} \end{bmatrix}, P) \tag{4.34}$$

where

$$\begin{bmatrix} \hat{x} \\ \hat{y} \\ \hat{V} \end{bmatrix} = (H^T R^{-1} H)^{-1} H^T R^{-1} Z \tag{4.35}$$

and

$$P = (H^T R^{-1} H)^{-1} \tag{4.36}$$

From the INS, two additional measurements related to own ship position are obtained

$$X_{0_m} = X_0 + v_{X_0} \tag{4.37}$$

$$Y_{0_m} = Y_0 + v_{Y_0} \tag{4.38}$$

where

$$E(v_{X_0}^2) = \sigma_{X_0}^2 \tag{4.39}$$

and we assume, at INS update time,

$$\sigma_{X_0} = 0.8 \ [nm] \tag{4.40}$$

and

$$\begin{aligned} E(v_{Y_0}^2) &= \sigma_{Y_0}^2 \\ \sigma_{Y_0} &= 75 \ [ft] \end{aligned} \tag{4.41}$$

so that the covariance matrix $P_{X_0,Y_0}$

$$P_{X_0,Y_0} = \begin{bmatrix} \sigma^2_{X_0} & 0 \\ 0 & \sigma^2_{Y_0} \end{bmatrix} \tag{4.42}$$

***Inclusion of Additional Positional Variables:*** $\gamma$***,*** $X_0$***,*** $Y_0$***,*** $X_P$***, and*** $Y_P$ **.** We replace $\gamma$ in the coordinate transformation Eqs. (3.1)

$$\begin{aligned} X_P &= xcos\gamma + ysin\gamma + X_0 \\ Y_P &= xsin\gamma - ycos\gamma + Y_0 \end{aligned}$$

with the estimate from Phase 1, $\hat{\gamma}$, where

$$\hat{\gamma} = \gamma + v_\gamma \tag{4.43}$$

and

$$\begin{aligned} v_\gamma &= \mathcal{N}(0, \sigma^2_\gamma) \\ \sigma^2_\gamma &= P^+_{2,2} \end{aligned} \tag{4.44}$$

We apply the small angle approximation and we obtain

$$X_P = cos\hat{\gamma}\ \ x + sin\hat{\gamma}\ \ y + X_0 + (Y^-_P - Y^-_0)v_\gamma \tag{4.45}$$

$$Y_P = sin\hat{\gamma}\ \ x - cos\hat{\gamma}\ \ y + Y_0 + (X^-_0 - X^-_P)v_\gamma \tag{4.46}$$

Hence, from now on, we have 5 positional variables: $(x, y, V, X_0, Y_0) \in \mathcal{R}^5$. The linear regression is

$$\begin{bmatrix} 0 \\ 0 \\ V_m \\ \cdots \\ X_{0_m} \\ Y_{0_m} \end{bmatrix} = \begin{bmatrix} 1 & 0 & -K_x & : & 0 & 0 \\ 0 & 1 & -K_y & : & 0 & 0 \\ 0 & 0 & 1 & : & 0 & 0 \\ \cdots & \cdots & \cdots & \cdots & \cdots & \cdots \\ 0 & 0 & 0 & : & 1 & 0 \\ 0 & 0 & 0 & : & 0 & 1 \end{bmatrix} \begin{bmatrix} x \\ y \\ V \\ \cdots \\ X_0 \\ Y_0 \end{bmatrix} + \begin{bmatrix} v_x \\ v_y \\ v_V \\ \cdots \\ v_{X_0} \\ v_{Y_0} \end{bmatrix} \tag{4.47}$$

and

$$R = \begin{bmatrix} P_{x,y}(1,1) & P_{x,y}(1,2) & 0 & : & 0 & 0 \\ P_{x,y}(2,1) & P_{x,y}(2,2) & 0 & : & 0 & 0 \\ 0 & 0 & \sigma_V^2 & : & 0 & 0 \\ \cdots & \cdots & \cdots & \cdots & \cdots & \cdots \\ 0 & 0 & 0 & : & \sigma_{X_0}^2 & 0 \\ 0 & 0 & 0 & : & 0 & \sigma_{Y_0}^2 \end{bmatrix} \tag{4.48}$$

It is important to note that now the parameter vector does not include the two angular navigation variables $\theta$ and $\gamma$ which have been previously estimated. The angular variables were estimated in Phase 1, and now are used in Phase 2. The positional variables are estimated in Phase 2. Thus, we have separated the angular and positional navigation variables' estimation.

Moreover, the linear regression (4.47)-(4.48), has a blocked structure. Thus, without solving the linear regression, we can directly state

$$X_0 = \mathcal{N}(X_{0_m}, \sigma_{X_0}^2) \tag{4.49}$$

$$Y_0 = \mathcal{N}(Y_{0_m}, \sigma_{Y_0}^2) \tag{4.50}$$

i.e.,

$$\hat{X}_0 = X_{0_m} \tag{4.51}$$

$$\hat{Y}_0 = Y_{0_m} \tag{4.52}$$

The MV solution to the upper left $3\times3$ linear regression block yields the estimate of $\hat{x}, \hat{y}, \hat{V}$ to be used in the geo-location of the unknown point P.

***Measurement Situation 1 - Geo-Location Using Optical Bearings-Only Measurements.*** Replacing $x$ and $y$ with the estimate $\hat{x}$ and $\hat{y}$ in the Eqs. (4.45) and (4.46), we perform the geo-location of the point P.

$$\begin{aligned} X_P &= cos\hat{\gamma}\ \hat{x} + sin\hat{\gamma}\ \hat{y} + \hat{X}_0 \\ Y_P &= sin\hat{\gamma}\ \hat{x} - cos\hat{\gamma}\ \hat{y} + \hat{Y}_0 \end{aligned} \tag{4.53}$$

In this calculation, we set

$$\hat{X}_0 = X_{0_m}, \qquad \hat{Y}_0 = Y_{0_m}$$

#### *4.3.1.1 Inclusion of Ground Object Position Information.*

Assuming that the ground object is at a "known" location, two additional position "measurements" may be generated:

$$X_{p_m} = X_P + v_{X_P} \tag{4.54}$$

$$Y_{p_m} = Y_P + v_{Y_P} \tag{4.55}$$

The prior information in Eqs. (4.54) and (4.55) is included in the linear regression and we augment the parameter vector, thus forming the complete 7 element parameter vector of positional variables

$$\begin{pmatrix} x & y & V & X_0 & Y_0 & X_P & Y_P \end{pmatrix} \in \mathcal{R}^7$$

Backing out $v_\gamma$ from Eq. (4.45) and then inserting it into Eq. (4.46), we obtain

$$X_P = \frac{\hat{x}^-}{X_P^- - X_0^-}x + \frac{\hat{y}^-}{X_P^- - X_0^-}y + X_0 + \frac{Y_P^- - Y_0^-}{X_P^- - X_0^-}Y_0 - \frac{Y_P^- - Y_0^-}{X_P^- - X_0^-}Y_P \tag{4.56}$$

where

$$\hat{x}^- \equiv (X_P^- - X_0^-)cos\hat{\gamma} + (Y_P^- - Y_0^-)sin\hat{\gamma} \tag{4.57}$$

$$\hat{y}^- \equiv (X_P^- - X_0^-)sin\hat{\gamma} - (Y_P^- - Y_0^-)cos\hat{\gamma} \tag{4.58}$$

Next, we insert Eq. (4.56) into Eq. (4.54) and obtain

$$X_{P_m} = \frac{\hat{x}^-}{X_P^- - X_0^-}x + \frac{\hat{y}^-}{X_P^- - X_0^-}y + X_0 + \frac{Y_P^- - Y_0^-}{X_P^- - X_0^-}Y_0 - \frac{Y_P^- - Y_0^-}{X_P^- - X_0^-}Y_P + v_{X_P} \tag{4.59}$$

and we back out $Y_P$, obtaining

$$Y_P = \frac{\hat{x}^-}{Y_P^- - Y_0^-}x + \frac{\hat{y}^-}{Y_P^- - Y_0^-}y + Y_0 + \frac{X_P^- - X_0^-}{Y_P^- - Y_0^-}X_0 - \frac{X_P^- - X_0^-}{Y_P^- - Y_0^-}X_P \tag{4.60}$$

Inserting Eq. (4.60) into Eq. (4.55), we obtain

$$Y_{P_m} = \frac{\hat{x}^-}{Y_P^- - Y_0^-}x + \frac{\hat{y}^-}{Y_P^- - Y_0^-}y + Y_0 + \frac{X_P^- - X_0^-}{Y_P^- - Y_0^-}X_0 - \frac{X_P^- - X_0^-}{Y_P^- - Y_0^-}X_P + v_{Y_P} \tag{4.61}$$

#### *4.3.1.2 Measurement Situation 2 - Inclusion of Ground Object Altitude Measurement.*

It is plausible that *a prior* information on the altitude of the ground object is available; or, point P might be at sea-level, i.e., $Y_{p_m} = 0$. Thus, the new "measurement" is included

$$Y_{p_m} = Y_P + v_{Y_P} \tag{4.62}$$

with the measurement error statistics

$$\begin{aligned} E(v_{Y_P}^2) &= \sigma_{Y_P}^2 \\ \sigma_{Y_P} &= 100 \ ft \end{aligned} \tag{4.63}$$

Including this new measurement into the linear regression formulation, we obtain the non-singular linear regression

$$Z = H\theta + V \tag{4.64}$$

where the measurement vector

$$Z = \begin{bmatrix} 0 & 0 & V_m & X_{0_m} & Y_{0_m} & Y_{p_m} \end{bmatrix}^T, \tag{4.65}$$

the regressor

$$H = \begin{bmatrix} 1 & 0 & -K_x & 0 & 0 & 0 \\ 0 & 1 & -K_y & 0 & 0 & 0 \\ 0 & 0 & 1 & 0 & 0 & 0 \\ 0 & 0 & 0 & 1 & 0 & 0 \\ 0 & 0 & 0 & 0 & 1 & 0 \\ \frac{\hat{x}^-}{Y_P^- - Y_0^-} & \frac{\hat{y}^-}{Y_P^- - Y_0^-} & 0 & \frac{X_P^- - X_0^-}{Y_P^- - Y_0^-} & 1 & -\frac{X_P^- - X_0^-}{Y_P^- - Y_0^-} \end{bmatrix}, \tag{4.66}$$

the parameter

$$\theta = \begin{bmatrix} x & y & V & X_0 & Y_0 & X_P \end{bmatrix}^T \tag{4.67}$$

and the equation error

$$V = \begin{bmatrix} v_x & v_y & v_V & v_{X_0} & v_{Y_0} & v_{Y_P} \end{bmatrix}^T \tag{4.68}$$

The coefficients $K_x$ and $K_y$ were estimated in Phase 1, and $\hat{x}^-$ and $\hat{y}^-$ are given in Eqs. (4.57) and (4.58). The equation error's covariance block diagonal R matrix needed in the

MV estimation formulae is

$$R = \begin{bmatrix} P_{x,y}(1,1) & P_{x,y}(1,2) & 0 & 0 & 0 & 0 \\ P_{x,y}(2,1) & P_{x,y}(2,2) & 0 & 0 & 0 & 0 \\ 0 & 0 & \sigma_V^2 & 0 & 0 & 0 \\ 0 & 0 & 0 & \sigma_{X_0}^2 & 0 & 0 \\ 0 & 0 & 0 & 0 & \sigma_{Y_0}^2 & 0 \\ 0 & 0 & 0 & 0 & 0 & \sigma_{Y_P}^2 \end{bmatrix} \tag{4.69}$$

Thus, using the MV estimation formulae (4.16) and (4.17), we obtain the MV parameter estimate $\hat{\theta} = (\hat{x}, \hat{y}, \hat{V}, \hat{X}_0, \hat{Y}_o, \hat{X}_p)$ and the parameter estimation error covariance $P^+$. Next, we revisit Eq. (4.60) for the estimation of $Y_P$ to complete the geo-location. The availability of $Y_P$ information will improve the own-ship position estimate.

***4.3.1.3 Inclusion of Slant Range Measurement.*** We consider an additional scenario where the slant range to the point P, the tracked ground object, is also measured. The measurement equation is

$$R_m = R + v_R \tag{4.70}$$

where $R$ is the true slant range and the measurement error statistics are

$$\begin{aligned} v_R &= \mathcal{N}(0, \sigma_R^2) \\ \sigma_R &= 200 \ \ ft. \end{aligned} \tag{4.71}$$

This measurement is treated as follows.
The non-linear geometric relationship

$$x^2 + y^2 = R^2 \tag{4.72}$$

holds. We use the identities

$$x = \hat{x}^- + (x - \hat{x}^-) \tag{4.73}$$

$$y = \hat{y}^- + (y - \hat{y}^-) \tag{4.74}$$

where $\hat{x}^-$ and $\hat{y}^-$ are the current best estimates of the $x$ and $y$ coordinates of P in the local reference frame. Inserting Eqs. (4.70), (4.73), and (4.74) into Eq. (4.72) yields

$$R_m^2 - 2R_m v_R \approx (\hat{x}^-)^2 + (\hat{y}^-)^2 + 2\hat{x}^-(x - \hat{x}^-) + 2\hat{y}^-(y - \hat{y}^-) \tag{4.75}$$

and thus

$$2\hat{x}^- x + 2\hat{y}^- y - (\hat{x}^-)^2 - (\hat{y}^-)^2 \approx R_m^2 - 2R_m v_R$$

Re-arranging, we obtain

$$\hat{x}^- x + \hat{y}^- y = \frac{1}{2}[R_m^2 + (\hat{x}^-)^2 + (\hat{y}^-)^2] - R_m v_R$$

We define the "measurement"

$$z = \frac{1}{2}[R_m^2 + (\hat{x}^-)^2 + (\hat{y}^-)^2] \tag{4.76}$$

and thus

$$z = \begin{bmatrix} \hat{x}^- & \hat{y}^- \end{bmatrix} \begin{bmatrix} x \\ y \end{bmatrix} + R_m v_R \tag{4.77}$$

This linearized measurement equation can be directly added to any of the previously discussed linear regressions in Sects. 4.3.1.2 and 4.3.1.4.

***Measurement Situation 3 - Bearings-Only Measurements and Slant Range.*** Including the slant range measurement in the linear regression in the

primary variables yields the augmented linear regression

$$\begin{bmatrix} 0 \\ 0 \\ V_m \\ z \end{bmatrix} = \begin{bmatrix} 1 & 0 & -K_x \\ 0 & 1 & -K_y \\ 0 & 0 & 1 \\ \hat{x}^- & \hat{y}^- & 0 \end{bmatrix} \begin{bmatrix} x \\ y \\ V \end{bmatrix} + \begin{bmatrix} v_x \\ v_y \\ v_V \\ R_m v_R \end{bmatrix} \tag{4.78}$$

The equation error covariance matrix is

$$R = \begin{bmatrix} P_{x,y_{11}} & P_{x,y_{12}} & 0 & 0 \\ P_{x,y_{21}} & P_{x,y_{22}} & 0 & 0 \\ 0 & 0 & \sigma_V^2 & 0 \\ 0 & 0 & 0 & R_m^2 \sigma_R^2 \end{bmatrix} \tag{4.79}$$

Obviously, iterations on $x$ and $y$ are required. We will use the initial guesses of

$$\hat{x}_0^- = R_m cos\hat{\gamma}_D, \quad \hat{y}_0^- = R_m sin\hat{\gamma}_D \tag{4.80}$$

***Measurement Situations 4 - Bearings-Only Measurements, Altitude of the Point P and Also Slant Range Measurement is Available.*** The objective here is simultaneously to estimate the A/C position and to geo-locate the point P using passive bearings measurements and a combination of a measurement of the slant range to the point P, and altitude estimate of point P.

Including the slant range measurement in the linear regression equation derived in Phase

2, we obtain the augmented $7 \times 6$ regressor

$$H = \begin{bmatrix} 1 & 0 & -K_x & 0 & 0 & 0 \\ 0 & 1 & -K_y & 0 & 0 & 0 \\ 0 & 0 & 1 & 0 & 0 & 0 \\ 0 & 0 & 0 & 1 & 0 & 0 \\ 0 & 0 & 0 & 0 & 1 & 0 \\ \frac{\hat{x}^-}{Y_P^- - Y_0^-} & \frac{\hat{y}^-}{Y_P^- - Y_0^-} & 0 & \frac{X_P^- - X_0^-}{Y_P^- - Y_0^-} & 1 & -\frac{X_P^- - X_0^-}{Y_P^- - Y_0^-} \\ \hat{x}^- & \hat{y}^- & 0 & 0 & 0 & 0 \end{bmatrix} \tag{4.81}$$

and measurement vector $Z$, parameter vector $\theta$, and measurement noise vector $V$,

$$Z = \begin{bmatrix} 0 \\ 0 \\ V_m \\ X_{0_m} \\ Y_{0_m} \\ Y_{p_m} \\ Sr_m \end{bmatrix}, \quad \theta = \begin{bmatrix} x \\ y \\ V \\ X_0 \\ Y_0 \\ X_P \end{bmatrix}, \quad V = \begin{bmatrix} v_x \\ v_y \\ v_V \\ v_{X_0} \\ v_{Y_0} \\ v_{Y_P} \\ R_m v_R \end{bmatrix} \tag{4.82}$$

respectively. The augmented block diagonal equation error covariance matrix is

$$R = \begin{bmatrix} P_{x,y}(1,1) & P_{x,y}(1,2) & 0 & 0 & 0 & 0 & 0 & \\ P_{x,y}(2,1) & P_{x,y}(2,2) & 0 & 0 & 0 & 0 & 0 & \\ 0 & 0 & \sigma_V^2 & 0 & 0 & 0 & 0 & \\ 0 & 0 & 0 & \sigma_{X_0}^2 & 0 & 0 & 0 & \\ 0 & 0 & 0 & 0 & \sigma_{Y_0}^2 & 0 & 0 & \\ 0 & 0 & 0 & 0 & 0 & \sigma_{Y_P}^2 & 0 & \\ 0 & 0 & 0 & 0 & 0 & 0 & 0 & R_m^2 v_R^2 \end{bmatrix} \tag{4.83}$$

Again, applying the MV estimation formulae, we calculate the minimum variance estimate (4.16) and (4.17),

$$\hat{\theta} = \begin{bmatrix} \hat{x} & \hat{y} & \hat{V} & \hat{X}_0 & \hat{Y}_0 & \hat{X_P} \end{bmatrix}^T \tag{4.84}$$

and the $6 \times 6$ estimation error covariance matrix $P^+$. The geo-location calculation is completed by estimating $Y_P$ via Eq. (4.60).

#### *4.3.1.4 Measurement Situation 5 - Inclusion of the Ground Object X - Coordinate Information.*

We consider a scenario in which the $X_P$ position of the ground object is also available. This leads us into a measurement situation in which complete information on the ground object is assumed "known".

Thus, an additional "measurement"

$$X_{p_m} = X_P + v_{X_P} \tag{4.85}$$

where

$$\begin{aligned} E(v_{X_P}^2) &= \sigma_{X_P}^2 \\ \sigma_{X_P} &= 100 \ ft \end{aligned} \tag{4.86}$$

is included in the linear regression equation (4.64) as the last row.

We obtain the new MV estimate $\hat{\theta} = (\hat{x}, \hat{y}, \hat{V}, \hat{X}_0, \hat{Y}_0, \hat{X}_P)$ and the estimation error covariance $P$ according to Eqs. (4.16) and (4.17) where the equation error covariance matrix R is again block diagonal. The geo-location parameter $Y_P$ is again obtained using Eq. (4.60)

***Measurement Situations 6 - Bearings-Only Measurements, Altitude and Position of the Point P Available, and Also Slant Range Measurement is Available.*** Similar to measurement Scenario 4, using passive bearings measurements and a combination of a measurement of the slant range to the point P, and

either a rough altitude estimate of point P (no measurement), or the position information of the point P, we aim to aid INS for its positional variables and to estimate the position of the ground object.

Including the slant range measurement in the linear regression equation derived in Phase 2, we obtain the augmented $8 \times 6$ regressor

$$H = \begin{bmatrix} 1 & 0 & -K_x & 0 & 0 & 0 \\ 0 & 1 & -K_y & 0 & 0 & 0 \\ 0 & 0 & 1 & 0 & 0 & 0 \\ 0 & 0 & 0 & 1 & 0 & 0 \\ 0 & 0 & 0 & 0 & 1 & 0 \\ \frac{\hat{x}^-}{Y_P^- - Y_0^-} & \frac{\hat{y}^-}{Y_P^- - Y_0^-} & 0 & \frac{X_P^- - X_0^-}{Y_P^- - Y_0^-} & 1 & -\frac{X_P^- - X_0^-}{Y_P^- - Y_0^-} \\ 0 & 0 & 0 & 0 & 0 & 1 \\ \hat{x}^- & \hat{y}^- & 0 & 0 & 0 & 0 \end{bmatrix} \tag{4.87}$$

and measurement vector $Z$, parameter vector $\theta$, and measurement noise vector $V$,

$$Z = \begin{bmatrix} 0 \\ 0 \\ V_m \\ X_{0_m} \\ Y_{0_m} \\ Y_{p_m} \\ X_{P_m} \\ Sr_m \end{bmatrix}, \quad \theta = \begin{bmatrix} x \\ y \\ V \\ X_0 \\ Y_0 \\ X_P \end{bmatrix}, \quad V = \begin{bmatrix} v_x \\ v_y \\ v_V \\ v_{X_0} \\ v_{Y_0} \\ v_{Y_P} \\ v_{X_P} \\ R_m v_R \end{bmatrix} \tag{4.88}$$

respectively. The augmented block diagonal equation error covariance matrix is

$$R = \begin{bmatrix} P_{x,y}(1,1) & P_{x,y}(1,2) & 0 & 0 & 0 & 0 & 0 & 0 \\ P_{x,y}(2,1) & P_{x,y}(2,2) & 0 & 0 & 0 & 0 & 0 & 0 \\ 0 & 0 & \sigma_V^2 & 0 & 0 & 0 & 0 & 0 \\ 0 & 0 & 0 & \sigma_{X_0}^2 & 0 & 0 & 0 & 0 \\ 0 & 0 & 0 & 0 & \sigma_{Y_0}^2 & 0 & 0 & 0 \\ 0 & 0 & 0 & 0 & 0 & \sigma_{Y_P}^2 & 0 & 0 \\ 0 & 0 & 0 & 0 & 0 & 0 & \sigma_{X_P}^2 & 0 \\ 0 & 0 & 0 & 0 & 0 & 0 & 0 & R_m^2 v_R^2 \end{bmatrix} \tag{4.89}$$

Again, applying the MV estimation formulae, we calculate the minimum variance estimate (4.16) and (4.17),

$$\hat{\theta} = \begin{bmatrix} \hat{x} & \hat{y} & \hat{V} & \hat{X_0} & \hat{Y_0} & \hat{X_P} \end{bmatrix}^T \tag{4.90}$$

and the $6 \times 6$ estimation error covariance matrix $P^+$. The geo-location calculation is completed by estimating $Y_P$ via Eq. (4.60).

***4.3.1.5 Simulation Results.*** We perform 5000 of MC experiments on each measurement situation and the results of the experiments are given in the following sections.

***Simulation Results - Measurement Situation 1.*** In Phase 1, no improvement in own-ship position estimate is obtained. Recall that an improvement in own-ship angular variables' estimates was obtained.

At this stage of our work, we have estimated $x$, $y$, and $V$ using bearings-only measurements. In parallel, we have calculated the coordinates of the ground object. The velocity estimation and geo-location, based on the linear regression derived above, are analyzed for variable flight altitude in Table 4.4, and analyzed for varying airspeed in Table 4.5.

It is observed that the velocity estimation performance has a random nature for both altitude and velocity variations. The 1-$\sigma$ error of A/C velocity before aiding (2.5 ft/sec)

Table 4.4 Measurement Situation 1 - Estimation performance for different flight altitudes. The velocity is 0.8 M, the measurement errors during the estimation process are $\sigma_{INS_{\theta\&\gamma}} = \frac{1}{8}$ deg, $\sigma_{INS_V} = 2.5$ ft/sec, $\sigma_{INS_{X_0}} = 0.8$ NM (1481.6 m), and $\sigma_{INS_{Y_0}} = 75$ ft. The predicted 1-$\sigma$ value of the velocity estimate is the same with $\sigma_{V_{INS}}$, 2.5 ft/sec.

| $h$ [ft] | $\hat{\sigma}^+_{E_V}$ [ft/sec] | $\hat{\sigma}^+_{E_{X_P}}$ [m] | $\bar{e}_{\hat{X}^+_P}$ [m] | $\hat{\sigma}^+_{E_{Y_P}}$ [ft] | $\bar{e}_{\hat{X}^+_P}$ [ft] |
|---|---|---|---|---|---|
| 1000 | 2.458 | 1478.11 | 12.11 | 74.52 | 1.27 |
| 3,000 | 2.522 | 1485.72 | 9.28 | 80.81 | 1.09 |
| 6,000 | 2.499 | 1503.41 | 27.97 | 110.13 | 1.78 |
| 10,000 | 2.490 | 1464.62 | 8.26 | 209.55 | 0.66 |
| 15,000 | 2.506 | 1486.04 | 29.76 | 28.88 | 1.38 |
| 20,000 | 2.496 | 1479.03 | 22.46 | 340.02 | 5.46 |

Table 4.5 Measurement Situation 1 - Estimation performance for different airspeeds. The flight altitude is 3,000 feet, and the measurement errors during the estimation process are as in Table 4.4.

| $Vel$ [M] | $\hat{\sigma}^+_{E_V}$ [ft/sec] | $\hat{\sigma}^+_{E_{X_P}}$ [m] | $\bar{e}_{\hat{X}^+_P}$ [m] | $\hat{\sigma}^+_{E_{Y_P}}$ [ft] | $\bar{e}_{\hat{Y}^+_P}$ [ft] |
|---|---|---|---|---|---|
| 0.5 | 2.484 | 1489.08 | 23.02 | 84.64 | 0.35 |
| 0.6 | 2.525 | 1471.16 | 0.46 | 80.92 | 0.91 |
| 0.7 | 2.539 | 1487.41 | 8.84 | 81.33 | 1.31 |
| 0.8 | 2.473 | 1479.82 | 30.59 | 81.68 | 0.05 |
| 0.9 | 2.546 | 1466.30 | 27.54 | 78.40 | 0.33 |
| 1 | 2.523 | 1482.84 | 37.23 | 77.49 | 0.21 |

is unchanged after aiding; that is, there is no significant improvement, the A/C velocity estimate is about the same. Geo-location performance, however, is basically determined by the INS-provided own-ship position estimate. As shown in Tables 4.4 and 4.5, the 1-$\sigma$ values for both $\hat{X}_P$ and $\hat{Y}_P$ are about the 1-$\sigma$ of the A/C $x$ and $y$-position errors. The increase in altitude, and decrease in A/C velocity result in a deterioration in geo-location performance. The latter is a result of the measurement arrangement, as explained in Sect. 4.1.

We conclude that in the Measurement Situation 1 the basic objective of INS position aiding is not met; however, we can perform a geo-location estimation, but it will be accurate as much as the INS-provided own-ship position measurement's accuracy. From this conclusion, we can not suggest this kind of scenario for any application.

***Simulation Results - Measurement Situation 2.*** The result of the simulations are documented in the following tables: Table 4.6 shows the velocity estimation and geo-location performance as a function of flight altitude. Own ship position estimation performance for varying flight altitudes is documented in Table 4.7. The results for various airspeeds, are presented in Tables 4.8 and 4.9.

Table 4.6 Measurement Situation 2 - Estimation performance for different flight altitudes. The A/C's speed is 0.8 M, and the measurement errors during the estimation process are $\sigma_{INS_{\theta\&\gamma}} = \frac{1}{8}$ deg, $\sigma_{INS_V} = 2.5$ ft/sec, $\sigma_{INS_{X_0}} = 0.8$ NM (1481.6 m), and $\sigma_{INS_{Y_0}} = 75$ ft.

| $h$ [ft] | $\hat{\sigma}^+_{E_V}$ [ft/sec] | $\hat{\sigma}^+_{E_{X_P}}$ [m] | $\bar{e}_{\hat{X}^+_P}$ [m] | $\hat{\sigma}^+_{E_{Y_P}}$ [ft] | $\bar{e}_{\hat{Y}^+_P}$ [ft] |
|---|---|---|---|---|---|
| 1000 | 2.485 | 1485.45 | 25.79 | 99.48 | 2.94 |
| 3,000 | 2.550 | 1486.75 | 44.13 | 97.75 | 2.09 |
| 6,000 | 2.521 | 1486.10 | 2.41 | 99.29 | 0.16 |
| 10,000 | 2.505 | 1497.33 | 25.97 | 99.42 | 2.10 |
| 15,000 | 2.490 | 1496.67 | 20.93 | 100.93 | 0.65 |
| 20,000 | 2.525 | 1540.67 | 130.41 | 101.03 | 3.14 |

Table 4.7 Measurement Situation 2 - Own ship position estimation performance for different flight altitudes. The A/C's speed is 0.8 M, and the measurement errors during the estimation process are given in Table 4.6 .

| $h$ [ft] | $\hat{\sigma}^+_{E_{X_0}}$ [m] | $\bar{e}_{\hat{X}^+_0}$ [m] | $\hat{\sigma}^+_{E_{Y_0}}$ [ft] | $\bar{e}_{\hat{Y}^+_0}$ [ft] |
|---|---|---|---|---|
| 1000 | 1485.29 | 27.56 | 75.47 | 0.13 |
| 3,000 | 1486.69 | 43.72 | 74.54 | 0.69 |
| 6,000 | 1485.14 | 2.64 | 74.91 | 0.39 |
| 10,000 | 1495.02 | 23.97 | 74.27 | 1.89 |
| 15,000 | 1479.78 | 3.23 | 75.96 | 0.52 |
| 20,000 | 1465.71 | 43.34 | 75.45 | 0.27 |

At this stage, a general observation concerning velocity estimation performance in all the experiments is in order: Velocity aiding is not significant. The velocity estimates are very close to the values prior to aiding. Geo-location performance depends on the INS provided own ship position information for $\hat{X}_P$, and, for $\hat{Y}_P$ estimation, the quality of the prior information on the altitude of the ground object is crucial. A decrease in geo-location accuracy is observed when the flight level is increased. The effect of airspeed variation on geo-location is random. Own ship position estimates errors, however, are usually close to

Table 4.8 Measurement Situation 2 - Estimation performance for different A/C speeds. The altitude is 3,000 feet, and the measurement errors during the estimation process are $\sigma_{INS_{\theta\&\gamma}} = \frac{1}{8}$ deg, $\sigma_{INS_V} = 2.5$ ft/sec, $\sigma_{INS_{X_0}} = 0.8$ NM (1481.6 m), and $\sigma_{INS_{Y_0}} = 75$ ft.

| $Vel$ [M] | $\hat{\sigma}^+_{E_V}$ [ft/sec] | $\hat{\sigma}^+_{E_{X_P}}$ [m] | $\bar{e}_{\hat{X}^+_P}$ [m] | $\hat{\sigma}^+_{E_{Y_P}}$ [ft] | $\bar{e}_{\hat{Y}^+_P}$ [ft] |
|---|---|---|---|---|---|
| 0.5 | 2.513 | 1444.26 | 13.74 | 100.91 | 3.47 |
| 0.6 | 2.502 | 1498.24 | 13.33 | 99.81 | 2.66 |
| 0.7 | 2.498 | 1465.90 | 17.65 | 100.03 | 0.89 |
| 0.8 | 2.465 | 1481.69 | 29.46 | 102.00 | 2.33 |
| 0.9 | 2.515 | 1482.03 | 24.65 | 101.84 | 0.80 |
| 1 | 2.469 | 1483.72 | 67.01 | 99.44 | 4.07 |

Table 4.9 Measurement Situation 2 - Own ship position estimation performance for different A/C speeds. The altitude is 3,000 feet; and the measurement errors during the estimation process are given in Table 4.8.

| $Vel$ [M] | $\hat{\sigma}^+_{E_{X_0}}$ [m] | $\bar{e}_{\hat{X}^+_0}$ [m] | $\hat{\sigma}^+_{E_{Y_0}}$ [ft] | $\bar{e}_{\hat{Y}^+_0}$ [ft] |
|---|---|---|---|---|
| 0.5 | 1443.85 | 13.24 | 73.89 | 0.24 |
| 0.6 | 1497.80 | 12.96 | 75.61 | 0.30 |
| 0.7 | 1465.79 | 18.53 | 74.23 | 1.21 |
| 0.8 | 1481.31 | 29.89 | 74.34 | 1.55 |
| 0.9 | 1481.92 | 23.63 | 75.43 | 0.47 |
| 1 | 1483.91 | 7.11 | 74.99 | 1.75 |

the unaided position estimates' 1-$\sigma$ values. The inclusion of the ground object's altitude information with a 100 feet uncertainty, barely aids the INS.

Table 4.10 shows the effect of including more accurate altitude information. The estimation accuracy increases when the information accuracy increases, as expected. Unfortunately, this level of accuracy is not readily available for prior $Y_P$ information, and the ensuing increase in position estimation accuracy is not enough for good INS aiding.

As a result, contrary to our expectations, we conclude that the inclusion of prior $Y_P$ information in the estimation process does not significantly contribute to INS aiding. The altitude information on the ground object, actually, is a measurement may be obtained by using the onboard sensors; or, it can be highly accurate if we choose a point on the surface of the sea (altitude is very close the zero). So, we do not suggest to use this algorithm in any aiding scheme.

Table 4.10 Measurement Situation 2 - Estimation performance as a function of measurement errors. The altitude and velocity are 3,000 feet and 0.8 M, respectively. The INS provided measurements, accuracy is as in Table 4.8.

| | $\hat{\sigma}^+_{E_V}$ [ft/sec] | $\hat{\sigma}^+_{E_{X_0}}$ [m] | $\hat{\sigma}^+_{E_{Y_0}}$ [ft] | $\hat{\sigma}^+_{E_{X_P}}$ [m] | $\hat{\sigma}^+_{E_{Y_P}}$ [ft] |
|---|---|---|---|---|---|
| $\sigma_{Y_P^-} = 100$ ft | 2.513 | 1487.06 | 75.69 | 1486.84 | 100.89 |
| $\sigma_{Y_P^-} = 50$ ft | 2.498 | 1483.48 | 75.31 | 1483.69 | 50.41 |
| $\sigma_{Y_P^-} = 10$ f | 2.525 | 1478.05 | 74.98 | 1477.79 | 10.00 |

***Simulation Results - Measurement Situation 3.*** Only the aircraft velocity estimate is calculated, since the parameter vector includes only the velocity state of the INS navigation output. The simulation results are shown in Table 4.11 which includes the statistics of the velocity estimate for varying altitudes and airspeeds. The

Table 4.11 Measurement Situation 3 - Airspeed Estimation performance for different airspeeds and altitudes. The measurement errors during the estimation process are $\sigma_{INS_{\theta\&\gamma}} = \frac{1}{8}$ deg, $\sigma_{INS_V} = 2.5$ ft/sec, $\sigma_{INS_{X_0}} = 0.8$ NM (1481.6 m), and $\sigma_{INS_{Y_0}} = 75$ ft. The slant range measurement has an 1-$\sigma$ error of 200 ft.

| $h$ [ft] | $\hat{\sigma}^+_{E_V}$ [ft/sec] | | $V$ [M] |
|---|---|---|---|
| 1000 | 2.479 | 2.476 | 0.5 |
| 3,000 | 2.473 | 2.471 | 0.6 |
| 6,000 | 2.478 | 2.542 | 0.7 |
| 10,000 | 2.445 | 2.487 | 0.8 |
| 15,000 | 2.420 | 2.484 | 0.9 |
| 20,000 | 2.415 | 2.528 | 1 |

estimates' 1-$\sigma$ values are below the pre-aiding velocity values; however, this improvement is not adequate to declare a successful aiding. Another observation is that the accuracy increases when the altitude increases. This contradicts the other experiments; however, when the altitude gets higher, the slant range also gets longer, so that the relative ranging error decreases, i.e., the signal-to-noise ratio of the slant range measurement increases.

This scenario shows that the bearings-only measurements supported by the slant range measurement to the ground object is not effective on INS position estimate. Hence, we conclude that this scenario can not be used as a unique means of aiding the INS optically.

***Simulation Results - Measurement Situation 4.*** In Measurement Situation 4, the effect of including the prior information on the altitude of the point P and the slant range to the point P measurement in the parameter estimation process is investigated and is documented in Tables 4.12 through 4.16. The estimate of the velocity $V$, and the geo-location of point P (the $\hat{X}_P$ and $\hat{Y}_P$ estimates) are shown in Table 4.12 as a function of altitude, and in Table 4.14 as a function of airspeed. Table 4.13 gives the aircraft position ($X_0$ and $Y_0$) estimates for various flight altitudes, and Table 4.15 gives the position statistics for different airspeeds. Compared to the measurement Situation in which only prior information on the altitude of point P is used, the estimates are slightly better; however, the estimation accuracy is again determined by the accuracy of the INS provided measurements. Finally, in Table 4.16, we show the different measurement error levels, and their statistics. Using passive slant range measurement devices, and obtaining a prior information on the ground object altitude, we still perform position estimate without radiating magnetic energy and still assume the ground object coordinates unknown. From this point of view, this scenario could have been proposed to use in an INS aiding schema, if the $X$-position estimate had been also improved.

Table 4.12 Measurement Situation 4 - Velocity estimate and geo-location performance for different flight altitudes. The A/C's speed is 0.8 M; and the measurement errors during the estimation process are $\sigma_{INS_{\theta\&\gamma}} = \frac{1}{8}$ deg, $\sigma_{INS_V} = 2.5$ ft/sec, $\sigma_{INS_{X_0}} = 0.8$ NM (1481.6 m), and $\sigma_{INS_{Y_0}} = 75$ ft. The *prior* information $Y_P^-$ and the measurement $R_m$ have the statistics $\sigma_{Y_P} = 100$ ft and $\sigma_{Sr} = 200$ ft.

| $h$ [ft] | $\hat{\sigma}^+_{E_V}$ [ft/sec] | $\hat{\sigma}^+_{E_{X_P}}$ [m] | $\bar{e}_{\hat{X}^+_P}$ [m] | $\hat{\sigma}^+_{E_{Y_P}}$ [ft] | $\bar{e}_{\hat{Y}^+_P}$ [ft] |
|---|---|---|---|---|---|
| 1000 | 2.464 | 1485.65 | 37.07 | 99.91 | 2.01 |
| 3,000 | 2.447 | 1492.70 | 13.26 | 98.72 | 0.26 |
| 6,000 | 2.546 | 1486.65 | 1.64 | 101.25 | 0.99 |
| 10,000 | 2.447 | 1480.34 | 27.69 | 100.71 | 0.22 |
| 15,000 | 2.468 | 1493.02 | 25.02 | 101.15 | 2.52 |
| 20,000 | 2.448 | 1489.25 | 19.19 | 99.09 | 0.89 |

Table 4.13 Measurement Situation 4 - Own ship position estimation performance for different flight altitudes. The A/C's speed is 0.8 M, and the measurement errors during the estimation process are given in Table 4.12.

| $h$ [ft] | $\bar{e}_{\hat{X}_0^+}$ [m] | $\hat{\sigma}^+_{E_{X_0}}$ [m] | $\bar{e}_{\hat{Y}_0^+}$ [ft] | $\hat{\sigma}^+_{E_{Y_0}}$ [ft] |
|---|---|---|---|---|
| 1000 | 38.67 | 1485.29 | 0.79 | 76.14 |
| 3,000 | 13.98 | 1492.82 | 1.36 | 74.53 |
| 6,000 | 1.81 | 1486.53 | 0.49 | 75.29 |
| 10,000 | 28.08 | 1480.12 | 0.66 | 74.43 |
| 15,000 | 26.00 | 1492.16 | 1.02 | 76.20 |
| 20,000 | 18.20 | 1488.61 | 0.10 | 74.66 |

Table 4.14 Measurement Situation 4 - Velocity estimation and geo-location performance for different airspeeds. The altitude is 3,000 ft, and the measurement errors during the estimation process are $\sigma_{INS_{\theta\&\gamma}} = \frac{1}{8}$ deg, $\sigma_{INS_V} = 2.5$ ft/sec, $\sigma_{INS_{X_0}} = 0.8$ NM (1481.6 m), and $\sigma_{INS_{Y_0}} = 75$ ft. The *prior* information $Y_P^-$ and the measurement $R_m$ have the statistics $\sigma_{Y_P} = 100$ ft and $\sigma_{Sr} = 200$ ft.

| $V$ [M] | $\hat{\sigma}^+_{E_V}$ [ft/sec] | $\hat{\sigma}^+_{E_{X_P}}$ [m] | $\bar{e}_{\hat{X}_P^+}$ [m] | $\hat{\sigma}^+_{E_{Y_P}}$ [ft] | $\bar{e}_{\hat{Y}_P^+}$ [ft] |
|---|---|---|---|---|---|
| 0.5 | 2.462 | 1464.74 | 2.20 | 98.81 | 1.17 |
| 0.6 | 2.508 | 1468.96 | 2.84 | 100.2 | 2.33 |
| 0.7 | 2.509 | 1465.51 | 0.04 | 99.94 | 1.36 |
| 0.8 | 2.503 | 1478.13 | 12.9 | 102.16 | 0.75 |
| 0.9 | 2.469 | 1474.04 | 15.11 | 101.31 | 0.09 |
| 1 | 2.512 | 1492.95 | 6.74 | 100.73 | 1.82 |

Table 4.15 Measurement Situation 4 - Own ship position estimation performance for different airspeeds. The altitude is 3,000 feet, and the measurement errors during the estimation process are given in Table 4.14.

| $h$ [ft] | $\bar{e}_{\hat{X}_0^+}$ [m] | $\hat{\sigma}^+_{E_{X_0}}$ [m] | $\bar{e}_{\hat{Y}_0^+}$ [ft] | $\hat{\sigma}^+_{E_{Y_0}}$ [ft] |
|---|---|---|---|---|
| 0.5 | 1.17 | 1465.07 | 1.91 | 75.67 |
| 0.6 | 1.49 | 1468.64 | 0.75 | 75.88 |
| 0.7 | 0.60 | 1465.64 | 0.32 | 73.90 |
| 0.8 | 13.81 | 1478.27 | 0.09 | 75.05 |
| 0.9 | 14.39 | 1473.95 | 0.92 | 75.07 |
| 1 | 7.53 | 1492.78 | 0.54 | 74.08 |

Table 4.16 Measurement Situation 4 - Estimation performance as a function of measurement errors. The altitude and velocity are 3,000 feet and 0.8 M, respectively. The measurements' accuracy provided by the INS are as in Table 4.14.

| | $\hat{\sigma}^+_{E_V}$ [ft/sec] | $\hat{\sigma}^+_{E_{X_0}}$ [m] | $\hat{\sigma}^+_{E_{Y_0}}$ [ft] | $\hat{\sigma}^+_{E_{X_P}}$ [m] | $\hat{\sigma}^+_{E_{Y_P}}$ [ft] |
|---|---|---|---|---|---|
| $\sigma_{Y_P^-} = 100$ ft, $\sigma_{R^-} = 200$ ft | 2.462 | 1509.91 | 75.09 | 1500.42 | 97.98 |
| $\sigma_{Y_P^-} = 50$ ft, $\sigma_{R^-} = 100$ ft | 2.420 | 1494.41 | 74.55 | 1494.89 | 49.29 |
| $\sigma_{Y_P^-} = 10$ ft, $\sigma_{R^-} = 20$ ft | 2.338 | 1484.73 | 74.60 | 1484.49 | 9.86 |

***Simulation Results - Measurement Situation 5.*** Simulation results for the measurement Situations where the additional, $Y_P$, information is included, are shown in Tables 4.17 through 4.21. Tables 4.17 and 4.18 show the velocity estimation and geo-location results, and own-ship position estimation performance for varying flight altitudes, respectively.

Table 4.17 Measurement Situation 5 - Velocity estimate, and geo-location performance for different flight altitudes. The A/C's speed is 0.8 M, and the measurement errors during the estimation process are $\sigma_{INS_{\theta\&\gamma}} = \frac{1}{8}$ deg, $\sigma_{INS_V} = 2.5$ ft/sec, $\sigma_{INS_{X_0}} = 0.8$ NM (1481.6 m), and $\sigma_{INS_{Y_0}} = 75$ ft. The additional *prior* information accuracy: $\sigma_{X_P} = \sigma_{Y_P} = 100$ ft.

| $h$ [ft] | $\hat{\sigma}^+_{E_V}$ [ft/sec] | $\hat{\sigma}^+_{E_{X_P}}$ [m] | $\bar{e}_{\hat{X}^+_P}$ [m] | $\hat{\sigma}^+_{E_{Y_P}}$ [ft] | $\bar{e}_{\hat{Y}^+_P}$ [ft] |
|---|---|---|---|---|---|
| 1000 | 2.535 | 30.34 | 0.46 | 100.07 | 2.35 |
| 3,000 | 2.487 | 29.87 | 0.34 | 98.12 | 0.31 |
| 6,000 | 2.479 | 30.88 | 0.18 | 98.75 | 0.25 |
| 10,000 | 2.522 | 30.38 | 0.42 | 98.69 | 0.17 |
| 15,000 | 2.485 | 30.35 | 0.27 | 101.1 | 0.13 |
| 20,000 | 2.507 | 31.01 | 0.54 | 100.04 | 3.18 |

It is observed that the positioning performance in this measurement Situation is good since the resultant 1-$\sigma$ value of the $X$-position estimate of the A/C is reduced considerably. The estimation and geo-location performance is documented in Tables 4.19 and 4.20 as a function of airspeed. The accuracy of the position estimate and of geo-location tends to decrease when the velocity decreases and/or the altitude increases. The statistics for varying error levels of the INS-provided measurements are given in Table 4.21.

Table 4.18 Measurement Situation 5 - Own ship position estimation performance for different flight altitudes. The A/C's speed is 0.8 M, and the measurement errors during the estimation process are given in Table 4.17.

| $h$ [ft] | $\bar{e}_{\hat{X}_0^+}$ [m] | $\hat{\sigma}^+_{E_{X_0}}$ [m] | $\hat{\sigma}^+_{X_0}$ [m] | $\bar{e}_{\hat{Y}_0^+}$ [ft] | $\hat{\sigma}^+_{E_{Y_0}}$ [ft] | $\hat{\sigma}^+_{Y_0}$ [ft] |
|---|---|---|---|---|---|---|
| 1000 | 1.88 | 34.62 | 36.13 | 1.36 | 74.88 | 74.99 |
| 3,000 | 1.41 | 36.68 | 37.42 | 0.51 | 74.68 | 74.99 |
| 6,000 | 0.96 | 45.66 | 44.55 | 0.88 | 74.86 | 74.99 |
| 10,000 | 3.64 | 71.45 | 72.33 | 2.33 | 75.12 | 74.99 |
| 15,000 | 3.19 | 94.89 | 94.72 | 0.35 | 75.11 | 74.99 |
| 20,000 | 4.64 | 130.46 | 127.32 | 0.34 | 76.47 | 74.99 |

Table 4.19 Measurement Situation 5 - Velocity estimation and geo-location performance for different airspeeds. The altitude is 3,000 feet; and the measurement errors during the estimation process are $\sigma_{INS_{\theta\&\gamma}} = \frac{1}{8}$ deg, $\sigma_{INS_V} = 2.5$ ft/sec, $\sigma_{INS_{X_0}} = 0.8$ NM (1481.6 m), and $\sigma_{INS_{Y_0}} = 75$ ft. The additional *prior* information accuracy: $\sigma_{X_P} = \sigma_{Y_P} = 100$ ft.

| $V$ [M] | $\hat{\sigma}^+_{E_V}$ [ft/sec] | $\hat{\sigma}^+_{E_{X_P}}$ [m] | $\bar{e}_{\hat{X}_P^+}$ [m] | $\hat{\sigma}^+_{E_{Y_P}}$ [ft] | $\bar{e}_{\hat{Y}_P^+}$ [ft] |
|---|---|---|---|---|---|
| 0.5 | 2.472 | 30.73 | 0.04 | 100.37 | 0.24 |
| 0.6 | 2.516 | 30.48 | 0.74 | 100.55 | 1.78 |
| 0.7 | 2.510 | 31.17 | 0.13 | 99.30 | 1.65 |
| 0.8 | 2.444 | 30.69 | 0.02 | 99.89 | 1.9 |
| 0.9 | 2.483 | 30.38 | 0.34 | 98.72 | 0.25 |
| 1 | 2.495 | 30.53 | 0.38 | 98.83 | 1.17 |

Measurement Situation 5 could be called "optical position fix-taking", because the positioning performance is comparable to that achieved with currently used fix-taking modes, however without ranging. The objective of this research, we recall, is INS aiding by optically tracking an "unknown" ground object. Now, the position of the ground object is known, however no active ranging is used.

Table 4.20 Measurement Situation 5 - Own ship position estimation performance for different airspeeds. The altitude is 3,000 feet, and the measurement errors during the estimation process are given in Table 4.19.

| $V$ [M] | $\bar{e}_{\hat{X}_0^+}$ [m] | $\hat{\sigma}^+_{E_{X_0}}$ [m] | $\hat{\sigma}^+_{X_0}$ [m] | $\bar{e}_{\hat{Y}_0^+}$ [ft] | $\hat{\sigma}^+_{E_{Y_0}}$ [ft] | $\hat{\sigma}^+_{Y_0}$ [ft] |
|---|---|---|---|---|---|---|
| 0.5 | 1.30 | 39.47 | 38.89 | 0.72 | 74.59 | 74.99 |
| 0.6 | 0.57 | 37.44 | 37.26 | 1.98 | 74.77 | 74.99 |
| 0.7 | 0.54 | 37.96 | 38.22 | 2.11 | 73.58 | 74.99 |
| 0.8 | 0.67 | 37.41 | 37.15 | 0.78 | 76.14 | 74.99 |
| 0.9 | 1.11 | 37.24 | 36.88 | 1.36 | 74.53 | 74.99 |
| 1 | 1.45 | 36.24 | 36.41 | 1.90 | 75.66 | 74.99 |

Table 4.21 Measurement Situation 5 - Estimation performance as a function of prior information accuracy. The altitude and velocity are 3,000 feet and 0.8 M, respectively. The measurements provided by the INS are given in Table 4.19.

| | $\hat{\sigma}^+_{E_V}$ [ft/sec] | $\hat{\sigma}^+_{E_{X_0}}$ [m] | $\hat{\sigma}^+_{E_{Y_0}}$ [ft] | $\hat{\sigma}^+_{E_{X_P}}$ [m] | $\hat{\sigma}^+_{E_{Y_P}}$ [ft] |
|---|---|---|---|---|---|
| $\sigma_{Y_P^-} = \sigma_{X_P^-} = 100$ ft | 2.487 | 37.02 | 76.95 | 30.26 | 99.43 |
| $\sigma_{Y_P^-} = \sigma_{X_P^-} = 50$ ft | 2.509 | 37.92 | 75.00 | 15.16 | 50.67 |
| $\sigma_{Y_P^-} = \sigma_{X_P^-} = 10$ ft | 2.422 | 15.96 | 73.98 | 3.05 | 9.97 |

***Simulation Results - Measurement Situation 6.*** In Measurement Situation 6, we also considered the case in which the $X_P$ information on the point P is included, and re-ran the same experiments. The results are documented in Tables 4.22, 4.23, 4.24, and 4.25. It can be seen that the inclusion of the $X_P$ prior information yields a decent parameter estimate $\hat{\theta}$, which is indicative of good INS aiding, although some deviations are observed.

Unfortunately, this scenario needs additional measurement $X_P^-$ to yield a good performance as shown in the Tables 4.22 to 4.25. Inclusion of $X_P^-$ is tantamount to say that this scenario is only used on the "known" ground object. Although we think that it can be used during the peace-time flights on our land, in any way, the current methods of fix-taking are already doing the same job, even more accurately. As a result, Scenario 6 results are favorable, but the Scenario is not the one we try to design.

Table 4.22 Measurement Situation 6 - Velocity estimation and geo-location performance for different flight altitudes. The A/C's speed is 0.8 M, and the measurement errors during the estimation process are $\sigma_{INS_{\theta\&\gamma}} = \frac{1}{8}$ deg, $\sigma_{INS_V} = 2.5$ ft/sec, $\sigma_{INS_{X_0}} = 0.8$ NM (1481.6 m), and $\sigma_{INS_{Y_0}} = 75$ ft. The *prior* information $X_P^-$ and $Y_P^-$, and the measurement $R_m$ have the statistics $\sigma_{X_P} = \sigma_{Y_P} = 100$ ft., and $\sigma_{Sr} = 200$ ft.

| $h$ [ft] | $\hat{\sigma}^+_{E_V}$ [ft/sec] | $\hat{\sigma}^+_{E_{X_P}}$ [m] | $\bar{e}_{\hat{X}_P^+}$ [m] | $\hat{\sigma}^+_{E_{Y_P}}$ [ft] | $\bar{e}_{\hat{Y}_P^+}$ [ft] |
|---|---|---|---|---|---|
| 1000 | 2.518 | 30.67 | 0.65 | 100.44 | 1.32 |
| 3,000 | 2.488 | 30.85 | 0.51 | 99.53 | 2.22 |
| 6,000 | 2.497 | 30.38 | 0.18 | 98.35 | 0.62 |
| 10,000 | 2.423 | 29.98 | 0.21 | 100.16 | 1.17 |
| 15,000 | 2.359 | 30.46 | 0.22 | 100.44 | 1.91 |
| 20,000 | 2.422 | 30.37 | 0.04 | 100.40 | 0.41 |

Table 4.23 Measurement Situation 6 - Own ship position estimation performance for different altitudes. The A/C's speed is 0.8 M, and the measurement errors during the estimation process are given in Table 4.22.

| $h$ [ft] | $\bar{e}_{\hat{X}_0^+}$ [m] | $\hat{\sigma}^+_{E_{X_0}}$ [m] | $\hat{\sigma}^+_{X_0}$ [m] | $\bar{e}_{\hat{Y}_0^+}$ [ft] | $\hat{\sigma}^+_{E_{Y_0}}$ [ft] | $\hat{\sigma}^+_{Y_0}$ [ft] |
|---|---|---|---|---|---|---|
| 1000 | 3.11 | 35.14 | 34.48 | 0.07 | 76.21 | 74.99 |
| 3,000 | 2.28 | 40.79 | 37.15 | 0.98 | 74.59 | 74.99 |
| 6,000 | 0.96 | 43.68 | 44.40 | 1.78 | 74.49 | 74.99 |
| 10,000 | 2.08 | 58.61 | 60.70 | 0.09 | 74.81 | 74.99 |
| 15,000 | 0.41 | 69.27 | 68.82 | 0.55 | 75.25 | 74.99 |
| 20,000 | 2.82 | 79.70 | 78.68 | 1.30 | 74.87 | 74.99 |

Table 4.24 Measurement Situation 6 - Velocity estimation and geo-location performance for different airspeeds. The flight altitude is 3,000 feet, and the measurement errors during the estimation process are $\sigma_{INS_{\theta\&\gamma}} = \frac{1}{8}$ deg, $\sigma_{INS_V} = 2.5$ ft/sec, $\sigma_{INS_{X_0}} = 0.8$ NM (1481.6 m), and $\sigma_{INS_{Y_0}} = 75$ ft. The *prior* information $X_P^-$ and $Y_P^-$ accuracy and the measurement $R_m$ have the statistics $\sigma_{X_P} = \sigma_{Y_P} = 100$ ft, and $\sigma_{SR} = 200$ ft.

| $V$ [M] | $\hat{\sigma}^+_{E_V}$ [ft/sec] | $\hat{\sigma}^+_{E_{X_P}}$ [m] | $\bar{e}_{\hat{X}_P^+}$ [m] | $\hat{\sigma}^+_{E_{Y_P}}$ [ft] | $\bar{e}_{\hat{Y}_P^+}$ [ft] |
|---|---|---|---|---|---|
| 0.5 | 2.481 | 30.17 | 0.91 | 99.00 | 1.69 |
| 0.6 | 2.440 | 30.50 | 0.31 | 98.45 | 0.78 |
| 0.7 | 2.476 | 30.84 | 0.04 | 99.39 | 0.97 |
| 0.8 | 2.467 | 30.05 | 0.82 | 99.76 | 0.09 |
| 0.9 | 2.536 | 30.28 | 0.27 | 98.70 | 3.34 |
| 1 | 2.505 | 30.60 | 0.24 | 99.28 | 0.57 |

Table 4.25 Measurement Situation 6 - Own ship position estimation performance for different airspeeds. The flight altitude is 3,000 feet, and the measurement errors during the estimation process are given in Table 4.24.

| $V$ [M] | $\bar{e}_{\hat{X}_0^+}$ [m] | $\hat{\sigma}^+_{E_{X_0}}$ [m] | $\hat{\sigma}^+_{X_0}$ [m] | $\bar{e}_{\hat{Y}_0^+}$ [ft] | $\hat{\sigma}^+_{E_{Y_0}}$ [ft] | $\hat{\sigma}^+_{Y_0}$ [ft] |
|---|---|---|---|---|---|---|
| 0.5 | 2.05 | 38.74 | 38.45 | 0.004 | 73.78 | 74.99 |
| 0.6 | 1.51 | 39.34 | 37.21 | 0.263 | 75.48 | 74.99 |
| 0.7 | 1.1 | 37.55 | 36.81 | 1.46 | 75.41 | 74.99 |
| 0.8 | 0.38 | 37.29 | 37.05 | 0.72 | 75.04 | 74.99 |
| 0.9 | 0.82 | 37.25 | 36.39 | 0.24 | 73.59 | 74.99 |
| 1 | 0.31 | 36.46 | 36.31 | 0.37 | 76.16 | 74.99 |

Table 4.26 Measurement Situation 6 - Estimation performance as a function of measurement errors. The flight altitude and velocity are 3,000 feet and 0.8 M, respectively. The INS provided measurements' accuracy is as in Table 4.24.

| | $\hat{\sigma}^+_{E_V}$ [ft/sec] | $\hat{\sigma}^+_{E_{X_0}}$ [m] | $\hat{\sigma}^+_{E_{Y_0}}$ [ft] | $\hat{\sigma}^+_{E_{X_P}}$ [m] | $\hat{\sigma}^+_{E_{Y_P}}$ [ft] |
|---|---|---|---|---|---|
| $\sigma_{Y_P^-} = \sigma_{X_P^-} = 100$ ft, $\sigma_{R^-} = 200$ ft | 2.528 | 37.22 | 75.32 | 29.88 | 99.3 |
| $\sigma_{Y_P^-} = \sigma_{X_P^-} = 50$ ft, $\sigma_{R^-} = 100$ ft | 2.435 | 22.91 | 75.41 | 15.13 | 50.35 |
| $\sigma_{Y_P^-} = \sigma_{X_P^-} = 10$ ft, $\sigma_{R^-} = 20$ ft | 2.067 | 14.61 | 74.77 | 3.04 | 10.06 |

***4.3.1.6 Comparison of The Measurement Situations.*** We investigate INS aiding by optically tracking an unknown ground object. Phase 1 entailed the estimation of the angular navigation variables. The estimation performance statistics of the algorithm which is applied to 6 different measurement scenarios is based on 5000 "independent" MC runs. Thus, in each measurement Situation, the random number generator is used to simulate white Gaussian noises for each measurement. As a result, different samples of noises are applied to each parameter in each run and results are documented in Tables 4.4 to 4.26. Based on these independent experiments, we analyzed the statistics scenario by scenario.

In this section, we compare the Scenarios' statistics parameter-wise. Fig 4.6 shows the experimental error variance of own ship $X$-position estimate. Measurement Situations 3 and 6 are clearly preferable to Measurement Situations 2 and 5. The estimation results in Measurement Situations 3 and 6 reflect the $X_P$ prior information accuracy. In Measure-

ment Situations 2 and 5, the error variance of the estimates is about 0.8 NM, since they are driven by the INS provided $X_0$ measurements.

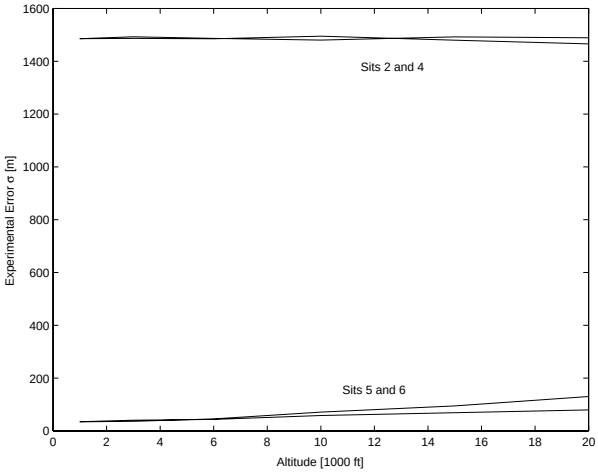


Figure 4.6 Own-ship X-Position Estimate: Comparison of Measurement Situations

The comparison of geo-location performance concerning the $Xp$ coordinate is given in Fig 4.7. The results are similar to the $X_0$ estimation performance results. Inclusion of prior information on $Xp$ in Measurement Situations 3 and 6 yields an estimation error variance of about 30 meters.

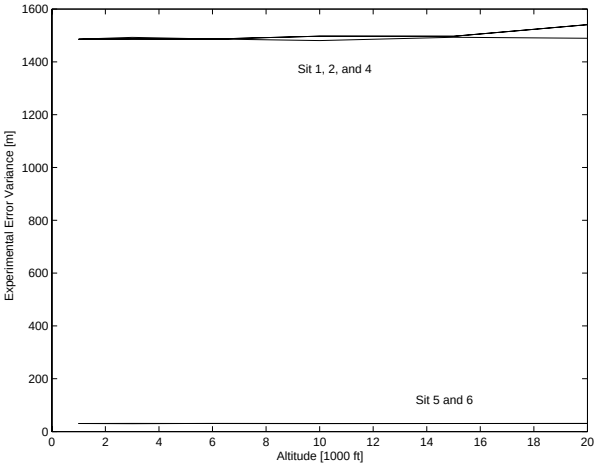


Figure 4.7 $X_P$ - Geo-location: Comparison of Measurement Situations

Estimation error $\sigma$ comparisons for own ship altitude estimation are shown in Fig 4.8. All Measurement Situations in this experiment include $Y_P^-$ prior information. The

1-$\sigma$ value of the INS provided altitude measurement is 75 feet; and the 100 feet accurate $Y_P^-$ prior information does not affect the estimation performance. After aiding, the results are random and the errors are about 75 feet. In Measurement Situations 5 and 6, inclusion of slant range measurement slightly reduces the estimation error.

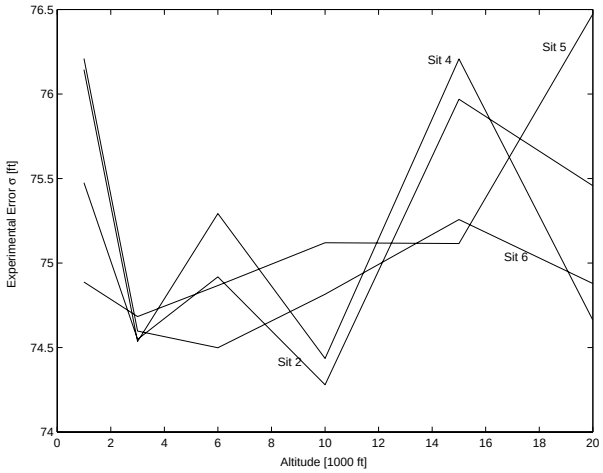


Figure 4.8 Own-ship Y-Position Estimate: Comparison of Measurement Situations

The ground object altitude estimation errors are compared in Fig 4.9. In Measurement Situation 1, the estimation error variance shows a considerable increase when the flight altitude increases. This measurement Situation simulates geo-location using bearings-only measurements. Remaining measurement Situations are driven by the quality of the prior information $Y_P^-$, hence the 100 feet positioning error variance is expected.

The velocity estimation performance comparison is shown in Fig 4.10. The results are slightly below the unaided velocity error $\sigma$ of 2.5 ft/sec. In Measurement Situations 4, 5, and 6, the inclusion of slant range measurement decreases the error variance.

Considering own-ship $X$-position and the ground object $X$-coordinate estimates, the measurement Situations including $X_P^-$ prior information clearly outperforms the remaining measurement Situations. Unfortunately, the objective of aiding INS by tracking an "unknown" ground object can not be satisfied in a scenario we use $X_P^-$ prior information. For own-ship $Y$-position and the ground object $Y$-coordinate estimates, inclusion of $Y_P^-$ prior information do not improve the estimation performance unless the prior information is very

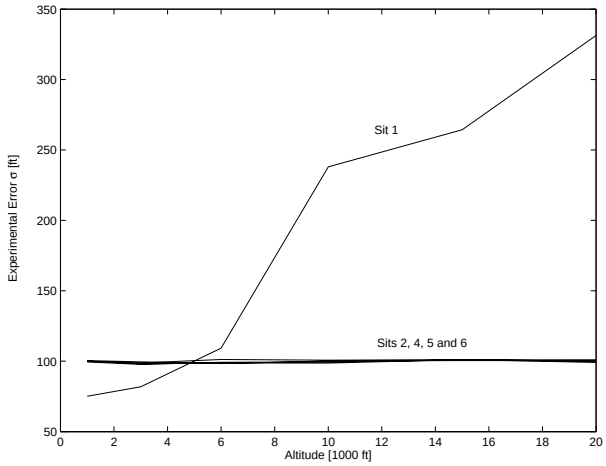


Figure 4.9 $Y_P$ - Geo-location Estimate: Comparison of Measurement Situations

accurate. Assuming the terrain is flat and the altitude of the ground objects do not change significantly within 1 NM, the difference between onboard baro-altimeter and radar altimeter may yield a prior information on the altitude of the ground object. Hence, we assumed 100 feet error $\sigma$ for $Y_P^-$ prior information. For more accurate prior information, however, we have to assume that the ground object coordinates are known. Own-ship velocity estimates results show that optical tracking Scenarios have not significant contribution to the INS velocity estimate error reduction.

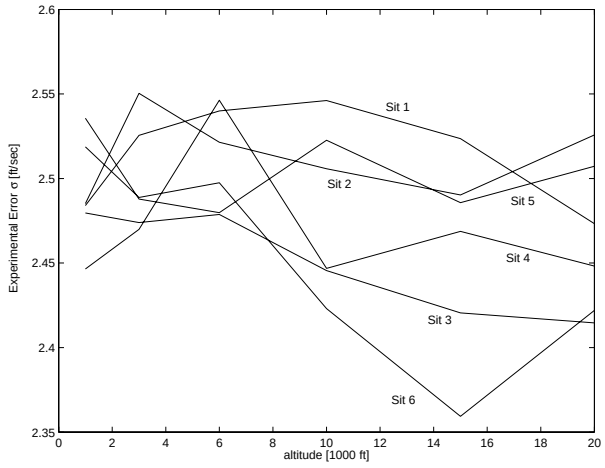


Figure 4.10 Velocity Estimate: Comparison of Measurement Situations

### *4.3.2 Singular Linear Regression.*

At the completion of Phase 1 , we have the estimates

$$\begin{aligned} \gamma_D &= \mathcal{N}(\hat{\gamma}_D, \sigma^2_{\gamma_D}) \\ \gamma &= \mathcal{N}(\hat{\gamma}, \sigma^2_{\gamma}) \end{aligned}$$

In other words,

$$\begin{aligned} \gamma_D &= \hat{\gamma}_D + v_{\gamma_D}, \qquad v_{\gamma_D} = \mathcal{N}(0, \sigma^2_{\gamma_D}) \\ \gamma &= \hat{\gamma} + v_{\gamma}, \qquad v_{\gamma} = \mathcal{N}(0, \sigma^2_{\gamma}) \end{aligned} \tag{4.91}$$

The measurement situation is shown in Fig 3.2. We recognize that

$$\begin{aligned} x &= R\, cos\gamma_D \\ y &= R\, sin\gamma_D \end{aligned} \tag{4.92}$$

where $R$ is the initial slant range to the point P. Replacing in Eqs. (4.92) $\gamma_D$ with $\hat{\gamma}_D$, and using Eqs (4.91), we obtain

$$\begin{aligned} x &\approx R\, cos\hat{\gamma}_D - R\, sin\hat{\gamma}_D.v_{\gamma_D} \\ y &\approx R\, sin\hat{\gamma}_D + R\, cos\hat{\gamma}_D.v_{\gamma_D} \end{aligned}$$

Furthermore, we recall the equalities

$$\begin{aligned} x &= K_x V \\ y &= K_y V \end{aligned}$$

where, the gains $K_x$ and $K_y$ obtained after the application of the SVD algorithm, are "clean".

Hence, we declare $R$ and $V$ the primary parameters and write the linear regression in $R$

and $V$:

$$\begin{bmatrix} 0 \\ 0 \\ V_m \end{bmatrix} = \begin{bmatrix} cos\hat{\gamma}_D & -K_x \\ sin\hat{\gamma}_D & -K_y \\ 0 & 1 \end{bmatrix} \begin{bmatrix} R \\ V \end{bmatrix} + \begin{bmatrix} -R\, sin\hat{\gamma}_D & 0 \\ R\, cos\hat{\gamma}_D & 0 \\ 0 & 1 \end{bmatrix} \begin{bmatrix} v_{\gamma_D} \\ v_V \end{bmatrix} \tag{4.93}$$

We also have the coordinate transformation Equations (3.1)

$$\begin{aligned} x\, cos\gamma + y\, sin\gamma &= X_P - X_0 \\ x\, sin\gamma - y\, cos\gamma &= Y_P - Y_0 \end{aligned} \tag{4.94}$$

Inserting Eqs. (4.92) into the coordinate transformation Equations (4.94), we obtain

$$\begin{aligned} R(cos\gamma_D.cos\gamma + sin\gamma_D.sin\gamma) &= X_P - X_0 \\ R(cos\gamma_D.sin\gamma - sin\gamma_D.cos\gamma) &= Y_P - Y_0 \end{aligned}$$

which yields

$$\begin{aligned} R\, cos(\gamma_D - \gamma) &= X_P - X_0 \\ R\, sin(\gamma_D - \gamma) &= Y_0 - Y_P \end{aligned} \tag{4.95}$$

Eqs. (4.91) yield

$$\gamma_D - \gamma = \hat{\gamma}_D - \hat{\gamma} + v_{\gamma_D} - v_\gamma$$

and thus, linearization yields

$$\begin{aligned} cos(\gamma_D - \gamma) &\approx cos(\hat{\gamma}_D - \hat{\gamma}) - sin(\hat{\gamma}_D - \hat{\gamma})v_{\gamma_D} + sin(\hat{\gamma}_D - \hat{\gamma})v_\gamma \\ sin(\gamma_D - \gamma) &\approx sin(\hat{\gamma}_D - \hat{\gamma}) + cos(\hat{\gamma}_D - \hat{\gamma})v_{\gamma_D} - cos(\hat{\gamma}_D - \hat{\gamma})v_\gamma \end{aligned} \tag{4.96}$$

Inserting Eqs. (4.96) into Eqs. (4.95), we obtain the linear regression in the complete parameter ($R$, $X_0$, $Y_0$, $X_P$, $Y_P$):

$$\begin{bmatrix} 0 \\ 0 \end{bmatrix} = \begin{bmatrix} cos(\hat{\gamma}_D - \hat{\gamma}) & 1 & 0 & -1 & 0 \\ sin(\hat{\gamma}_D - \hat{\gamma}) & 0 & -1 & 0 & 1 \end{bmatrix} \begin{bmatrix} R \\ X_0 \\ Y_0 \\ X_P \\ Y_P \end{bmatrix} + \\ + \begin{bmatrix} -sin(\hat{\gamma}_D - \hat{\gamma}) & sin(\hat{\gamma}_D - \hat{\gamma}) \\ cos(\hat{\gamma}_D - \hat{\gamma}) & -cos(\hat{\gamma}_D - \hat{\gamma}) \end{bmatrix} \begin{bmatrix} v_{\gamma_D} \\ v_\gamma \end{bmatrix} \tag{4.97}$$

We have the additional non-linear equality constraint:

$$\sqrt{(X_0 - X_P)^2 + (Y_0 - Y_P)^2} - R = 0$$

We treat the above non-linear equality constraint $f(\vec{X}) = 0$, where $\vec{X} = (R, X_0, Y_0, X_P, Y_P)$ and

$$f(R, X_0, Y_0, X_P, Y_P) = R - \sqrt{(X_0 - X_P)^2 + (Y_0 - Y_P)^2} \tag{4.98}$$

as follows.

The linearization of Eq. (4.98) about a prior parameter estimate yields the additional linear regression equation

$$0 = \begin{bmatrix} \sqrt{(\hat{X}_0^- - \hat{X}_P^-)^2 + (\hat{Y}_0^- - \hat{Y}_P^-)^2}, & (\hat{X}_P^- - \hat{X}_0^-), & (\hat{Y}_P^- - \hat{Y}_0^-), & (\hat{X}_0^- - \hat{X}_P^-), & (\hat{Y}_0^- - \hat{Y}_P^-) \end{bmatrix} \begin{bmatrix} R \\ X_0 \\ Y_0 \\ X_P \\ Y_P \end{bmatrix} \tag{4.99}$$

We also perform the following algebraic manipulations:

In Eq. (4.99) we eliminate

$$\hat{X}_P^- - \hat{X}_0^- = \hat{R}^- \sqrt{1 - \left( \frac{\hat{Y}_P^- - \hat{Y}_0^-}{\hat{R}^-} \right)^2}$$

and divide the equation by $\hat{R}^-$, where the superscript "-" denotes a prior estimate of the parameter. The linearization (4.99) of $f(\vec{X}) = 0$ is developed in Appendix C.

At this point, we use the INS-provided measurements $V_m$, $X_{o_m}$, $Y_{o_m}$, the linear regression equations (4.93) and (4.98), and the constraint (4.99) which were derived so far, and we form the basic linear regression

$$\begin{bmatrix} V_m \\ 0 \\ 0 \\ 0 \\ 0 \\ 0 \\ X_{o_m} \\ Y_{o_m} \end{bmatrix} = \begin{bmatrix} 1 & 0 & 0 & 0 & 0 & 0 \\ -K_x & cos\hat{\gamma}_D & 0 & 0 & 0 & 0 \\ -K_y & sin\hat{\gamma}_D & 0 & 0 & 0 & 0 \\ 0 & cos(\hat{\gamma}_D - \hat{\gamma}) & 1 & 0 & -1 & 0 \\ 0 & sin(\hat{\gamma}_D - \hat{\gamma}) & 0 & -1 & 0 & 1 \\ 0 & 1 & \sqrt{1 - \left(\frac{\hat{Y}_P^- - \hat{Y}_0^-}{\hat{R}^-}\right)^2} & \frac{\hat{Y}_P^- - \hat{Y}_0^-}{\hat{R}^-} & -\sqrt{1 - \left(\frac{\hat{Y}_P^- - \hat{Y}_0^-}{\hat{R}^-}\right)^2} & \frac{\hat{Y}_0^- - \hat{Y}_P^-}{\hat{R}^-} \\ 0 & 0 & 1 & 0 & 0 & 0 \\ 0 & 0 & 0 & 1 & 0 & 0 \end{bmatrix} \begin{bmatrix} V \\ R \\ X_0 \\ Y_0 \\ X_P \\ Y_P \end{bmatrix}$$
$$+ \begin{bmatrix} 1 & 0 & 0 & 0 & 0 \\ 0 & 0 & 0 & 0 & -\hat{R}^- sin\hat{\gamma}_D \\ 0 & 0 & 0 & 0 & \hat{R}^- cos\hat{\gamma}_D \\ 0 & 0 & 0 & sin(\hat{\gamma}_D - \hat{\gamma}) & -sin(\hat{\gamma}_D - \hat{\gamma}) \\ 0 & 0 & 0 & -cos(\hat{\gamma}_D - \hat{\gamma}) & cos(\hat{\gamma}_D - \hat{\gamma}) \\ 0 & 0 & 0 & 0 & 0 \\ 0 & 1 & 0 & 0 & 0 \\ 0 & 0 & 1 & 0 & 0 \end{bmatrix} \begin{bmatrix} v_V \\ v_{X_0} \\ v_{Y_0} \\ v_\gamma \\ v_{\gamma_D} \end{bmatrix} \tag{4.100}$$

***4.3.2.1 Measurement Scenarios.*** In Sect. 4.3.2 we have obtained the basic linear regression (4.100) of the form

$$Z = H\theta + \Gamma V \tag{4.101}$$

Based on this linear regression, we simulate 6 different measurement scenarios whose derivations are given as following.

***Scenario 1.*** In this measurement situation, we assume that the aircraft's $X_0$ and $Y_0$ position and aircraft's velocity are provided by the INS with 1-$\sigma$ errors of 0.8 nm, 75 ft, and 2.5 ft/sec, respectively.

The regressor H

$$\begin{bmatrix} 1 & 0 & 0 & 0 & 0 & 0 \\ -K_x & cos\hat{\gamma}_D & 0 & 0 & 0 & 0 \\ -K_y & sin\hat{\gamma}_D & 0 & 0 & 0 & 0 \\ 0 & cos(\hat{\gamma}_D - \hat{\gamma}) & 1 & 0 & -1 & 0 \\ 0 & sin(\hat{\gamma}_D - \hat{\gamma}) & 0 & -1 & 0 & 1 \\ 0 & 1 & \sqrt{1 - \left(\frac{\hat{Y}_P^- - \hat{Y}_0^-}{\hat{R}^-}\right)^2} & \frac{\hat{Y}_P^- - \hat{Y}_0^-}{\hat{R}^-} & -\sqrt{1 - \left(\frac{\hat{Y}_P^- - \hat{Y}_0^-}{\hat{R}^-}\right)^2} & \frac{\hat{Y}_0^- - \hat{Y}_P^-}{\hat{R}^-} \\ 0 & 0 & 1 & 0 & 0 & 0 \\ 0 & 0 & 0 & 1 & 0 & 0 \end{bmatrix} \tag{4.102}$$

and

$$Z = \begin{bmatrix} V_m & 0 & 0 & 0 & 0 & 0 & X_{o_m} & Y_{o_m} \end{bmatrix}^T \tag{4.103}$$

$$\theta = \begin{bmatrix} V \\ R \\ X_0 \\ Y_0 \\ X_P \\ Y_P \end{bmatrix}, \quad \Gamma = \begin{bmatrix} 1 & 0 & 0 & 0 & 0 \\ 0 & 0 & 0 & 0 & -\hat{R}^- sin\hat{\gamma}_D \\ 0 & 0 & 0 & 0 & \hat{R}^- cos\hat{\gamma}_D \\ 0 & 0 & 0 & sin(\hat{\gamma}_D - \hat{\gamma}) & -sin(\hat{\gamma}_D - \hat{\gamma}) \\ 0 & 0 & 0 & -cos(\hat{\gamma}_D - \hat{\gamma}) & cos(\hat{\gamma}_D - \hat{\gamma}) \\ 0 & 0 & 0 & 0 & 0 \\ 0 & 1 & 0 & 0 & 0 \\ 0 & 0 & 1 & 0 & 0 \end{bmatrix}, \quad V = \begin{bmatrix} v_V \\ v_{X_0} \\ v_{Y_0} \\ v_\gamma \\ v_{\gamma_D} \end{bmatrix}$$

The $8 \times 8$ equation error covariance matrix $R = E\{\Gamma V V^T \Gamma^T\}$ is

$$R = \Gamma \begin{bmatrix} \sigma_V^2 & 0 & 0 & 0 & 0 \\ 0 & \sigma_{X_0}^2 & 0 & 0 & 0 \\ 0 & 0 & \sigma_{Y_0}^2 & 0 & 0 \\ 0 & 0 & 0 & \sigma_\gamma^2 & 0 \\ 0 & 0 & 0 & 0 & \sigma_{\gamma_D}^2 \end{bmatrix} \Gamma^T \tag{4.104}$$

R has a rank of 5.

Obviously, we need to iterate on $Y_0$, $Y_P$, and $R$. The initial guesses for the above are $\hat{Y}_0^- = Y_{0m}$, $\hat{Y}_P^- = 0$. Considering optimal measurement geometry introduced in Sect. 4.1, initial guess for the slant range measurement can be chosen as $\hat{R}^- = \frac{7}{3} \times$altitude.

Eqs. (4.138) - (4.141) in the sequel yield the MV estimate and predicted estimation error variance matrix. INS aiding and geo-location are jointly performed.

***Scenario 2.*** In this measurement scenario, the linear regression is augmented with the prior information on $Y_P$, with $\sigma_{Y_P} = 100$ ft. Thus, we include the "measurement"

$$Y_{P_m} = Y_P + v_{Y_P} \tag{4.105}$$

We obtain the augmented linear regression (4.101), where the regressor

$$H = \begin{bmatrix} 1 & 0 & 0 & 0 & 0 & 0 \\ -K_x & cos\hat{\gamma}_D & 0 & 0 & 0 & 0 \\ -K_y & sin\hat{\gamma}_D & 0 & 0 & 0 & 0 \\ 0 & cos(\hat{\gamma}_D - \hat{\gamma}) & 1 & 0 & -1 & 0 \\ 0 & sin(\hat{\gamma}_D - \hat{\gamma}) & 0 & -1 & 0 & 1 \\ 0 & 1 & \sqrt{1 - \left(\frac{\hat{Y}_P^- - \hat{Y}_0^-}{\hat{R}^-}\right)^2} & \frac{\hat{Y}_P^- - \hat{Y}_0^-}{\hat{R}^-} & -\sqrt{1 - \left(\frac{\hat{Y}_P^- - \hat{Y}_0^-}{\hat{R}^-}\right)^2} & \frac{\hat{Y}_0^- - \hat{Y}_P^-}{\hat{R}^-} \\ 0 & 0 & 1 & 0 & 0 & 0 \\ 0 & 0 & 0 & 1 & 0 & 0 \\ 0 & 0 & 0 & 0 & 0 & 1 \end{bmatrix} \quad (4.106)$$

and

$$Z = \begin{bmatrix} V_m \\ 0 \\ 0 \\ 0 \\ 0 \\ 0 \\ X_{o_m} \\ Y_{o_m} \\ Y_{P_m} \end{bmatrix}, \quad \Gamma = \begin{bmatrix} 1 & 0 & 0 & 0 & 0 & 0 \\ 0 & 0 & 0 & 0 & -\hat{R}^- sin\hat{\gamma}_D & 0 \\ 0 & 0 & 0 & 0 & \hat{R}^- cos\hat{\gamma}_D & 0 \\ 0 & 0 & 0 & sin(\hat{\gamma}_D - \hat{\gamma}) & -sin(\hat{\gamma}_D - \hat{\gamma}) & 0 \\ 0 & 0 & 0 & -cos(\hat{\gamma}_D - \hat{\gamma}) & cos(\hat{\gamma}_D - \hat{\gamma}) & 0 \\ 0 & 0 & 0 & 0 & 0 & 0 \\ 0 & 1 & 0 & 0 & 0 & 0 \\ 0 & 0 & 1 & 0 & 0 & 0 \\ 0 & 0 & 0 & 0 & 0 & 1 \end{bmatrix}, \quad V = \begin{bmatrix} v_V \\ v_{X_0} \\ v_{Y_0} \\ v_\gamma \\ v_{\gamma_D} \\ v_{Y_P} \end{bmatrix} \quad (4.107)$$

The $9 \times 9$ equation error covariance matrix R is

$$R = \Gamma \begin{bmatrix} \sigma_V^2 & 0 & 0 & 0 & 0 & 0 \\ 0 & \sigma_{X_0}^2 & 0 & 0 & 0 & 0 \\ 0 & 0 & \sigma_{Y_0}^2 & 0 & 0 & 0 \\ 0 & 0 & 0 & \sigma_\gamma^2 & 0 & 0 \\ 0 & 0 & 0 & 0 & \sigma_{\gamma_D}^2 & 0 \\ 0 & 0 & 0 & 0 & 0 & \sigma_{Y_P}^2 \end{bmatrix} \Gamma^T \quad (4.108)$$

and the rank of R is 6.

***Scenario 3.*** We augment the linear regression by including the slant range to the point P measurement. The new measurement equation is

$$R_m = R + v_R \tag{4.109}$$

where 1-$\sigma_R$ is 200 feet.

In the augmented linear regression (4.101) the regressor

$$H = \begin{bmatrix} 1 & 0 & 0 & 0 & 0 & 0 \\ -K_x & cos\hat{\gamma}_D & 0 & 0 & 0 & 0 \\ -K_y & sin\hat{\gamma}_D & 0 & 0 & 0 & 0 \\ 0 & cos(\hat{\gamma}_D - \hat{\gamma}) & 1 & 0 & -1 & 0 \\ 0 & sin(\hat{\gamma}_D - \hat{\gamma}) & 0 & -1 & 0 & 1 \\ 0 & 1 & \sqrt{1 - \left(\frac{\hat{Y}_P^- - \hat{Y}_0^-}{\hat{R}^-}\right)^2} & \frac{\hat{Y}_P^- - \hat{Y}_0^-}{\hat{R}^-} & -\sqrt{1 - \left(\frac{\hat{Y}_P^- - \hat{Y}_0^-}{\hat{R}^-}\right)^2} & \frac{\hat{Y}_0^- - \hat{Y}_P^-}{\hat{R}^-} \\ 0 & 0 & 1 & 0 & 0 & 0 \\ 0 & 0 & 0 & 1 & 0 & 0 \\ 0 & 1 & 0 & 0 & 0 & 0 \end{bmatrix} \tag{4.110}$$

and

$$Z = \begin{bmatrix} V_m \\ 0 \\ 0 \\ 0 \\ 0 \\ 0 \\ X_{o_m} \\ Y_{o_m} \\ R_m \end{bmatrix}, \quad \Gamma = \begin{bmatrix} 1 & 0 & 0 & 0 & 0 & 0 \\ 0 & 0 & 0 & 0 & -\hat{R}^- sin\hat{\gamma}_D & 0 \\ 0 & 0 & 0 & 0 & \hat{R}^- cos\hat{\gamma}_D & 0 \\ 0 & 0 & 0 & sin(\hat{\gamma}_D - \hat{\gamma}) & -sin(\hat{\gamma}_D - \hat{\gamma}) & 0 \\ 0 & 0 & 0 & -cos(\hat{\gamma}_D - \hat{\gamma}) & cos(\hat{\gamma}_D - \hat{\gamma}) & 0 \\ 0 & 0 & 0 & 0 & 0 & 0 \\ 0 & 1 & 0 & 0 & 0 & 0 \\ 0 & 0 & 1 & 0 & 0 & 0 \\ 0 & 0 & 0 & 0 & 0 & 1 \end{bmatrix}, \quad V = \begin{bmatrix} v_V \\ v_{X_0} \\ v_{Y_0} \\ v_\gamma \\ v_{\gamma_D} \\ v_{R_m} \end{bmatrix} \tag{4.111}$$

The $9 \times 9$ equation error covariance matrix R is

$$R = \Gamma \begin{bmatrix} \sigma_V^2 & 0 & 0 & 0 & 0 & 0 \\ 0 & \sigma_{X_0}^2 & 0 & 0 & 0 & 0 \\ 0 & 0 & \sigma_{Y_0}^2 & 0 & 0 & 0 \\ 0 & 0 & 0 & \sigma_{\gamma}^2 & 0 & 0 \\ 0 & 0 & 0 & 0 & \sigma_{\gamma_D}^2 & 0 \\ 0 & 0 & 0 & 0 & 0 & \sigma_{R_m}^2 \end{bmatrix} \Gamma^T \tag{4.112}$$

and rank(R)=6.

***Scenario 4.*** In this measurement scenario, we assume that both the altitude prior information and slant range measurement are available. Augmenting the linear regression by including the slant range and $Y_P$ information, we obtain for the measurement situation 4 the singular linear regression (4.101) with the regressor

$$H = \begin{bmatrix} 1 & 0 & 0 & 0 & 0 & 0 \\ -K_x & cos\hat{\gamma}_D & 0 & 0 & 0 & 0 \\ -K_y & sin\hat{\gamma}_D & 0 & 0 & 0 & 0 \\ 0 & cos(\hat{\gamma}_D - \hat{\gamma}) & 1 & 0 & -1 & 0 \\ 0 & sin(\hat{\gamma}_D - \hat{\gamma}) & 0 & -1 & 0 & 1 \\ 0 & 1 & \sqrt{1 - \left(\frac{\hat{Y}_P^- - \hat{Y}_0^-}{\hat{R}^-}\right)^2} & \frac{\hat{Y}_P^- - \hat{Y}_0^-}{\hat{R}^-} & -\sqrt{1 - \left(\frac{\hat{Y}_P^- - \hat{Y}_0^-}{\hat{R}^-}\right)^2} & \frac{\hat{Y}_0^- - \hat{Y}_P^-}{\hat{R}^-} \\ 0 & 0 & 1 & 0 & 0 & 0 \\ 0 & 0 & 0 & 1 & 0 & 0 \\ 0 & 0 & 0 & 0 & 0 & 1 \\ 0 & 1 & 0 & 0 & 0 & 0 \end{bmatrix} \tag{4.113}$$

$$Z = \begin{bmatrix} V_m \\ 0 \\ 0 \\ 0 \\ 0 \\ 0 \\ X_{o_m} \\ Y_{o_m} \\ Y_{P_m} \\ R_m \end{bmatrix}, \quad \Gamma = \begin{bmatrix} 1 & 0 & 0 & 0 & 0 & 0 & 0 \\ 0 & 0 & 0 & 0 & -\hat{R}^- sin\hat{\gamma}_D & 0 & 0 \\ 0 & 0 & 0 & 0 & \hat{R}^- cos\hat{\gamma}_D & 0 & 0 \\ 0 & 0 & 0 & sin(\hat{\gamma}_D - \hat{\gamma}) & -sin(\hat{\gamma}_D - \hat{\gamma}) & 0 & 0 \\ 0 & 0 & 0 & -cos(\hat{\gamma}_D - \hat{\gamma}) & cos(\hat{\gamma}_D - \hat{\gamma}) & 0 & 0 \\ 0 & 0 & 0 & 0 & 0 & 0 & 0 \\ 0 & 1 & 0 & 0 & 0 & 0 & 0 \\ 0 & 0 & 1 & 0 & 0 & 0 & 0 \\ 0 & 0 & 0 & 0 & 0 & 1 & 0 \\ 0 & 0 & 0 & 0 & 0 & 0 & 1 \end{bmatrix}, \quad V = \begin{bmatrix} v_V \\ v_{X_0} \\ v_{Y_0} \\ v_\gamma \\ v_{\gamma_D} \\ v_{Y_P} \\ v_{R_m} \end{bmatrix} \quad (4.114)$$

The $10 \times 10$ equation error covariance matrix R is

$$R = \Gamma \begin{bmatrix} \sigma_V^2 & 0 & 0 & 0 & 0 & 0 & 0 \\ 0 & \sigma_{X_0}^2 & 0 & 0 & 0 & 0 & 0 \\ 0 & 0 & \sigma_{Y_0}^2 & 0 & 0 & 0 & 0 \\ 0 & 0 & 0 & \sigma_\gamma^2 & 0 & 0 & 0 \\ 0 & 0 & 0 & 0 & \sigma_{\gamma_D}^2 & 0 & 0 \\ 0 & 0 & 0 & 0 & 0 & \sigma_{Y_P}^2 & 0 \\ 0 & 0 & 0 & 0 & 0 & 0 & \sigma_{R_m}^2 \end{bmatrix} \Gamma^T \quad (4.115)$$

and rank(R)=7.

***Scenario 5.*** In this measurement scenario, we augment the linear regression by including the complete prior information on the ground object. Thus, the "measurement" equations are included

$$Y_{P_m} = Y_P + v_{Y_P} \quad (4.116)$$

$$X_{P_m} = X_P + v_{X_P} \quad (4.117)$$

where $\sigma_{Y_P} = \sigma_{X_P} = 100$ ft.

In the augmented linear regression (4.101) for the measurement situation 5, the regressor

$$H = \begin{bmatrix} 1 & 0 & 0 & 0 & 0 & 0 \\ -K_x & cos\hat{\gamma}_D & 0 & 0 & 0 & 0 \\ -K_y & sin\hat{\gamma}_D & 0 & 0 & 0 & 0 \\ 0 & cos(\hat{\gamma}_D - \hat{\gamma}) & 1 & 0 & -1 & 0 \\ 0 & sin(\hat{\gamma}_D - \hat{\gamma}) & 0 & -1 & 0 & 1 \\ 0 & 1 & \sqrt{1 - \left(\frac{\hat{Y}_P^- - \hat{Y}_0^-}{\hat{R}^-}\right)^2} & \frac{\hat{Y}_P^- - \hat{Y}_0^-}{\hat{R}^-} & -\sqrt{1 - \left(\frac{\hat{Y}_P^- - \hat{Y}_0^-}{\hat{R}^-}\right)^2} & \frac{\hat{Y}_0^- - \hat{Y}_P^-}{\hat{R}^-} \\ 0 & 0 & 1 & 0 & 0 & 0 \\ 0 & 0 & 0 & 1 & 0 & 0 \\ 0 & 0 & 0 & 0 & 0 & 1 \\ 0 & 0 & 0 & 0 & 1 & 0 \end{bmatrix} \quad (4.118)$$

and

$$Z = \begin{bmatrix} V_m \\ 0 \\ 0 \\ 0 \\ 0 \\ 0 \\ X_{o_m} \\ Y_{o_m} \\ Y_{P_m} \\ X_{P_m} \end{bmatrix}, \quad \Gamma = \begin{bmatrix} 1 & 0 & 0 & 0 & 0 & 0 & 0 \\ 0 & 0 & 0 & 0 & -\hat{R}^- sin\hat{\gamma}_D & 0 & 0 \\ 0 & 0 & 0 & 0 & \hat{R}^- cos\hat{\gamma}_D & 0 & 0 \\ 0 & 0 & 0 & sin(\hat{\gamma}_D - \hat{\gamma}) & -sin(\hat{\gamma}_D - \hat{\gamma}) & 0 & 0 \\ 0 & 0 & 0 & -cos(\hat{\gamma}_D - \hat{\gamma}) & cos(\hat{\gamma}_D - \hat{\gamma}) & 0 & 0 \\ 0 & 0 & 0 & 0 & 0 & 0 & 0 \\ 0 & 1 & 0 & 0 & 0 & 0 & 0 \\ 0 & 0 & 1 & 0 & 0 & 0 & 0 \\ 0 & 0 & 0 & 0 & 0 & 1 & 0 \\ 0 & 0 & 0 & 0 & 0 & 0 & 1 \end{bmatrix}, \quad V = \begin{bmatrix} v_V \\ v_{X_0} \\ v_{Y_0} \\ v_\gamma \\ v_{\gamma_D} \\ v_{Y_P} \\ v_{X_P} \end{bmatrix} \quad (4.119)$$

The $10 \times 10$ equation error covariance matrix is

$$R = \Gamma \begin{bmatrix} \sigma_V^2 & 0 & 0 & 0 & 0 & 0 & 0 \\ 0 & \sigma_{X_0}^2 & 0 & 0 & 0 & 0 & 0 \\ 0 & 0 & \sigma_{Y_0}^2 & 0 & 0 & 0 & 0 \\ 0 & 0 & 0 & \sigma_{\gamma}^2 & 0 & 0 & 0 \\ 0 & 0 & 0 & 0 & \sigma_{\gamma_D}^2 & 0 & 0 \\ 0 & 0 & 0 & 0 & 0 & \sigma_{Y_P}^2 & 0 \\ 0 & 0 & 0 & 0 & 0 & 0 & \sigma_{X_P}^2 \end{bmatrix} \Gamma^T \tag{4.120}$$

and rank(R)=7.

***Scenario 6.*** The prior information on the ground object's position ($X_P$ and $Y_P$) and the slant range measurement R are augmented into the linear regression. Their 1-$\sigma$ error values are as in the previously discussed Scenarios 4 and 5.

In the augmented linear regression (4.101) for the measurement situation 6, the regressor

$$H = \begin{bmatrix} 1 & 0 & 0 & 0 & 0 & 0 \\ -K_x & cos\hat{\gamma}_D & 0 & 0 & 0 & 0 \\ -K_y & sin\hat{\gamma}_D & 0 & 0 & 0 & 0 \\ 0 & cos(\hat{\gamma}_D - \hat{\gamma}) & 1 & 0 & -1 & 0 \\ 0 & sin(\hat{\gamma}_D - \hat{\gamma}) & 0 & -1 & 0 & 1 \\ 0 & 1 & \sqrt{1 - \left(\frac{\hat{Y}_P^- - \hat{Y}_0^-}{\hat{R}^-}\right)^2} & \frac{\hat{Y}_P^- - \hat{Y}_0^-}{\hat{R}^-} & -\sqrt{1 - \left(\frac{\hat{Y}_P^- - \hat{Y}_0^-}{\hat{R}^-}\right)^2} & \frac{\hat{Y}_0^- - \hat{Y}_P^-}{\hat{R}^-} \\ 0 & 0 & 1 & 0 & 0 & 0 \\ 0 & 0 & 0 & 1 & 0 & 0 \\ 0 & 0 & 0 & 0 & 0 & 1 \\ 0 & 0 & 0 & 0 & 1 & 0 \\ 0 & 1 & 0 & 0 & 0 & 0 \end{bmatrix} \tag{4.121}$$

and

$$Z = \begin{bmatrix} V_m \\ 0 \\ 0 \\ 0 \\ 0 \\ 0 \\ X_{o_m} \\ Y_{o_m} \\ Y_{P_m} \\ X_{P_m} \\ R_m \end{bmatrix}, \quad \Gamma = \begin{bmatrix} 1 & 0 & 0 & 0 & 0 & 0 & 0 & 0 \\ 0 & 0 & 0 & 0 & -\hat{R}^- sin\hat{\gamma}_D & 0 & 0 & 0 \\ 0 & 0 & 0 & 0 & \hat{R}^- cos\hat{\gamma}_D & 0 & 0 & 0 \\ 0 & 0 & 0 & sin(\hat{\gamma}_D - \hat{\gamma}) & -sin(\hat{\gamma}_D - \hat{\gamma}) & 0 & 0 & 0 \\ 0 & 0 & 0 & -cos(\hat{\gamma}_D - \hat{\gamma}) & cos(\hat{\gamma}_D - \hat{\gamma}) & 0 & 0 & 0 \\ 0 & 0 & 0 & 0 & 0 & 0 & 0 & 0 \\ 0 & 1 & 0 & 0 & 0 & 0 & 0 & 0 \\ 0 & 0 & 1 & 0 & 0 & 0 & 0 & 0 \\ 0 & 0 & 0 & 0 & 0 & 1 & 0 & 0 \\ 0 & 0 & 0 & 0 & 0 & 0 & 1 & 0 \\ 0 & 0 & 0 & 0 & 0 & 0 & 0 & 1 \end{bmatrix}, \quad V = \begin{bmatrix} v_V \\ v_{X_0} \\ v_{Y_0} \\ v_\gamma \\ v_{\gamma_D} \\ v_{Y_P} \\ v_{X_P} \\ v_{R_m} \end{bmatrix} \quad (4.122)$$

The $11 \times 11$ equation error covariance matrix is

$$R = \Gamma \begin{bmatrix} \sigma_V^2 & 0 & 0 & 0 & 0 & 0 & 0 & 0 \\ 0 & \sigma_{X_0}^2 & 0 & 0 & 0 & 0 & 0 & 0 \\ 0 & 0 & \sigma_{Y_0}^2 & 0 & 0 & 0 & 0 & 0 \\ 0 & 0 & 0 & \sigma_\gamma^2 & 0 & 0 & 0 & 0 \\ 0 & 0 & 0 & 0 & \sigma_{\gamma_D}^2 & 0 & 0 & 0 \\ 0 & 0 & 0 & 0 & 0 & \sigma_{Y_P}^2 & 0 & 0 \\ 0 & 0 & 0 & 0 & 0 & 0 & \sigma_{X_P}^2 & 0 \\ 0 & 0 & 0 & 0 & 0 & 0 & 0 & \sigma_{R_m}^2 \end{bmatrix} \Gamma^T \quad (4.123)$$

and rank(R)=8.

***4.3.2.2 Solution to Singular Linear Regression.*** The 6 linear regressions of the form (4.101) for Scenarios 1-6 have an equation error matrix $R$ which is rank deficient. We henceforth refer to the linear regressions (4.102)-(4.104), (4.106)-(4.108), (4.110)-(4.112), (4.113)-(4.115), (4.118)-(4.120), (4.121)-(4.123) for the measurement Scenarios 1-6, respectively, as singular. The solution of singular linear regressions requires the

following

**Theorem 7**

Consider a singular linear regression in the standard form

$$Z = H\theta + \Gamma V \tag{4.124}$$

where the parameter vector $\theta \in \mathcal{R}^n$, the measurement vector $Z \in \mathcal{R}^N$, $H$ is a $N \times n$ regressor matrix of rank $n$, $N \geq n$, and $\Gamma$ is an $N \times l$ noise input matrix. The Gaussian random noise vector $V \in \mathcal{R}^l$, with statistics $V = \mathcal{N}(0, R_1)$, and the equation error covariance matrix

$$R = E\{(\Gamma V)(\Gamma V)^T\} = \Gamma E(VV^T)\Gamma^T = \Gamma R_1 \Gamma^T$$

The $N \times N$ error covariance matrix $R \geq 0$, and $R \not> 0$. Assume that

$$\text{rank}(R){=}m \qquad \text{and} \qquad N - n < m < N$$

The MV parameter estimate is then given by

$$\hat{\theta}_1 = P_{\theta_1}(H_{1,1} - H_{1,2}H_{2,2}^{-1}H_{2,1})^T D^{\frac{1}{2}}(z_1 - H_{1,2}H_{2,2}^{-1})$$

where

$$P_{\theta_1} = \left[(H_{1,1} - H_{1,2}H_{2,2}^{-1}H_{2,1})^T D^{-1}(H_{1,1} - H_{1,2}H_{2,2}^{-1}H_{2,1})\right]^{-1}$$

$$\hat{\theta}_2 = H_{2,2}^{-1}z_2 - H_{2,2}^{-1}H_{2,1}\left[(H_{1,1} - H_{1,2}H_{2,2}^{-1}H_{2,1})^T D^{-1}(H_{1,1} - H_{1,2}H_{2,2}^{-1}H_{2,1})\right]^{-1}. \\ .(H_{1,1} - H_{1,2}H_{2,2}^{-1}H_{2,1})^T D^{-1}(z_1 - H_{1,2}H_{2,2}^{-1}z_2)$$

and

$$P_{\theta_2} = H_{2,2}^{-1}H_{2,1}\left[(H_{1,1} - H_{1,2}H_{2,2}^{-1}H_{2,1})^T D^{-1}(H_{1,1} - H_{1,2}H_{2,2}^{-1}H_{2,1})\right]^{-1} H_{2,1}^T(H_{2,2}^{-1})^T$$

The parameter $\theta$ is partitioned $\theta = \binom{\theta_1}{\theta_2}$, and the matrices $H_{1,1}$, $H_{1,2}$, $H_{2,1}$, $H_{2,2}$ and the orthogonal matrix $D$ are specified in Eqs. (4.132), (4.128), (4.134), (4.131) and (4.125), respectively.

PROOF

1. Perform the Singular Value Decomposition [1] (SVD) of the real symmetric positive semidefinite matrix R.

$$R = TST^T$$

where T is an $N \times N$ orthonormal matrix, S is diagonal

$$S = \begin{bmatrix} D & : & 0 \\ \cdots & : & \cdots \\ 0 & : & 0 \end{bmatrix} \tag{4.125}$$

and D is also diagonal. D is an $m \times m$ diagonal sub-matrix of S, with positive elements. Thus,

$$R = T \begin{bmatrix} D^{\frac{1}{2}} & : & 0 \\ \cdots & : & \cdots \\ 0 & : & 0 \end{bmatrix} \begin{bmatrix} D^{\frac{1}{2}} & : & 0 \\ \cdots & : & \cdots \\ 0 & : & 0 \end{bmatrix} T^T = T \begin{bmatrix} D^{\frac{1}{2}} \\ \cdots \\ 0 \end{bmatrix} \begin{bmatrix} D^{\frac{1}{2}} & \vdots & 0 \end{bmatrix} T^T$$

2. Define the Gaussian random vector $W \in \mathcal{R}^N$,

$$W = \begin{bmatrix} D^{-\frac{1}{2}} & : & 0 \\ \cdots & : & \cdots \\ 0 & : & I_{N-m} \end{bmatrix} T^T \Gamma V \tag{4.126}$$

We calculate

$$
\begin{aligned}
E\left\{WW^T\right\} &= \begin{bmatrix} D^{-\frac{1}{2}} & : & 0 \\ \cdots & : & \cdots \\ 0 & : & I_{N-m} \end{bmatrix} T^T E\left\{\Gamma V V^T \Gamma^T\right\} T \begin{bmatrix} D^{-\frac{1}{2}} & : & 0 \\ \cdots & : & \cdots \\ 0 & : & I_{N-m} \end{bmatrix} \\
&= \begin{bmatrix} D^{-\frac{1}{2}} & : & 0 \\ \cdots & : & \cdots \\ 0 & : & I_{N-m} \end{bmatrix} T^T R T \begin{bmatrix} D^{-\frac{1}{2}} & : & 0 \\ \cdots & : & \cdots \\ 0 & : & I_{N-m} \end{bmatrix} \\
&= \begin{bmatrix} D^{-\frac{1}{2}} & : & 0 \\ \cdots & : & \cdots \\ 0 & : & I_{N-m} \end{bmatrix} T^T T \begin{bmatrix} D^{\frac{1}{2}} & : & 0 \\ \cdots & : & \cdots \\ 0 & : & 0 \end{bmatrix} \begin{bmatrix} D^{\frac{1}{2}} & : & 0 \\ \cdots & : & \cdots \\ 0 & : & 0 \end{bmatrix} T^T T \begin{bmatrix} D^{-\frac{1}{2}} & : & 0 \\ \cdots & : & \cdots \\ 0 & : & I_{N-m} \end{bmatrix} \\
&= \begin{bmatrix} D^{-\frac{1}{2}} & : & 0 \\ \cdots & : & \cdots \\ 0 & : & I_{N-m} \end{bmatrix} \begin{bmatrix} D & : & 0 \\ \cdots & : & \cdots \\ 0 & : & 0 \end{bmatrix} \begin{bmatrix} D^{-\frac{1}{2}} & : & 0 \\ \cdots & : & \cdots \\ 0 & : & I_{N-m} \end{bmatrix} \\
&= \begin{bmatrix} I_m & : & 0 \\ \cdots & : & \cdots \\ 0 & : & 0 \end{bmatrix}
\end{aligned}
$$

Hence, we conclude that

$$
W = \begin{bmatrix} w_1 \\ \cdots \\ 0 \end{bmatrix}
$$

where

$$
w_1 \in \mathcal{R}^m
$$

and

$$
w_1 = \mathcal{N}(0, I_m)
$$

3. Multiply the linear regression (4.124) from the left by the matrix

$$\begin{bmatrix} D^{-\frac{1}{2}} & : & 0 \\ \cdots & : & \cdots \\ 0 & : & I_{N-m} \end{bmatrix} T^T$$

Thus, we obtain

$$\begin{bmatrix} D^{-\frac{1}{2}} & : & 0 \\ \cdots & : & \cdots \\ 0 & : & I_{N-m} \end{bmatrix} T^T Z = \begin{bmatrix} D^{-\frac{1}{2}} & : & 0 \\ \cdots & : & \cdots \\ 0 & : & I_{N-m} \end{bmatrix} T^T H\theta + W$$

Define the partitioned vector

$$T^T Z = \begin{bmatrix} z_1 \\ \cdots \\ z_2 \end{bmatrix} \tag{4.127}$$

and the partitioned matrix

$$T^T H = \begin{bmatrix} H_1 \\ \cdots \\ H_2 \end{bmatrix} \tag{4.128}$$

where $z_1 \in \mathcal{R}^m$, $z_2 \in \mathcal{R}^{N-m}$, $H_1$ is an $m \times n$ matrix, and $H_2$ is an $(N-m) \times n$ matrix.

Hence, we have obtained the reduced order non-singular standard linear regression

$$D^{-\frac{1}{2}} z_1 = D^{-\frac{1}{2}} H_1 \theta + w_1, \qquad E\{w_1 w_1^T\} = I_m \tag{4.129}$$

and a set of $N-m$ linear equality constraints

$$z_2 = H_2 \theta \tag{4.130}$$

4. Without loss of generality, partition $H_2$ as follows:

$$H_2 = \left[ H_{2,1} \vdots H_{2,2} \right] \tag{4.131}$$

where $H_{2,2}$ is an $(N-m) \times (N-m)$ non-singular matrix.

Similarly, partition the vector

$$\theta = \begin{bmatrix} \theta_1 \\ \dots \\ \theta_2 \end{bmatrix} \tag{4.132}$$

where $\theta_2 \in \mathcal{R}^{N-m}$. With this notation, the linear system (4.130) is

$$z_2 = H_{2,1}\theta_1 + H_{2,2}\theta_2$$

and, backing out $\theta_2$, we obtain

$$\theta_2 = H_{2,2}^{-1} z_2 - H_{2,2}^{-1} H_{2,1} \theta_1 \tag{4.133}$$

5. Similar to $H_2$, partition $H_1$ as follows

$$H_1 = \left[ H_{1,1} \vdots H_{1,2} \right] \tag{4.134}$$

where $H_{1,1}$ is an $m \times (n+m-N)$ matrix, and $H_{1,2}$ is an $m \times (N-m)$ matrix.

Thus, the linear regression (4.129) is

$$z_1 = H_{1,1}\theta_1 + H_{1,2}\theta_2 + D^{\frac{1}{2}} w_1 \tag{4.135}$$

Inserting Eq. (4.133) into Eq. (4.135) yields the reduced linear regression

$$\underbrace{z_1 - H_{1,2}H_{2,2}^{-1} z_2}_{\mathbf{Z}} = \underbrace{\left(H_{1,1} - H_{1,2}H_{2,2}^{-1}H_{2,1}\right)}_{\mathbf{H}} \theta_1 + \underbrace{D^{\frac{1}{2}} w_1}_{\mathbf{V}} \tag{4.136}$$

where the equation error matrix is

$$R = E\{D^{\frac{1}{2}} w_1 w_1^T D^{\frac{1}{2}}\} = D \tag{4.137}$$

6. Finally, assume that

$$rank(H_{1,1} - H_{1,2}H_{2,2}^{-1}H_{2,1}) = n + m - N$$

and apply the standard MV estimation formulae (4.16) and (4.17) to the linear regression (4.136)

We obtain

$$\hat{\theta}_1 = P_{\theta_1}(H_{1,1} - H_{1,2}H_{2,2}^{-1}H_{2,1})^T D^{\frac{1}{2}}(z_1 - H_{1,2}H_{2,2}^{-1}) \tag{4.138}$$

where

$$P_{\theta_1} = \left[(H_{1,1} - H_{1,2}H_{2,2}^{-1}H_{2,1})^T D^{-1}(H_{1,1} - H_{1,2}H_{2,2}^{-1}H_{2,1})\right]^{-1} \tag{4.139}$$

Using Eq. (4.133), obtain

$$\hat{\theta}_2 = H_{2,2}^{-1}z_2 - H_{2,2}^{-1}H_{2,1}\left[(H_{1,1} - H_{1,2}H_{2,2}^{-1}H_{2,1})^T D^{-1}(H_{1,1} - H_{1,2}H_{2,2}^{-1}H_{2,1})\right]^{-1}. \\ .(H_{1,1} - H_{1,2}H_{2,2}^{-1}H_{2,1})^T D^{-1}(z_1 - H_{1,2}H_{2,2}^{-1}z_2) \tag{4.140}$$

and

$$P_{\theta_2} = H_{2,2}^{-1}H_{2,1}\left[(H_{1,1} - H_{1,2}H_{2,2}^{-1}H_{2,1})^T D^{-1}(H_{1,1} - H_{1,2}H_{2,2}^{-1}H_{2,1})\right]^{-1}. \\ .H_{2,1}^T(H_{2,2}^{-1})^T \tag{4.141}$$

□

The above derivation is summarized in the following algorithm.

SINGULAR LINEAR REGRESSION ALGORITHM

Consider the singular linear regression (4.124). Assume $n \leq N$ and $N > m > N - n \geq 0$.

1. Perform the SVD of R and obtain the $N \times N$ orthonormal matrix T and $m \times m$ diagonal matrix D with positive elements.

2. Form the vectors $z_1$, $z_2$, and the matrices $H_{1,1}$, $H_{1,2}$, $H_{2,1}$, and $H_{2,2}$ as in Eqs. (4.127), (4.128), (4.134), and (4.131).
   Assume

$$\begin{aligned} rank(H_{2,2}) &= N - m \\ rank(H_{1,1} - H_{1,2}H_{2,2}^{-1}H_{2,1}) &= n + m - N \end{aligned}$$

3. The MV parameter estimate and estimation error covariance are given by formulae (4.138) - (4.141).

□

***4.3.2.3 Simulation Results.*** The number of bearing measurements N is 10. For each of the Scenarios 1 - 6, $N_{MC} = 5000$ MC runs are performed. The following statistics are obtained:

The experimentally obtained mean error (bias) in the parameter estimate $\hat{\theta}$ (after aiding) is

$$\bar{e}_{\hat{\theta}^+} = \frac{1}{N_{MC}} \sum_{i=1}^{N_{MC}} (\hat{\theta}_i^+ - \theta) \tag{4.142}$$

where $\hat{\theta}_i^+$ is the parameter estimate in the i th MC experiment.

The experimentally obtained standard deviation of the parameter estimate (after aiding) is calculated according to

$$\hat{\sigma}_{E_\theta}^+ = \sqrt{\frac{\sum_{i=1}^{N_{MC}} (\hat{\theta}_i^+ - \theta)^2}{N_{MC} - 1}} \tag{4.143}$$

The predicted parameter estimation error variance (after aiding) is

$$\hat{\sigma}_{\theta}^{+} = \begin{bmatrix} \sqrt{P_{11}^{+}} & \cdots \\ \vdots & \ddots \end{bmatrix} \tag{4.144}$$

Finally, the experimentally obtained probability of the $i$-th parameter component estimate being within a 1-$\sigma$ distance from the true parameter is calculated as follows.

$$P_{E_{1-\sigma}} = \frac{\text{Number of times } \left( |\hat{\theta}_i^{+} - \theta| \leq \hat{\sigma}_{\theta}^{+} \right)}{N_{MC}} \tag{4.145}$$

***Scenario 1.*** The statistics for Scenario 1 as a function of altitude and airspeed, respectively, are shown in Tables 4.27 and 4.28. It is observed that the estimation performance is completely dependent on the accuracy of the measurement provided by the (unaided) INS. Thus, the own-ship position estimates $\hat{X}_0^{+}$ and $\hat{Y}_0^{+}$ are very close to the unaided values of these parameters ($\hat{X}_0^{-}$ and $\hat{Y}_0^{-}$), and the predicted estimation error variances of $\hat{X}_0^{+}$ and $\hat{Y}_0^{+}$ are close to the measurement error variances of the (unaided) INS. This means that there is no significant improvement in own-ship position estimate accuracy. Moreover, the positional estimation accuracy is directly reflected in geo-location performance; that is, geo-location accuracy is as good as the unaided INS provided position accuracy. The aircraft altitude estimate's accuracy decreases when the flight altitude increases, whereas the predicted altitude estimation error variance does not increase. It means that altitude estimation performance in measurement Scenario 1 is poor. The same applies to slant range to the point P estimation accuracy, even though the predicted and experimental estimation error variance errors are close, which is good. The active Air-to-Ground Ranging (AGR) modes that are currently used for slant range estimation yield better accuracy, as required for air-to-ground delivery.

Similarly, the aircraft's velocity estimate's standard deviation variance in all flight conditions is about 2.5 feet/sec. This is equal to the value prior to aiding. Contrary to the trend brought about by altitude increase, any increase in the aircraft's velocity renders the estimates $\hat{Y}_P$ and $\hat{R}$ more accurate; but even at the best flight condition,

Table 4.27 Estimation performance as a function of altitude - Scenario 1.

| | $h$ [ft] | 1000 | 3,000 | 6,000 | 10,000 | 15,000 | 20,000 |
|---|---|---|---|---|---|---|---|
| $V$ [ft/sec] | $\bar{e}_{\hat{V}^+}$ | 0.008 | 0.043 | 0.226 | 1.769 | 7.974 | 0.04 |
| | $\hat{\sigma}^+_{E_V}$ | 2.458 | 2.518 | 2.508 | 2.469 | 2.476 | 2.532 |
| | $\hat{\sigma}^+_V$ | 2.499 | 2.499 | 2.499 | 2.498 | 2.488 | 2.499 |
| | $P_{E_{1-\sigma}}$ | 0.845 | 0.834 | 0.86 | 0.957 | 1.0 | 0.839 |
| $X_0$ [m] | $\bar{e}_{\hat{X}_0^+}$ | 0.01 | 0.008 | 0.028 | 0.011 | 0.007 | 0.009 |
| | $\hat{\sigma}^+_{E_{X_0}}$ | 1480.7 | 1496.8 | 1484.4 | 1464.5 | 1488.1 | 1484.9 |
| | $\hat{\sigma}^+_{X_0}$ | 1481.59 | 1481.59 | 1481.59 | 1481.59 | 1481.59 | 1481.59 |
| | $P_{E_{1-\sigma}}$ | 0.845 | 0.836 | 0.83 | 0.835 | 0.837 | 0.834 |
| $Y_0$ [ft] | $\bar{e}_{\hat{Y}_0^+}$ | 0.201 | 1.379 | 1.471 | 0.708 | 0.228 | 0.441 |
| | $\hat{\sigma}^+_{E_{Y_0}}$ | 76.88 | 75.67 | 76.07 | 74.95 | 74.7 | 75.49 |
| | $\hat{\sigma}^+_{Y_0}$ | 75 | 75 | 75 | 75 | 75 | 75 |
| | $P_{E_{1-\sigma}}$ | 0.838 | 0.83 | 0.837 | 0.84 | 0.839 | 0.838 |
| $X_P$ [m] | $\bar{e}_{\hat{X}_P^+}$ | 9.834 | 7.57 | 27.77 | 0.62 | 63.24 | 8.06 |
| | $\hat{\sigma}^+_{E_{X_P}}$ | 1480.7 | 1496.7 | 1484.3 | 1464.7 | 1487.9 | 1485.1 |
| | $\hat{\sigma}^+_{X_P}$ | 1481.6 | 1481.6 | 1481.6 | 1481.7 | 1481.8 | 1481.9 |
| | $P_{E_{1-\sigma}}$ | 0.845 | 0.836 | 0.83 | 0.837 | 0.849 | 0.832 |
| $Y_P$ [ft] | $\bar{e}_{\hat{Y}_P^+}$ | 0.172 | 1.241 | 3.036 | 24.43 | 156.3 | 4.03 |
| | $\hat{\sigma}^+_{E_{Y_P}}$ | 77.07 | 78.49 | 84.02 | 105.54 | 125.05 | 189.32 |
| | $\hat{\sigma}^+_{Y_P}$ | 75.06 | 75.59 | 77.31 | 81.2 | 88.18 | 97.29 |
| | $P_{E_{1-\sigma}}$ | 0.833 | 0.831 | 0.816 | 0.7 | 0.296 | 0.687 |
| $R$ [ft] | $\bar{e}_{\hat{R}^+}$ | 0.03 | 0.41 | 3.67 | 45.24 | 278.5 | 6.06 |
| | $\hat{\sigma}^+_{E_R}$ | 8.16 | 24.29 | 45.79 | 78.02 | 103.2 | 165.1 |
| | $\hat{\sigma}^+_R$ | 7.99 | 22.16 | 39.9 | 62.36 | 85.45 | 121.02 |
| | $P_{E_{1-\sigma}}$ | 0.834 | 0.827 | 0.823 | 0.914 | 0.99 | 0.779 |

Table 4.28 Estimation performance as a function of airspeed - Scenario 1.

| | $Vel$ [M] | 0.5 | 0.6 | 0.7 | 0.8 | 0.9 | 1.0 |
|---|---|---|---|---|---|---|---|
| $V$ [ft/sec] | $\bar{e}_{\hat{V}^+}$ | 0.005 | 0.007 | 0.031 | 0.014 | 0.017 | 0.015 |
| | $\hat{\sigma}^+_{E_V}$ | 2.484 | 2.543 | 2.464 | 2.536 | 2.491 | 2.505 |
| | $\hat{\sigma}^+_V$ | 2.499 | 2.499 | 2.499 | 2.498 | 2.488 | 2.499 |
| | $P_{E_{1-\sigma}}$ | 0.845 | 0.84 | 0.844 | 0.842 | 0.846 | 0.843 |
| $X_0$ [m] | $\bar{e}_{\hat{X}_0^+}$ | 15.05 | 10.65 | 32.41 | 1.511 | 3.637 | 14.5 |
| | $\hat{\sigma}^+_{E_{X_0}}$ | 1473.6 | 1475.9 | 1462.1 | 1473.5 | 1487.2 | 1473.2 |
| | $\hat{\sigma}^+_{X_0}$ | 1481.59 | 1481.59 | 1481.59 | 1481.59 | 1481.59 | 1481.59 |
| | $P_{E_{1-\sigma}}$ | 0.837 | 0.833 | 0.847 | 0.844 | 0.841 | 0.834 |
| $Y_0$ [ft] | $\bar{e}_{\hat{Y}_0^+}$ | 0.12 | 0.49 | 0.302 | 0.609 | 1.72 | 0.108 |
| | $\hat{\sigma}^+_{E_{Y_0}}$ | 75.11 | 76.3 | 74.88 | 76.51 | 74.43 | 74.77 |
| | $\hat{\sigma}^+_{Y_0}$ | 75 | 75 | 75 | 75 | 75 | 75 |
| | $P_{E_{1-\sigma}}$ | 0.844 | 0.835 | 0.844 | 0.834 | 0.836 | 0.845 |
| $X_P$ [m] | $\bar{e}_{\hat{X}_P^+}$ | 8.78 | 16.97 | 65.96 | 16.28 | 43.99 | 6.92 |
| | $\hat{\sigma}^+_{E_{X_P}}$ | 1560.6 | 1561.2 | 1577.5 | 1519.8 | 1646.8 | 1540.8 |
| | $\hat{\sigma}^+_{X_P}$ | 1481.6 | 1481.6 | 1481.6 | 1481.7 | 1481.8 | 1481.9 |
| | $P_{E_{1-\sigma}}$ | 0.837 | 0.834 | 0.849 | 0.845 | 0.843 | 0.835 |
| $Y_P$ [ft] | $\bar{e}_{\hat{Y}_P^+}$ | 0.434 | 0.576 | 0.733 | 0.372 | 1.54 | 0.141 |
| | $\hat{\sigma}^+_{E_{Y_P}}$ | 79.64 | 79.05 | 78.00 | 78.87 | 76.27 | 76.45 |
| | $\hat{\sigma}^+_{Y_P}$ | 76.47 | 76.03 | 75.76 | 75.58 | 75.46 | 75.37 |
| | $P_{E_{1-\sigma}}$ | 0.83 | 0.83 | 0.832 | 0.825 | 0.831 | 0.841 |
| $R$ [ft] | $\bar{e}_{\hat{R}^+}$ | 0.396 | 0.048 | 0.64 | 0.118 | 0.03 | 0.08 |
| | $\hat{\sigma}^+_{E_R}$ | 38.72 | 31.96 | 27.52 | 24.27 | 21.22 | 19.13 |
| | $\hat{\sigma}^+_R$ | 35.36 | 29.47 | 25.29 | 22.14 | 19.71 | 17.71 |
| | $P_{E_{1-\sigma}}$ | 0.826 | 0.826 | 0.827 | 0.817 | 0.82 | 0.818 |

the achieved accuracy is close the unaided accuracy. In all experiments, the empirically obtained probability of the estimates falling within a predicted 1-$\sigma$ of the true parameters is above 80 %.

In conclusion, Scenario 1 represents the basic measurement situation which relies on passive measurements only, does not use and/or require the ground object's position and additional range measurement, and no electro-magnetic energy is transmitted and/or received. An improvement in aircraft's angular navigation variables estimates is obtained. However, as for the positional navigation variables, this tactically advantageous measurement scenario does not yield good INS aiding.

***Scenario 2.*** The estimation performance in measurement Scenario 2 as a function of altitude is documented in Table 4.29 , and as a function of airspeed in Table 4.30. We expect to observe an enhancement in estimation performance because of the inclusion of *prior* information on the altitude of the ground object. Indeed, the estimate $\hat{Y}_P^+$ has an experimental $\sigma$ of 60 feet, although the uncertainty in the *prior* information is 100 feet. The own-ship altitude estimate $\hat{Y}_0^+$ is also improved, e.g., we obtain an experimental 1-$\sigma$ of 60 feet versus the pre-aiding $\sigma$ of 75 feet. Enhancements in the estimation accuracy of $V$, $X_0$ and $X_P$ are not significant. The slant range to the point P estimation performance is better than in Scenario 1; however, its accuracy is still not comparable to the AGR modes' accuracy. As before, an increase in velocity and/or decrease in altitude result in better estimation performance. Moreover, the $\hat{Y}_P$ and $\hat{R}$ estimation performance deterioration induced by an increase in altitude is now mitigated. Contrary to previous observations however, an increase in altitude and/or decrease in the aircraft's velocity make the estimation performance slightly more accurate than other parameters' estimation accuracy.

The effect of inclusion of more accurate $Y_P$ information is analyzed in Table 4.31. The accuracy of the ground object's *prior* altitude information does not have a significant effect on the $\hat{V}^+$, $\hat{X}_0^+$, $\hat{X}_P^+$, and $\hat{R}^+$ estimates. The estimation performance of $\hat{Y}_0^+$ and $\hat{Y}_P^+$, however, reflects the accuracy afforded by the augmented measurement.

Table 4.29 Estimation performance as a function of altitude - Scenario 2.

| | $h$ [ft] | 1000 | 3,000 | 6,000 | 10,000 | 15,000 | 20,000 |
|---|---|---|---|---|---|---|---|
| $V$ [ft/sec] | $\bar{e}_{\hat{Y}^+}$ | 0.0002 | 0.026 | 0.025 | 0.04 | 0.016 | 0.026 |
| | $\hat{\sigma}^+_{E_V}$ | 2.502 | 2.518 | 2.466 | 2.414 | 2.395 | 2.45 |
| | $\hat{\sigma}^+_V$ | 2.499 | 2.493 | 2.472 | 2.426 | 2.344 | 2.232 |
| | $P_{E_{1-\sigma}}$ | 0.842 | 0.828 | 0.841 | 0.847 | 0.836 | 0.817 |
| $X_0$ [m] | $\bar{e}_{\hat{X}_0^+}$ | 15.64 | 30.07 | 0.78 | 3.06 | 1.15 | 10.05 |
| | $\hat{\sigma}^+_{E_{X_0}}$ | 1471.1 | 1481.1 | 1482.2 | 1447.6 | 1479.3 | 1462.2 |
| | $\hat{\sigma}^+_{X_0}$ | 1481.59 | 1481.59 | 1481.59 | 1481.59 | 1481.59 | 1481.59 |
| | $P_{E_{1-\sigma}}$ | 0.847 | 0.839 | 0.84 | 0.84 | 0.838 | 0.844 |
| $Y_0$ [ft] | $\bar{e}_{\hat{Y}_0^+}$ | 0.433 | 1.386 | 0.255 | 1.218 | 1.66 | 0.454 |
| | $\hat{\sigma}^+_{E_{Y_0}}$ | 60.74 | 61.68 | 60.66 | 64.21 | 68.65 | 74.27 |
| | $\hat{\sigma}^+_{Y_0}$ | 60.01 | 60.09 | 60.37 | 60.97 | 62.00 | 63.32 |
| | $P_{E_{1-\sigma}}$ | 0.836 | 0.828 | 0.843 | 0.831 | 0.807 | 0.803 |
| $X_P$ [m] | $\bar{e}_{\hat{X}_P^+}$ | 29.18 | 8.67 | 1.04 | 3.29 | 0.98 | 10.33 |
| | $\hat{\sigma}^+_{E_{X_P}}$ | 1518.1 | 1567.8 | 1482.3 | 1447.5 | 1479.4 | 1463.1 |
| | $\hat{\sigma}^+_{X_P}$ | 1481.6 | 1481.6 | 1481.6 | 1481.7 | 1481.7 | 1481.8 |
| | $P_{E_{1-\sigma}}$ | 0.847 | 0.839 | 0.841 | 0.842 | 0.837 | 0.844 |
| $Y_P$ [ft] | $\bar{e}_{\hat{Y}_P^+}$ | 0.425 | 1.479 | 0.361 | 2.19 | 2.238 | 0.247 |
| | $\hat{\sigma}^+_{E_{Y_P}}$ | 60.72 | 62.65 | 63.66 | 72.94 | 83.25 | 95.97 |
| | $\hat{\sigma}^+_{Y_P}$ | 60.03 | 60.3 | 61.16 | 63.04 | 66.13 | 69.97 |
| | $P_{E_{1-\sigma}}$ | 0.837 | 0.823 | 0.833 | 0.798 | 0.778 | 0.765 |
| $R$ [ft] | $\bar{e}_{\hat{R}^+}$ | 0.022 | 0.013 | 0.94 | 2.27 | 0.66 | 0.61 |
| | $\hat{\sigma}^+_{E_R}$ | 8.33 | 24.95 | 42.8 | 68.13 | 90.94 | 115.2 |
| | $\hat{\sigma}^+_R$ | 7.99 | 22.09 | 39.49 | 60.48 | 82.77 | 105.72 |
| | $P_{E_{1-\sigma}}$ | 0.831 | 0.81 | 0.834 | 0.823 | 0.81 | 0.82 |

In conclusion, the inclusion of *prior* information on the ground object's altitude does not significantly help INS aiding. Note however that in Scenario 2, we are still exclusively using passive measurements only, and we still assume the ground object's position is unknown. Hence, the main advantage achieved in Scenario 2 compared to Scenario 1 is an improvement in the $\hat{Y}_0^+$ and $\hat{Y}_P^+$ estimates.

Table 4.30 Estimation performance as a function of airspeed - Scenario 2.

| | $Vel$ [M] | 0.5 | 0.6 | 0.7 | 0.8 | 0.9 | 1.0 |
|---|---|---|---|---|---|---|---|
| $V$ [ft/sec] | $\bar{e}_{\hat{V}^+}$ | 0.029 | 0.017 | 0.027 | 0.011 | 0.054 | 0.014 |
| | $\hat{\sigma}^+_{E_V}$ | 2.494 | 2.462 | 2.519 | 2.527 | 2.508 | 2.49 |
| | $\hat{\sigma}^+_V$ | 2.482 | 2.487 | 2.49 | 2.493 | 2.494 | 2.496 |
| | $P_{E_{1-\sigma}}$ | 0.836 | 0.84 | 0.84 | 0.838 | 0.845 | 0.844 |
| $X_0$ [m] | $\bar{e}_{\hat{X}_0^+}$ | 12.54 | 5.71 | 8.0 | 22.43 | 15.63 | 6.33 |
| | $\hat{\sigma}^+_{E_{X_0}}$ | 1472.6 | 1468.6 | 1498.2 | 1502.2 | 1495.4 | 1469.6 |
| | $\hat{\sigma}^+_{X_0}$ | 1481.59 | 1481.56 | 1481.59 | 1481.59 | 1481.56 | 1481.59 |
| | $P_{E_{1-\sigma}}$ | 0.841 | 0.843 | 0.841 | 0.833 | 0.839 | 0.847 |
| $Y_0$ [ft] | $\bar{e}_{\hat{Y}_0^+}$ | 0.42 | 1.547 | 0.966 | 0.246 | 0.804 | 1.07 |
| | $\hat{\sigma}^+_{E_{Y_0}}$ | 60.14 | 61.09 | 60.87 | 60.05 | 60.18 | 59.82 |
| | $\hat{\sigma}^+_{Y_0}$ | 60.24 | 60.17 | 60.12 | 60.09 | 60.07 | 60.06 |
| | $P_{E_{1-\sigma}}$ | 0.842 | 0.834 | 0.844 | 0.845 | 0.841 | 0.835 |
| $X_P$ [m] | $\bar{e}_{\hat{X}_P^+}$ | 6.19 | 12.91 | 31.18 | 7.86 | 40.12 | 19.33 |
| | $\hat{\sigma}^+_{E_{X_P}}$ | 1535.6 | 1526.4 | 1583.3 | 1545.7 | 1599.0 | 1503.3 |
| | $\hat{\sigma}^+_{X_P}$ | 1481.63 | 1481.58 | 1481.61 | 1481.61 | 1481.59 | 1481.6 |
| | $P_{E_{1-\sigma}}$ | 0.841 | 0.843 | 0.842 | 0.833 | 0.841 | 0.848 |
| $Y_P$ [ft] | $\bar{e}_{\hat{Y}_P^+}$ | 0.254 | 1.191 | 1.205 | 0.786 | .374 | 0.892 |
| | $\hat{\sigma}^+_{E_{Y_P}}$ | 61.33 | 61.95 | 61.71 | 61.52 | 60.77 | 60.64 |
| | $\hat{\sigma}^+_{Y_P}$ | 60.75 | 60.53 | 60.39 | 60.29 | 60.23 | 60.19 |
| | $P_{E_{1-\sigma}}$ | 0.841 | 0.832 | 0.842 | 0.831 | 0.836 | 0.836 |
| $R$ [ft] | $\bar{e}_{\hat{R}^+}$ | 0.253 | 0.382 | 0.327 | 0.487 | 0.586 | 0.161 |
| | $\hat{\sigma}^+_{E_R}$ | 37.23 | 30.66 | 27.8 | 24.9 | 21.93 | 19.41 |
| | $\hat{\sigma}^+_R$ | 35.15 | 29.46 | 25.18 | 22.06 | 19.62 | 17.68 |
| | $P_{E_{1-\sigma}}$ | 0.826 | 0.824 | 0.817 | 0.816 | 0.82 | 0.812 |

Table 4.31 Estimation performance as a function of different measurement errors - Scenario 2. The altitude and velocity are 3,000 feet and 0.8 M, respectively.

| | $\hat{\sigma}^+_{E_V}$[ft/sec] | $\hat{\sigma}^+_{E_{X_0}}$ [m] | $\hat{\sigma}^+_{E_{Y_0}}$ [ft] | $\hat{\sigma}^+_{E_{X_P}}$ [m] | $\hat{\sigma}^+_{E_{Y_P}}$ [ft] | $\hat{\sigma}^+_{E_R}$[ft] |
|---|---|---|---|---|---|---|
| $\sigma_{Y_P^-} = \sigma_{X_P^-} = 100$ ft | 2.47 | 1472.6 | 58.84 | 1529.1 | 59.78 | 24.41 |
| $\sigma_{Y_P^-} = \sigma_{X_P^-} = 50$ ft | 2.41 | 1468.6 | 43.59 | 1535.4 | 41.72 | 24.10 |
| $\sigma_{Y_P^-} = \sigma_{X_P^-} = 10$ ft | 2.46 | 1475.7 | 22.4 | 1562.1 | 9.91 | 24.18 |

***Scenario 3.*** In this scenario, we expect an enhancement in estimation accuracy since we include the slant range to point P measurement in the estimation process. Table 4.32 shows the estimation performance in Scenario 3 as a function of flight altitude. The predicted estimation error variance of the $\hat{X}_0^+$, and $\hat{Y}_0^+$ estimates are equal to the "measurement" error variance of the INS provided measurements because these parameters are uncorrelated with the slant range parameter. Their experimental variances are driven by the unaided INS accuracy. The estimation accuracy of $\hat{Y}_P^+$ is determined by the accuracy of $\hat{Y}_0^+$ at low altitudes; it deteriorates as the altitude increases. The velocity estimates are slightly more accurate at the higher altitudes. The slant range measurement makes almost no difference in the slant range to the target estimate at lower altitudes, however it yields a lightly better estimate at higher altitudes.

The estimation performance in Scenario 3 as a function of airspeed is investigated in Table 4.33. The predicted variance of the parameter vector $\theta$ estimation error decreases, which results from an increase in airspeed. The velocity estimation performance shows an opposite trend: the higher the airspeed, the lower the predicted and experimental velocity estimation error variance. The results of the experiments performed for different airspeeds are similar to the altitude results.

The enhancement of the estimation performance when a more accurate slant range measurement is used is evident in Table 4.34. The velocity estimates are improved significantly. The other parameters' estimates also improve, but not significantly. In both the changing altitude and velocity cases, the probability of the parameter estimation error falling within a 1-predicted-$\sigma$ is higher than 80%.

We conclude that in the measurement situation at hand in which the position and altitude of the ground object are not known, the inclusion of the slant range to the ground object measurement in the estimation process does not result in a significant improvement in positional navigation variable estimate and geo-location performance.

Table 4.32 Estimation performance as a function of altitude - Scenario 3.

| | $h$ [ft] | 1000 | 3,000 | 6,000 | 10,000 | 15,000 | 20,000 |
|---|---|---|---|---|---|---|---|
| $V$ [ft/sec] | $\bar{e}_{\hat{V}^+}$ | 0.019 | 0.0016 | 0.012 | 0.01 | 0.023 | 0.038 |
| | $\hat{\sigma}^+_{E_V}$ | 2.530 | 2.484 | 2.444 | 2.389 | 2.337 | 2.199 |
| | $\hat{\sigma}^+_V$ | 2.498 | 2.484 | 2.452 | 2.386 | 2.287 | 2.153 |
| | $P_{E_{1-\sigma}}$ | 0.832 | 0.841 | 0.839 | 0.843 | 0.836 | 0.836 |
| $X_0$ [m] | $\bar{e}_{\hat{X}_0^+}$ | 15.69 | 1.18 | 35.29 | 13.91 | 0.19 | 23.82 |
| | $\hat{\sigma}^+_{E_{X_0}}$ | 1506.6 | 1458.1 | 1481.2 | 1473.3 | 1481.7 | 1468.1 |
| | $\hat{\sigma}^+_{X_0}$ | 1481.59 | 1481.59 | 1481.59 | 1481.59 | 1481.59 | 1481.59 |
| | $P_{E_{1-\sigma}}$ | 0.844 | 0.839 | 0.83 | 0.84 | 0.839 | 0.842 |
| $Y_0$ [ft] | $\bar{e}_{\hat{Y}_0^+}$ | 2.195 | 1.724 | 0.143 | 0.215 | 0.371 | 0.136 |
| | $\hat{\sigma}^+_{E_{Y_0}}$ | 75.42 | 75.46 | 74.91 | 75.46 | 75.7 | 74.55 |
| | $\hat{\sigma}^+_{Y_0}$ | 75 | 75 | 75 | 75 | 75 | 75 |
| | $P_{E_{1-\sigma}}$ | 0.834 | 0.848 | 0.846 | 0.839 | 0.83 | 0.84 |
| $X_P$ [m] | $\bar{e}_{\hat{X}_P^+}$ | 15.69 | 0.682 | 34.89 | 12.78 | 0.32 | 23.99 |
| | $\hat{\sigma}^+_{E_{X_P}}$ | 1506.7 | 1458.6 | 1481.4 | 1474.7 | 1481.8 | 1468.8 |
| | $\hat{\sigma}^+_{X_P}$ | 1481.6 | 1481.6 | 1481.6 | 1481.7 | 1481.7 | 1481.8 |
| | $P_{E_{1-\sigma}}$ | 0.844 | 0.839 | 0.83 | 0.84 | 0.839 | 0.84 |
| $Y_P$ [ft] | $\bar{e}_{\hat{Y}_P^+}$ | 2.29 | 1.697 | 0.359 | 1.88 | 2.27 | 3.3 |
| | $\hat{\sigma}^+_{E_{Y_P}}$ | 75.68 | 78.18 | 83.32 | 100.58 | 124.1 | 150.5 |
| | $\hat{\sigma}^+_{Y_P}$ | 75.06 | 75.57 | 77.22 | 80.73 | 86.34 | 92.57 |
| | $P_{E_{1-\sigma}}$ | 0.833 | 0.837 | 0.823 | 0.783 | 0.754 | 0.725 |
| $R$ [ft] | $\bar{e}_{\hat{R}^+}$ | 0.032 | 0.05 | 0.05 | 1.59 | 2.13 | 1.48 |
| | $\hat{\sigma}^+_{E_R}$ | 8.38 | 24.91 | 43.14 | 69.21 | 94.11 | 118.96 |
| | $\hat{\sigma}^+_R$ | 7.99 | 22.07 | 39.11 | 59.73 | 80.69 | 101.64 |
| | $P_{E_{1-\sigma}}$ | 0.827 | 0.815 | 0.819 | 0.813 | 0.812 | 0.807 |

Table 4.33 Estimation performance as a function of airspeed - Scenario 3.

| | $Vel$ [M] | 0.5 | 0.6 | 0.7 | 0.8 | 0.9 | 1.0 |
|---|---|---|---|---|---|---|---|
| $V$ [ft/sec] | $\bar{e}_{\hat{V}^+}$ | 0.002 | 0.016 | 0.003 | 0.021 | 0.063 | 0.018 |
| | $\hat{\sigma}^+_{E_V}$ | 2.44 | 2.492 | 2.509 | 2.506 | 2.475 | 2.495 |
| | $\hat{\sigma}^+_V$ | 2.461 | 2.473 | 2.48 | 2.484 | 2.488 | 2.49 |
| | $P_{E_{1-\sigma}}$ | 0.84 | 0.841 | 0.837 | 0.842 | 0.834 | 0.845 |
| $X_0$ [m] | $\bar{e}_{\hat{X}_0^+}$ | 23.18 | 10.05 | 4.55 | 8.15 | 5.38 | 28.0 |
| | $\hat{\sigma}^+_{E_{X_0}}$ | 1499.6 | 1479.5 | 1478.6 | 1465.0 | 1488.9 | 1465.1 |
| | $\hat{\sigma}^+_{X_0}$ | 1481.59 | 1481.59 | 1481.59 | 1481.59 | 1481.59 | 1481.59 |
| | $P_{E_{1-\sigma}}$ | 0.834 | 0.845 | 0.845 | 0.84 | 0.838 | 0.841 |
| $Y_0$ [ft] | $\bar{e}_{\hat{Y}_0^+}$ | 0.486 | 0.996 | 0.46 | 2.324 | 0.1 | 0.704 |
| | $\hat{\sigma}^+_{E_{Y_0}}$ | 73.72 | 74.87 | 74.43 | 75.41 | 73.93 | 74.23 |
| | $\hat{\sigma}^+_{Y_0}$ | 75 | 75 | 75 | 75 | 75 | 75 |
| | $P_{E_{1-\sigma}}$ | 0.841 | 0.842 | 0.837 | 0.851 | 0.841 | 0.836 |
| $X_P$ [m] | $\bar{e}_{\hat{X}_P^+}$ | 21.56 | 13.04 | 3.12 | 5.89 | 4.743 | 27.86 |
| | $\hat{\sigma}^+_{E_{X_P}}$ | 1502.5 | 1493.1 | 1481.3 | 1471.5 | 1489.0 | 1465.2 |
| | $\hat{\sigma}^+_{X_P}$ | 1481.6 | 1481.6 | 1481.6 | 1481.6 | 1481.6 | 1481.6 |
| | $P_{E_{1-\sigma}}$ | 0.833 | 0.845 | 0.845 | 0.839 | 0.839 | 0.841 |
| $Y_P$ [ft] | $\bar{e}_{\hat{Y}_P^+}$ | 0.89 | 0.638 | 0.198 | 2.097 | 0.058 | 0.926 |
| | $\hat{\sigma}^+_{E_{Y_P}}$ | 77.46 | 77.81 | 77.44 | 78.3 | 76.28 | 76.06 |
| | $\hat{\sigma}^+_{Y_P}$ | 76.45 | 76.01 | 75.75 | 75.58 | 75.46 | 75.37 |
| | $P_{E_{1-\sigma}}$ | 0.834 | 0.834 | 0.831 | 0.841 | 0.838 | 0.829 |
| $R$ [ft] | $\bar{e}_{\hat{R}^+}$ | 0.047 | 0.024 | 0.062 | 0.263 | 0.306 | 0.388 |
| | $\hat{\sigma}^+_{E_R}$ | 36.82 | 31.04 | 27.89 | 24.8 | 21.72 | 19.42 |
| | $\hat{\sigma}^+_R$ | 34.95 | 29.3 | 25.06 | 22.06 | 19.61 | 17.67 |
| | $P_{E_{1-\sigma}}$ | 0.829 | 0.829 | 0.813 | 0.821 | 0.809 | 0.823 |

Table 4.34 Estimation performance as a function of different measurement errors - Scenario 3. The altitude and velocity are 3,000 feet and 0.8 M, respectively.

| | $\hat{\sigma}^+_{E_V}$[ft/sec] | $\hat{\sigma}^+_{E_{X_0}}$ [m] | $\hat{\sigma}^+_{E_{Y_0}}$ [ft] | $\hat{\sigma}^+_{E_{X_P}}$ [m] | $\hat{\sigma}^+_{E_{Y_P}}$ [ft] | $\hat{\sigma}^+_{E_R}$[ft] |
|---|---|---|---|---|---|---|
| $\sigma_{R^-} = 200$ ft | 2.464 | 1502.2 | 72.22 | 1502.4 | 75.37 | 24.29 |
| $\sigma_{R^-} = 100$ ft | 2.422 | 1495.5 | 73.61 | 1496.2 | 76.2 | 23.91 |
| $\sigma_{R^-} = 20$ ft | 1.79 | 1469.64 | 72.66 | 1522.7 | 74.72 | 15.25 |

***Scenario 4.*** The estimation performance statistics for Scenario 4 are given in Tables 4.35, 4.36, and 4.37. A general observation concerning these results is that the inclusion of the *prior* altitude information on the ground object and the slant range measurement yield estimation performance consistent with the advantages of both measurement Scenarios 2 and 3. The 75 feet 1-$\sigma$ own-ship altitude error is reduced to 60 feet. The $X$-position estimate of the aircraft has still the same deviation from the true $X$-position as in the unaided case. The estimation accuracy of $X_P$ closely tracks the estimation accuracy of $X_0$. The velocity estimate stays unchanged. The ground object altitude estimate $\hat{Y}_P^+$ shows an improvement similar to that of $\hat{Y}_0^+$, and the slant range to the ground object estimate also improves.

Table 4.35 Estimation performance as a function of altitude - Scenario 4.

| | $h$ [ft] | 1000 | 3,000 | 6,000 | 10,000 | 15,000 | 20,000 |
|---|---|---|---|---|---|---|---|
| $V$ [ft/sec] | $\bar{e}_{\hat{V}^+}$ | 0.027 | 0.042 | 0.055 | 0.034 | 0.034 | 0.081 |
| | $\hat{\sigma}^+_{E_V}$ | 2.483 | 2.551 | 2.417 | 2.375 | 2.231 | 2.133 |
| | $\hat{\sigma}^+_V$ | 2.488 | 2.484 | 2.426 | 2.32 | 2.188 | 2.045 |
| | $P_{E_{1-\sigma}}$ | 0.843 | 0.839 | 0.846 | 0.84 | 0.843 | 0.827 |
| $X_0$ [m] | $\bar{e}_{\hat{X}_0^+}$ | 6.07 | 9.79 | 8.62 | 21.16 | 24.17 | 21.69 |
| | $\hat{\sigma}^+_{E_{X_0}}$ | 1479.6 | 1507.7 | 1492.2 | 1491.8 | 1481.5 | 1463.1 |
| | $\hat{\sigma}^+_{X_0}$ | 1481.59 | 1481.59 | 1481.59 | 1481.59 | 1481.59 | 1481.59 |
| | $P_{E_{1-\sigma}}$ | 0.844 | 0.837 | 0.842 | 0.837 | 0.8379 | 0.836 |
| $Y_0$ [ft] | $\bar{e}_{\hat{Y}_0^+}$ | 0.142 | 0.558 | 1.065 | 0.404 | 0.554 | 0.668 |
| | $\hat{\sigma}^+_{E_{Y_0}}$ | 59.25 | 59.97 | 60.56 | 63.25 | 65.61 | 66.11 |
| | $\hat{\sigma}^+_{Y_0}$ | 60.04 | 60.07 | 60.35 | 60.91 | 61.8 | 62.75 |
| | $P_{E_{1-\sigma}}$ | 0.846 | 0.842 | 0.835 | 0.835 | 0.824 | 0.836 |
| $X_P$ [m] | $\bar{e}_{\hat{X}_P^+}$ | 6.17 | 10.0 | 10.13 | 17.04 | 21.44 | 20.12 |
| | $\hat{\sigma}^+_{E_{X_P}}$ | 1479.5 | 1507.7 | 1493.2 | 1508.1 | 1492.5 | 1465.5 |
| | $\hat{\sigma}^+_{X_P}$ | 1481.6 | 1481.6 | 1481.6 | 1481.7 | 1481.7 | 1481.7 |
| | $P_{E_{1-\sigma}}$ | 0.844 | 0.838 | 0.842 | 0.837 | 0.837 | 0.837 |
| $Y_P$ [ft] | $\bar{e}_{\hat{Y}_P^+}$ | 0.62 | 0.244 | 0.375 | 0.033 | 1.49 | 0.457 |
| | $\hat{\sigma}^+_{E_{Y_P}}$ | 59.62 | 60.76 | 63.27 | 70.83 | 75.96 | 78.44 |
| | $\hat{\sigma}^+_{Y_P}$ | 60.14 | 60.23 | 61.1 | 62.82 | 65.43 | 68.32 |
| | $P_{E_{1-\sigma}}$ | 0.842 | 0.84 | 0.83 | 0.817 | 0.798 | 0.806 |
| $R$ [ft] | $\bar{e}_{\hat{R}^+}$ | 0.39 | 0.32 | 1.06 | 1.61 | 1.75 | 1.44 |
| | $\hat{\sigma}^+_{E_R}$ | 17.69 | 20.07 | 41.25 | 63.88 | 75.87 | 84.33 |
| | $\hat{\sigma}^+_R$ | 16.67 | 18.22 | 38.68 | 57.94 | 71.35 | 81.04 |
| | $P_{E_{1-\sigma}}$ | 0.828 | 0.817 | 0.832 | 0.825 | 0.826 | 0.836 |

The measurement Scenario 4 is investigated for different altitudes in Table 4.35. Except the velocity estimate, all the other parameter estimates are better at low altitudes. The velocity estimate's predicted and experimental $\sigma$ decreases as the altitude increases.

Table 4.36 Estimation performance as a function of airspeed - Scenario 4.

| | $Vel$ [M] | 0.5 | 0.6 | 0.7 | 0.8 | 0.9 | 1.0 |
|---|---|---|---|---|---|---|---|
| $V$ [ft/sec] | $\bar{e}_{\hat{V}^+}$ | 0.053 | 0.026 | 0.071 | 0.038 | 0.046 | 0.006 |
| | $\hat{\sigma}^+_{E_V}$ | 2.461 | 2.464 | 2.521 | 2.485 | 2.466 | 2.46 |
| | $\hat{\sigma}^+_V$ | 2.444 | 2.461 | 2.471 | 2.478 | 2.482 | 2.486 |
| | $P_{E_{1-\sigma}}$ | 0.849 | 0.839 | 0.845 | 0.845 | 0.847 | 0.848 |
| $X_0$ [m] | $\bar{e}_{\hat{X}_0^+}$ | 32.62 | 5.09 | 15.58 | 17.77 | 0.149 | 26.85 |
| | $\hat{\sigma}^+_{E_{X_0}}$ | 1498.7 | 1467.0 | 1475.9 | 1479.6 | 1453.5 | 1492.1 |
| | $\hat{\sigma}^+_{X_0}$ | 1481.59 | 1481.59 | 1481.59 | 1481.59 | 1481.59 | 1481.59 |
| | $P_{E_{1-\sigma}}$ | 0.839 | 0.846 | 0.849 | 0.845 | 0.845 | 0.837 |
| $Y_0$ [ft] | $\bar{e}_{\hat{Y}_0^+}$ | 0.123 | 0.436 | 1.154 | 0.226 | 1.594 | 0.863 |
| | $\hat{\sigma}^+_{E_{Y_0}}$ | 60.64 | 60.27 | 59.41 | 60.11 | 61.42 | 59.71 |
| | $\hat{\sigma}^+_{Y_0}$ | 60.23 | 60.16 | 60.12 | 60.09 | 60.07 | 60.06 |
| | $P_{E_{1-\sigma}}$ | 0.842 | 0.842 | 0.841 | 0.845 | 0.845 | 0.842 |
| $X_P$ [m] | $\bar{e}_{\hat{X}_P^+}$ | 33.05 | 5.04 | 17.28 | 17.89 | 0.325 | 26.06 |
| | $\hat{\sigma}^+_{E_{X_P}}$ | 1498.8 | 1466.9 | 1480.7 | 1479.7 | 1453.6 | 1492.1 |
| | $\hat{\sigma}^+_{X_P}$ | 1481.6 | 1481.6 | 1481.6 | 1481.7 | 1481.7 | 1481.7 |
| | $P_{E_{1-\sigma}}$ | 0.838 | 0.846 | 0.849 | 0.844 | 0.844 | 0.837 |
| $Y_P$ [ft] | $\bar{e}_{\hat{Y}_P^+}$ | 0.654 | 0.505 | 0.615 | 0.113 | 1.528 | 0.705 |
| | $\hat{\sigma}^+_{E_{Y_P}}$ | 61.66 | 61.55 | 60.57 | 61.08 | 61.7 | 60.22 |
| | $\hat{\sigma}^+_{Y_P}$ | 60.72 | 60.51 | 60.38 | 60.29 | 60.23 | 60.19 |
| | $P_{E_{1-\sigma}}$ | 0.833 | 0.833 | 0.839 | 0.842 | 0.845 | 0.844 |
| $R$ [ft] | $\bar{e}_{\hat{R}^+}$ | 1.053 | 0.175 | 0.929 | 0.398 | 0.367 | 0.014 |
| | $\hat{\sigma}^+_{E_R}$ | 36.11 | 30.38 | 27.29 | 24.3 | 21.19 | 19.09 |
| | $\hat{\sigma}^+_R$ | 34.6 | 29.13 | 25.05 | 21.98 | 19.56 | 17.61 |
| | $P_{E_{1-\sigma}}$ | 0.837 | 0.83 | 0.831 | 0.825 | 0.828 | 0.824 |

The effect of aircraft velocity changes are also investigated and the statistics are documented in Table 4.36. A modest increase in estimation accuracy is observed when the velocity increases. As in the previous scenarios, the velocity estimate follows an opposite trend. In Table 4.37, the effects of different accuracy levels of slant range to P measurements and *prior* information on the ground object's altitude estimate are investigated. Notable improvements occur when the accuracy of the measurements is increased. How-

Table 4.37 Estimation performance as a function of different measurement errors - Scenario 4. The altitude and velocity are 3,000 feet and 0.8 M, respectively.

| | $\hat{\sigma}^+_{E_V}$[ft/sec] | $\hat{\sigma}^+_{E_{X_0}}$ [m] | $\hat{\sigma}^+_{E_{Y_0}}$ [ft] | $\hat{\sigma}^+_{E_{X_P}}$ [m] | $\hat{\sigma}^+_{E_{Y_P}}$ [ft] | $\hat{\sigma}^+_{E_R}$[ft] |
|---|---|---|---|---|---|---|
| $\sigma_{Y_P^-} = 100$ ft, $\sigma_{R^-} = 200$ ft | 2.371 | 1466.3 | 59.95 | 1466.24 | 61.21 | 22.93 |
| $\sigma_{Y_P^-} = 50$ ft, $\sigma_{R^-} = 100$ ft | 2.371 | 1472.6 | 42.75 | 1472.6 | 41.8 | 23.03 |
| $\sigma_{Y_P^-} = 10$ ft, $\sigma_{R^-} = 20$ ft | 1.742 | 1487.3 | 19.23 | 1487.4 | 9.66 | 14.97 |

ever, the quality of own-ship position estimate is still dominated by the accuracy of the unaided INS position estimate.

***Scenario 5.*** The measurement Scenario 5 is investigated for different flight altitudes and for different airspeeds and the estimation performance statistics are given in Tables 4.38 and 4.39, respectively. The own-ship $X$-position estimate $\hat{X}_0^+$ yields an experimental $\sigma$ of about 30 meters. Reducing the positional estimation error from 0.8 nm to a positioning error $\sigma$ of 30 meters is a significant improvement. The $\hat{Y}_0$ estimation error $\sigma$ is also reduced to 60 feet from a 75 feet error. In parallel, geo-location performance is within the 1-$\sigma$ of the ground object *prior* information accuracy. Furthermore, the altitude estimate of the ground object is now more accurate. Velocity and slant range estimates do not significantly change in this scenario. As before, flight conditions of low altitude and high speed yield better estimation performance.

The accuracy of the prior information $X_{P_m}$ and $Y_{P_m}$ is now increased, and the estimation performance statistics are analyzed in Table 4.40. An estimation error standard deviation of 7 meters for $X$, and 21 feet for own-ship $Y_0$-position is very good and could be called "position fix-taking", since that accuracy may be better than in the current fix-taking modes.

In conclusion: Since in this scenario we include both *prior* $X$ and $Y$ position information on the ground object, the best performance so far is obtained. True, the scenario loses its "tracking an unknown ground object" characteristic, but still, it is a passive INS aiding scheme. The inclusion of the ground object's coordinates information enhances estimation

Table 4.38 Estimation performance as a function of altitude - Scenario 5.

| | $h$ [ft] | 1000 | 3,000 | 6,000 | 10,000 | 15,000 | 20,000 |
|---|---|---|---|---|---|---|---|
| $V$ [ft/sec] | $\bar{e}_{\hat{V}^+}$ | 0.013 | 0.012 | 0.081 | 0.384 | 1.444 | 2.364 |
| | $\hat{\sigma}^+_{E_V}$ | 2.48 | 2.449 | 2.475 | 2.42 | 2.42 | 2.49 |
| | $\hat{\sigma}^+_V$ | 2.498 | 2.493 | 2.472 | 2.425 | 2.341 | 2.231 |
| | $P_{E_{1-\sigma}}$ | 0.847 | 0.849 | 0.848 | 0.876 | 0.939 | 0.968 |
| $X_0$ [m] | $\bar{e}_{\hat{X}_0^+}$ | 0.66 | 0.169 | 0.257 | 1.76 | 12.3 | 29.11 |
| | $\hat{\sigma}^+_{E_{X_0}}$ | 30.03 | 31.14 | 32.7 | 35.89 | 40.11 | 47.13 |
| | $\hat{\sigma}^+_{X_0}$ | 30.58 | 31.07 | 32.27 | 34.41 | 37.24 | 40.83 |
| | $P_{E_{1-\sigma}}$ | 0.842 | 0.841 | 0.837 | 0.827 | 0.728 | 0.598 |
| $Y_0$ [ft] | $\bar{e}_{\hat{Y}_0^+}$ | 0.61 | 0.647 | 0.239 | 1.55 | 9.163 | 21.35 |
| | $\hat{\sigma}^+_{E_{Y_0}}$ | 60.77 | 60.75 | 60.32 | 63.61 | 67.21 | 70.01 |
| | $\hat{\sigma}^+_{Y_0}$ | 60.01 | 60.09 | 60.37 | 60.98 | 62.0 | 63.29 |
| | $P_{E_{1-\sigma}}$ | 0.839 | 0.84 | 0.842 | 0.838 | 0.857 | 0.887 |
| $X_P$ [m] | $\bar{e}_{\hat{X}_P^+}$ | 0.67 | 0.075 | 0.624 | 0.675 | 0.544 | 0.035 |
| | $\hat{\sigma}^+_{E_{X_P}}$ | 29.97 | 30.44 | 30.19 | 31.2 | 30.16 | 30.59 |
| | $\hat{\sigma}^+_{X_P}$ | 30.472 | 30.472 | 30.472 | 30.472 | 30.472 | 30.472 |
| | $P_{E_{1-\sigma}}$ | 0.841 | 0.847 | 0.847 | 0.843 | 0.848 | 0.842 |
| $Y_P$ [ft] | $\bar{e}_{\hat{Y}_P^+}$ | 0.555 | 0.043 | 0.717 | 3.77 | 18.79 | 37.91 |
| | $\hat{\sigma}^+_{E_{Y_P}}$ | 60.82 | 61.93 | 63.88 | 70.55 | 79.9 | 90.04 |
| | $\hat{\sigma}^+_{Y_P}$ | 60.04 | 60.3 | 61.16 | 63.04 | 66.13 | 69.87 |
| | $P_{E_{1-\sigma}}$ | 0.838 | 0.836 | 0.833 | 0.795 | 0.715 | 0.641 |
| $R$ [ft] | $\bar{e}_{\hat{R}^+}$ | 0.01 | 0.515 | 1.256 | 9.52 | 50.47 | 112.17 |
| | $\hat{\sigma}^+_{E_R}$ | 9.59 | 23.66 | 42.34 | 65.93 | 89.48 | 116.05 |
| | $\hat{\sigma}^+_R$ | 9.18 | 22.13 | 39.47 | 60.57 | 82.63 | 105.28 |
| | $P_{E_{1-\sigma}}$ | 0.829 | 0.827 | 0.828 | 0.853 | 0.927 | 0.969 |

performance and thus INS aiding action. We could consider this scenario a robust way of aiding the INS by optically tracking a "known" ground object.

Table 4.39 Estimation performance as a function of airspeed - Scenario 5.

| | $Vel$ [M] | 0.5 | 0.6 | 0.7 | 0.8 | 0.9 | 1.0 |
|---|---|---|---|---|---|---|---|
| $V$ [ft/sec] | $\bar{e}_{\hat{V}^+}$ | 0.035 | 0.01 | 0.017 | 0.037 | 0.004 | 0.01 |
| | $\hat{\sigma}^+_{E_V}$ | 2.5 | 2.487 | 2.516 | 2.518 | 2.502 | 2.504 |
| | $\hat{\sigma}^+_V$ | 2.482 | 2.488 | 2.491 | 2.493 | 2.494 | 2.495 |
| | $P_{E_{1-\sigma}}$ | 0.843 | 0.838 | 0.839 | 0.838 | 0.841 | 0.84 |
| $X_0$ [m] | $\bar{e}_{\hat{X}_0^+}$ | 0.178 | 0.198 | 0.101 | 0.505 | 0.186 | 0.257 |
| | $\hat{\sigma}^+_{E_{X_0}}$ | 32.01 | 31.59 | 31.05 | 31.1 | 31.00 | 30.72 |
| | $\hat{\sigma}^+_{X_0}$ | 31.98 | 31.53 | 31.26 | 31.08 | 30.95 | 30.86 |
| | $P_{E_{1-\sigma}}$ | 0.84 | 0.842 | 0.839 | 0.844 | 0.839 | 0.838 |
| $Y_0$ [ft] | $\bar{e}_{\hat{Y}_0^+}$ | 0.406 | 0.236 | 0.142 | 1.817 | 0.455 | 0.144 |
| | $\hat{\sigma}^+_{E_{Y_0}}$ | 60.63 | 60.14 | 61.34 | 61.03 | 59.77 | 60.35 |
| | $\hat{\sigma}^+_{Y_0}$ | 60.24 | 60.16 | 60.12 | 60.09 | 60.07 | 60.06 |
| | $P_{E_{1-\sigma}}$ | 0.838 | 0.843 | 0.834 | 0.842 | 0.832 | 0.84 |
| $X_P$ [m] | $\bar{e}_{\hat{X}_P^+}$ | 0.32 | 0.266 | 0.016 | 0.672 | 0.257 | 0.234 |
| | $\hat{\sigma}^+_{E_{X_P}}$ | 30.42 | 30.52 | 30.14 | 30.32 | 30.43 | 30.33 |
| | $\hat{\sigma}^+_{X_P}$ | 30.472 | 30.472 | 30.472 | 30.472 | 30.472 | 30.472 |
| | $P_{E_{1-\sigma}}$ | 0.838 | 0.841 | 0.841 | 0.852 | 0.844 | 0.839 |
| $Y_P$ [ft] | $\bar{e}_{\hat{Y}_P^+}$ | 0.523 | 0.448 | 0.179 | 1.749 | 0.679 | 0.199 |
| | $\hat{\sigma}^+_{E_{Y_P}}$ | 62.07 | 61.11 | 62.84 | 61.73 | 59.97 | 61.02 |
| | $\hat{\sigma}^+_{Y_P}$ | 60.76 | 60.52 | 60.39 | 60.3 | 60.23 | 60.19 |
| | $P_{E_{1-\sigma}}$ | 0.841 | 0.837 | 0.831 | 0.845 | 0.839 | 0.838 |
| $R$ [ft] | $\bar{e}_{\hat{R}^+}$ | 0.456 | 0.279 | 0.251 | 0.507 | 0.292 | 0.198 |
| | $\hat{\sigma}^+_{E_R}$ | 36.96 | 30.48 | 27.3 | 24.54 | 21.56 | 19.45 |
| | $\hat{\sigma}^+_R$ | 35.26 | 29.4 | 25.2 | 22.11 | 19.69 | 17.67 |
| | $P_{E_{1-\sigma}}$ | 0.832 | 0.84 | 0.823 | 0.82 | 0.822 | 0.823 |

Table 4.40 Estimation performance as a function of different measurement errors - Scenario 5. The altitude and velocity are 3,000 feet and 0.8 M, respectively.

| | $\hat{\sigma}^+_{E_V}$[ft/sec] | $\hat{\sigma}^+_{E_{X_0}}$ [m] | $\hat{\sigma}^+_{E_{Y_0}}$ [ft] | $\hat{\sigma}^+_{E_{X_P}}$ [m] | $\hat{\sigma}^+_{E_{Y_P}}$ [ft] | $\hat{\sigma}^+_{E_R}$[ft] |
|---|---|---|---|---|---|---|
| $\sigma_{Y_P^-} = \sigma_{X_P^-} = 100$ ft | 2.453 | 31.1 | 59.87 | 30.37 | 60.74 | 23.77 |
| $\sigma_{Y_P^-} = \sigma_{X_P^-} = 50$ ft | 2.475 | 16.64 | 42.99 | 15.22 | 41.27 | 23.92 |
| $\sigma_{Y_P^-} = \sigma_{X_P^-} = 10$ ft | 2.423 | 7.25 | 21.47 | 3.06 | 9.7 | 23.34 |

***Scenario 6.*** In this final measurement scenario, complete *prior* information and the slant range measurement are included in the estimation algorithm. Tables 4.41, 4.42, and 4.43 show the estimation performance statistics for this "measurement rich" scenario.

The estimation performance as a function of altitude is given in Table 4.41. The experimental $\sigma$ and the predicted $\sigma$ values of the $X_0$ estimation error are close and are about 30 meters. The reduction from 0.8 nm (1481.6 meters) of the estimation error $\sigma$ to 30 meters is a desirable result. An increase in altitude causes a slight decrease in $X_0$ estimation accuracy. Own-ship altitude estimation error is also reduced; however, the reduction of error to 60 feet from 75 feet is not that significant; it responds to altitude changes similar to the $X_0$ estimate. We recall that the uncertainty in the coordinates of the ground object ($\sigma_{X_P}$ and $\sigma_{Y_P}$) is 100 feet. The experimental variance of the $\hat{X}_P$ estimation error is maintained within this bound while $\hat{\sigma}_{Y_P}$ is reduced to 60 feet. For both $\hat{X}_P$ and $\hat{Y}_P$, lower altitudes yield better performance. The velocity estimation error variance is reduced, as flight altitude increases. The slant range estimate shows a slight improvement in comparison to the previous scenarios, since additional information is used.

The estimation performance versus airspeed statistics are given in Table 4.42. Increasing airspeed makes the estimates more accurate. However, the accuracy enhancements resulting from higher velocities are not significant. The predicted $X_P$ estimation error variance does not change with airspeed whereas the ground object's $X$-coordinate estimation error $\sigma$ is about 100 feet ($\approx$ 30 m) for all airspeeds.

To increase the estimation accuracy, we also performed experiments using high, and very high accuracy measurements. The statistics are given Table 4.43. Clearly, if we have accurate measurements, the estimates produced by the algorithm are very good.

Table 4.41 Estimation performance as a function of altitude - Scenario 6.

| | $h$ [ft] | 1000 | 3,000 | 6,000 | 10,000 | 15,000 | 20,000 |
|---|---|---|---|---|---|---|---|
| $V$ [ft/sec] | $\bar{e}_{\hat{V}^+}$ | 0.028 | 0.013 | 0.068 | 0.018 | 0.008 | 0.037 |
| | $\hat{\sigma}^+_{E_V}$ | 2.504 | 2.475 | 2.434 | 2.31 | 2.212 | 2.133 |
| | $\hat{\sigma}^+_V$ | 2.496 | 2.478 | 2.425 | 2.321 | 2.188 | 2.044 |
| | $P_{E_{1-\sigma}}$ | 0.841 | 0.844 | 0.85 | 0.842 | 0.839 | 0.842 |
| $X_0$ [m] | $\bar{e}_{\hat{X}_0^+}$ | 0.21 | 0.252 | 0.3 | 0.549 | 0.437 | 0.024 |
| | $\hat{\sigma}^+_{E_{X_0}}$ | 30.57 | 31.2 | 32.38 | 34.96 | 37.59 | 40.36 |
| | $\hat{\sigma}^+_{X_0}$ | 30.59 | 31.06 | 32.19 | 34.09 | 35.33 | 36.02 |
| | $P_{E_{1-\sigma}}$ | 0.842 | 0.837 | 0.837 | 0.828 | 0.83 | 0.814 |
| $Y_0$ [ft] | $\bar{e}_{\hat{Y}_0^+}$ | 0.239 | 0.037 | 0.913 | 2.22 | 0.109 | 0.136 |
| | $\hat{\sigma}^+_{E_{Y_0}}$ | 60.54 | 59.89 | 61.42 | 62.55 | 63.97 | 65.49 |
| | $\hat{\sigma}^+_{Y_0}$ | 60.01 | 60.09 | 60.36 | 60.9 | 61.76 | 62.74 |
| | $P_{E_{1-\sigma}}$ | 0.835 | 0.843 | 0.841 | 0.839 | 0.837 | 0.831 |
| $X_P$ [m] | $\bar{e}_{\hat{X}_P^+}$ | 0.214 | 0.23 | 0.107 | 0.171 | 0.435 | 0.31 |
| | $\hat{\sigma}^+_{E_{X_P}}$ | 30.44 | 30.46 | 30.37 | 30.73 | 30.88 | 30.32 |
| | $\hat{\sigma}^+_{X_P}$ | 30.472 | 30.472 | 30.472 | 30.472 | 30.472 | 30.472 |
| | $P_{E_{1-\sigma}}$ | 0.841 | 0.839 | 0.838 | 0.836 | 0.838 | 0.847 |
| $Y_P$ [ft] | $\bar{e}_{\hat{Y}_P^+}$ | 0.165 | 0.261 | 0.047 | 1.608 | 1.487 | 1.432 |
| | $\hat{\sigma}^+_{E_{Y_P}}$ | 60.82 | 60.75 | 64.53 | 69.92 | 74.54 | 77.9 |
| | $\hat{\sigma}^+_{Y_P}$ | 60.04 | 60.3 | 61.12 | 62.8 | 65.41 | 68.3 |
| | $P_{E_{1-\sigma}}$ | 0.835 | 0.837 | 0.823 | 0.814 | 0.808 | 0.797 |
| $R$ [ft] | $\bar{e}_{\hat{R}^+}$ | 0.045 | 0.049 | 1.557 | 1.323 | 0.707 | 1.76 |
| | $\hat{\sigma}^+_{E_R}$ | 10.23 | 23.89 | 41.65 | 61.313 | 74.57 | 84.88 |
| | $\hat{\sigma}^+_R$ | 9.56 | 21.91 | 38.67 | 57.95 | 71.44 | 81.11 |
| | $P_{E_{1-\sigma}}$ | 0.829 | 0.822 | 0.833 | 0.836 | 0.837 | 0.834 |

Table 4.42 Estimation performance as a function of airspeed - Scenario 6.

| | $Vel$ [M] | 0.5 | 0.6 | 0.7 | 0.8 | 0.9 | 1.0 |
|---|---|---|---|---|---|---|---|
| $V$ [ft/sec] | $\bar{e}_{\hat{V}^+}$ | 0.053 | 0.01 | 0.032 | 0.01 | 0.026 | 0.005 |
| | $\hat{\sigma}^+_{E_V}$ | 2.449 | 2.412 | 2.39 | 2.467 | 2.494 | 2.492 |
| | $\hat{\sigma}^+_V$ | 2.444 | 2.461 | 2.471 | 2.477 | 2.482 | 2.485 |
| | $P_{E_{1-\sigma}}$ | 0.848 | 0.85 | 0.85 | 0.841 | 0.837 | 0.833 |
| $X_0$ [m] | $\bar{e}_{\hat{X}_0^+}$ | 0.191 | 0.005 | 0.614 | 0.188 | 0.319 | 0.374 |
| | $\hat{\sigma}^+_{E_{X_0}}$ | 32.0 | 30.81 | 31.54 | 31.07 | 31.1 | 30.94 |
| | $\hat{\sigma}^+_{X_0}$ | 31.93 | 31.51 | 31.24 | 31.07 | 30.94 | 30.86 |
| | $P_{E_{1-\sigma}}$ | 0.839 | 0.844 | 0.834 | 0.84 | 0.832 | 0.843 |
| $Y_0$ [ft] | $\bar{e}_{\hat{Y}_0^+}$ | 0.87 | 0.68 | 0.321 | 0.271 | 1.971 | 2.212 |
| | $\hat{\sigma}^+_{E_{Y_0}}$ | 61.26 | 59.73 | 59.93 | 60.03 | 61.13 | 59.39 |
| | $\hat{\sigma}^+_{Y_0}$ | 60.23 | 60.16 | 60.12 | 60.09 | 60.07 | 60.06 |
| | $P_{E_{1-\sigma}}$ | 0.828 | 0.839 | 0.84 | 0.84 | 0.839 | 0.838 |
| $X_P$ [m] | $\bar{e}_{\hat{X}_P^+}$ | 0.513 | 0.012 | 0.471 | 0.222 | 0.38 | 0.002 |
| | $\hat{\sigma}^+_{E_{X_P}}$ | 30.43 | 29.8 | 30.74 | 30.41 | 30.52 | 30.39 |
| | $\hat{\sigma}^+_{X_P}$ | 30.47 | 30.47 | 30.47 | 30.47 | 30.47 | 30.47 |
| | $P_{E_{1-\sigma}}$ | 0.839 | 0.843 | 0.834 | 0.839 | 0.834 | 0.844 |
| $Y_P$ [ft] | $\bar{e}_{\hat{Y}_P^+}$ | 1.241 | 0.918 | 0.247 | 0.069 | 1.488 | 2.146 |
| | $\hat{\sigma}^+_{E_{Y_P}}$ | 62.97 | 60.58 | 60.99 | 61.09 | 61.85 | 60.04 |
| | $\hat{\sigma}^+_{Y_P}$ | 60.72 | 60.52 | 60.38 | 60.29 | 60.23 | 60.19 |
| | $P_{E_{1-\sigma}}$ | 0.825 | 0.833 | 0.83 | 0.836 | 0.841 | 0.833 |
| $R$ [ft] | $\bar{e}_{\hat{R}^+}$ | 1.1 | 0.035 | 0.437 | 0.206 | 0.09 | 0.147 |
| | $\hat{\sigma}^+_{E_R}$ | 36.29 | 29.61 | 25.72 | 23.7 | 21.28 | 19.44 |
| | $\hat{\sigma}^+_R$ | 34.6 | 29.13 | 24.99 | 22.0 | 19.57 | 17.63 |
| | $P_{E_{1-\sigma}}$ | 0.837 | 0.844 | 0.837 | 0.824 | 0.82 | 0.812 |

Table 4.43 Estimation performance as a function of different measurement errors - Scenario 6. The altitude and velocity are 3,000 feet and 0.8 M, respectively.

| [ft] | $\hat{\sigma}^+_{E_V}$[ft/sec] | $\hat{\sigma}^+_{E_{X_0}}$ [m] | $\hat{\sigma}^+_{E_{Y_0}}$ [ft] | $\hat{\sigma}^+_{E_{X_P}}$ [m] | $\hat{\sigma}^+_{E_{Y_P}}$ [ft] | $\hat{\sigma}^+_{E_R}$[ft] |
|---|---|---|---|---|---|---|
| $\sigma_{Y_P^-}, \sigma_{X_P^-} = 100$, $\sigma_{R^-} = 200$ | 2.427 | 30.77 | 59.52 | 30.07 | 60.34 | 23.35 |
| $\sigma_{Y_P^-}, \sigma_{X_P^-} = 50$, $\sigma_{R^-} = 100$ | 2.406 | 16.59 | 42.57 | 15.36 | 41.59 | 23.07 |
| $\sigma_{Y_P^-}, \sigma_{X_P^-} = 10$, $\sigma_{R^-} = 20$ | 1.71 | 5.44 | 19.12 | 3.07 | 9.81 | 14.94 |

#### *4.3.2.4 Comparison of the Measurement Scenarios.*

Phase 1 entailed the estimation of the angular navigation variables and in Phase 2 the positional navigation variables are etimated. The estimation performance statistics of the algorithm which is applied to six different measurement scenarios is based on 5000 "independent" MC runs. In each scenario, the random number generator is used to simulate white Gaussian noise for each measurement. The results documented in Tables 4.27 to 4.43 were obtained with different samples of noise applied to the variables in each run across the measurement scenarios. Based on these independent experiments, we now analyze the estimation statistics for each estimation parameter.

Fig 4.11 shows the comparison of the experimental error variance of own-ship $X$-position estimate for the 6 measurement scenarios. Measurement Scenarios 5 and 6 are clearly preferable to Scenarios 1, 2, 3, and 4. The estimation results in Scenarios 5 and 6 reflect the $X_P$ prior information accuracy. In Scenarios 1, 2, 3, and 4, the error standard deviation of the estimates is about 0.8 NM, since they are driven by the INS provided $X_0$ measurements.

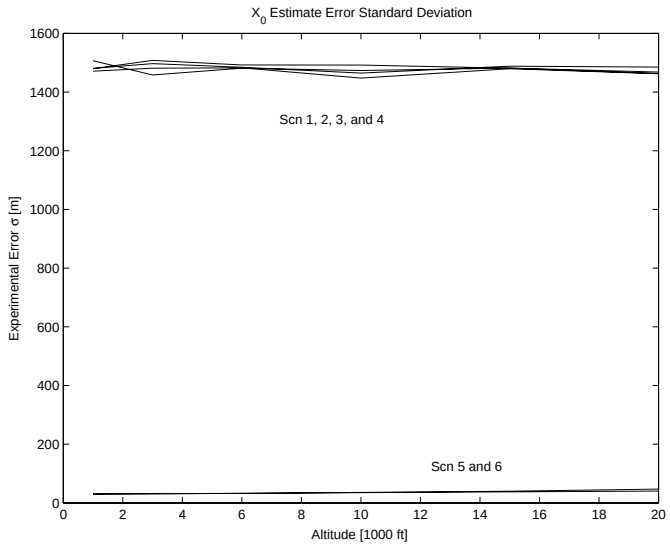


Figure 4.11 Own-ship X-Position Estimate: Comparison of Scenarios

The comparison of geo-location performance concerning the $Xp$ coordinate is given in Fig 4.12. The results are similar to the $X_0$ estimation performance results. Inclusion

of prior information on $X_P$ in Scenarios 5 and 6 yields an estimation error $\sigma$ of about 30 meters.

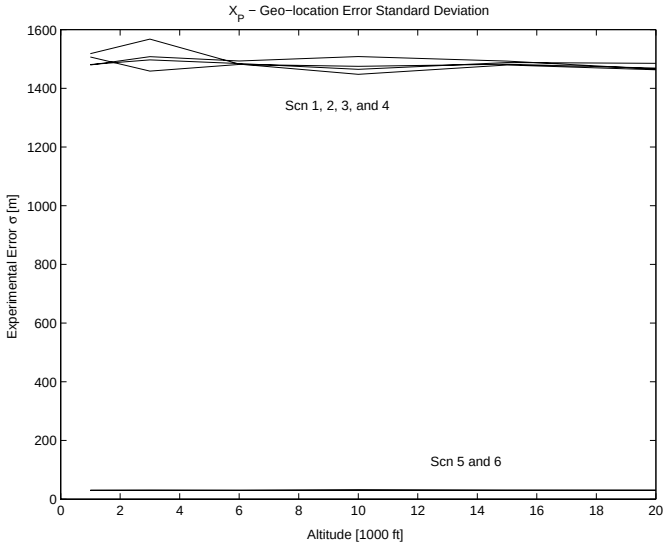


Figure 4.12 $X_P$ - Geo-location: Comparison of Scenarios

Estimation error variance comparisons for own-ship altitude estimation are shown in Fig 4.13. Scenarios 1 and 3 in this experiment do not include $\hat{Y}_P^-$ prior information. The 1-$\sigma$ value of the INS provided altitude measurement is 75 feet; and after aiding, the recorded estimation errors are about 75 feet for Scenarios 1 and 3. Scenarios 2, 4, 5, and 6 include $\hat{Y}_P^-$ prior information. At low altitudes, the estimation error is reduced to 60 feet with the inclusion of 100 feet accurate $\hat{Y}_P^-$ prior information. The estimation performance accuracy decreases with altitude. However, if the slant range measurement is also included, the deterioration of accuracy with altitude is less, pronounced as is the case in Scenarios 4 and 6.

The ground object altitude estimation errors are compared in Fig 4.14. In Scenario 1 and 3, the estimation error variance shows a considerable increase when the flight altitude increases. Scenarios 1 and 3 do not include $\hat{Y}_P^-$ prior information. In the remaining scenarios, an improvement similar to the improvement in own-ship altitude estimation is observed; the results are very similar in both cases.

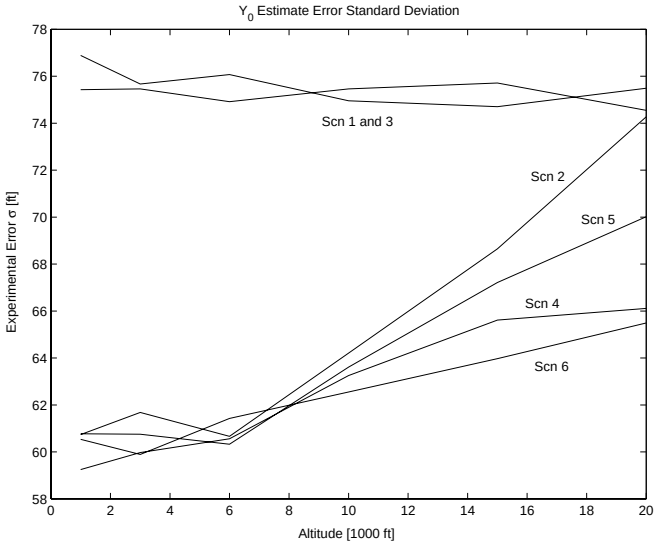


Figure 4.13 Own-ship Y-Position Estimate: Comparison of Scenarios

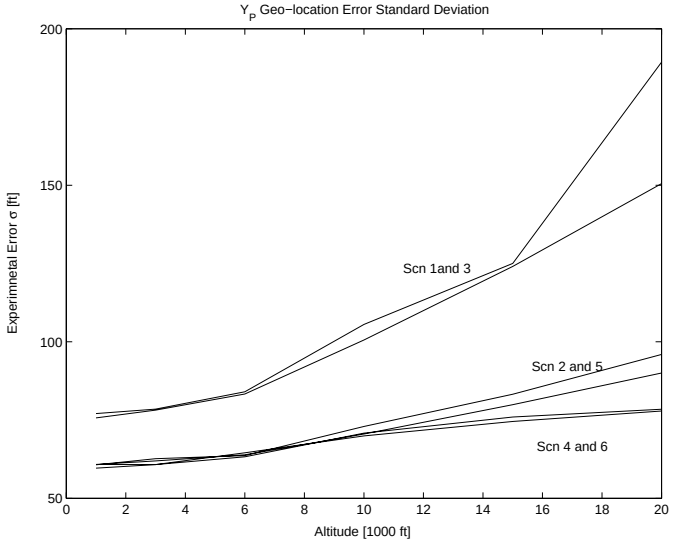


Figure 4.14 $Y_P$ - Geo-location Estimate: Comparison of Scenarios

The velocity estimation performance comparison is shown in Fig 4.15. The results are better than the unaided velocity error variance of 2.5 ft/sec. In Scenarios 3, 4, and 6, the inclusion of slant range measurement decreases the error variance.

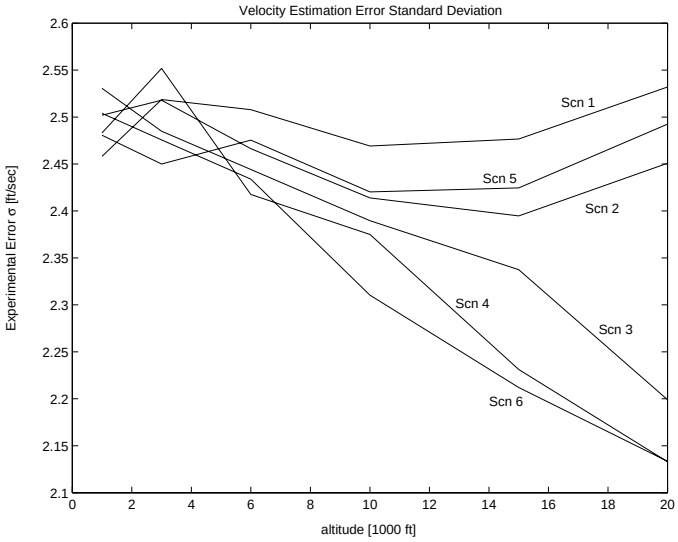


Figure 4.15 Velocity Estimate: Comparison of Scenarios

***4.3.3 Additional Comparison of the Scenarios and the Measurement Situations.*** We investigated INS aiding by optically tracking an unknown ground object. Two different algorithms were developed. Common to both, Phase 1 includes the estimation of the angular navigation variables. The estimation performance statistics of the two algorithms which are applied to six different measurement situations are based on 5000 "independent" MC runs. Thus, in each scenario, the random number generator is used to simulate white Gaussian noise for each variable and measurement. As a result, different samples of noise are applied to each parameter in each run. We analyzed the particular scenario statistics based on these independent experiments.

In this stage of our work, we repeat the MC experiments and we compare the estimates' statistics for the various scenarios when the same measurement noise realization is used in all scenarios. This comparison is performed in three cases and the results are shown in Figures 4.16 to 4.31.

***4.3.3.1 Case 1.*** In Case 1, we assume that the INS provides measurements with the statistics

$$\sigma_{X_0} = 0.8 \ nm, \qquad \sigma_{Y_0} = 75 \ feet, \qquad \sigma_V = 2.5 \ ft/sec$$

The prior information on the ground object's position, and the slant range measurement statistics are specified by

$$\sigma_{X_P} = 100 \ ft, \qquad \sigma_{Y_P} = 100 \ ft, \qquad \sigma_R = 200 \ ft$$

A fixed set of random measurements is used in all scenarios.

In Figure 4.16, the own-ship $X$-position estimation error is analyzed. In Scns 5, 6 and in Sits 5, and 6, a very good estimate is obtained. The remaining parameters' errors are relatively high. The reason for this significant accuracy difference comes from having the *prior* information on the "unknown" ground object. The inclusion of slant range measurement usually improves the estimation accuracy. Moreover, in Scn 5 and 6, the results are better than the results in Sits 5 and 6, even in the case where the same measurements realizations is used. The estimation errors in the other Scenarios and measurement Situations are close, and in the big picture, it is not very significant to observe which one performs better since the estimation accuracy in Scns 5 and 6 is satisfactory.

In Fig 4.17, we investigate the $X_P$ estimation errors. The results are almost the same as in the $X_0$ comparison. In the Scenarios and measurement Situations having $\hat{Y}_P^-$ and $\hat{X}_P^-$ information (Sit 3, 6 and Scn 5, 6) the smaller estimation error is recorded. Scns 1, 2, 3, 4, and Sits 2 and 4 including $Y_P^-$ and/or $R_m$ information, result in a larger error; nevertheless, in measurement Sits 2 and 4 the errors are larger than the errors in Scns 1, 2, 3, and 4. The accuracy of the estimates in Scns 5 and 6 and in the measurement Sits 5 and 6 are almost equal; therefore, we conclude that the inclusion of the ground object coordinates information significantly enhances the estimation performance.

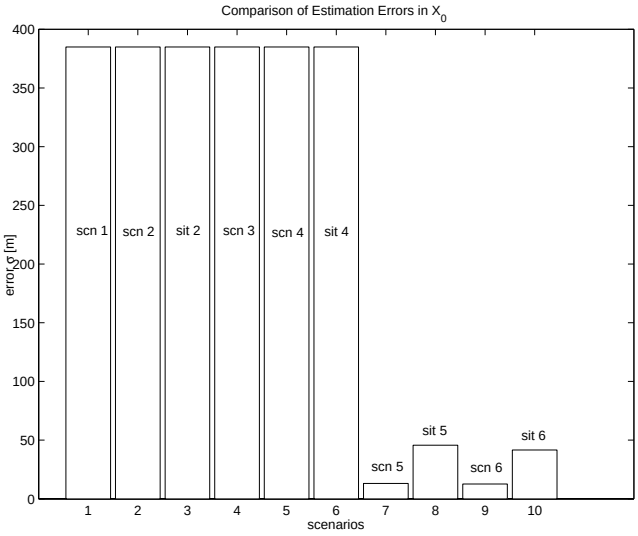


Figure 4.16 Own-ship $X$-Position Estimate - Case 1: Comparison of Scenarios

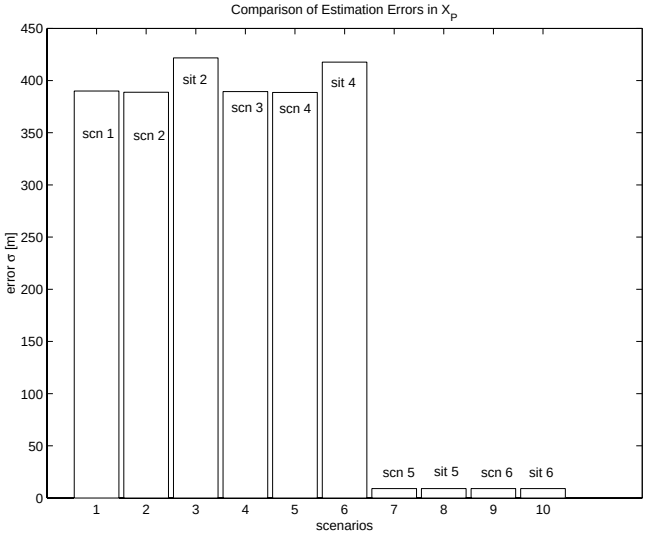


Figure 4.17 $X_P$ - Geo-location - Case 1: Comparison of Scenarios

Comparisons of own-ship altitude estimation performance are shown in Fig 4.18. All scenarios in which $\hat{Y}_P^-$ information is included (Scns 2, 4, 5, and 6), except Scn 3, yield own-ship altitude information more accurately than in Scn 3, and Sits 2, 4, 5, and 6.

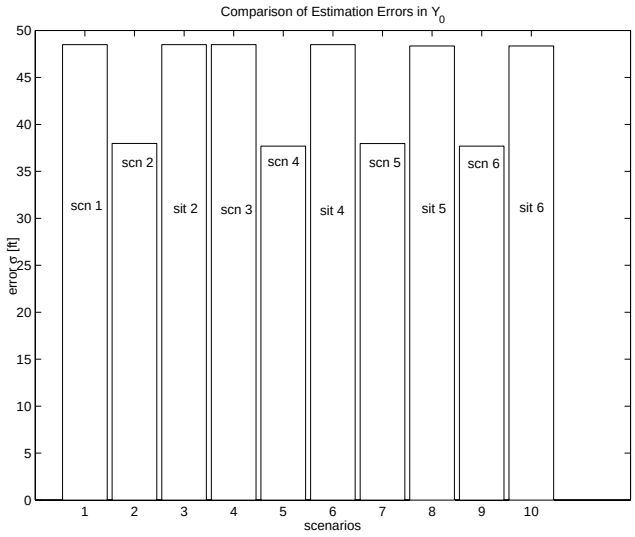


Figure 4.18 Own-ship $Y$-Position Estimate - Case 1: Comparison of Scenarios

The ground object altitude estimation errors are compared in Fig 4.19. The results in the figure are similar to the $Y_0$ results. In all Scenarios, performance is better than Situations. In Scns 1 and 3 the errors are relatively larger than in the other Scenarios, because of a lack of $Y_P^-$ information. In Scns 2, 4, 5, and 6 the estimation error is similar.

The velocity estimation performance comparison in Fig 4.20 shows that the most accurate estimates are obtained in Scns 4 and 6. The worst estimates are produced in Scns 1, and 2, and in measurement Sit 5. We conclude that inclusion of the slant range measurement $R_m$ and ground object altitude information $\hat{Y}_P^-$ is the reason for having better accuracy than in the others cases. The slant range measurement is not included in the worst three.

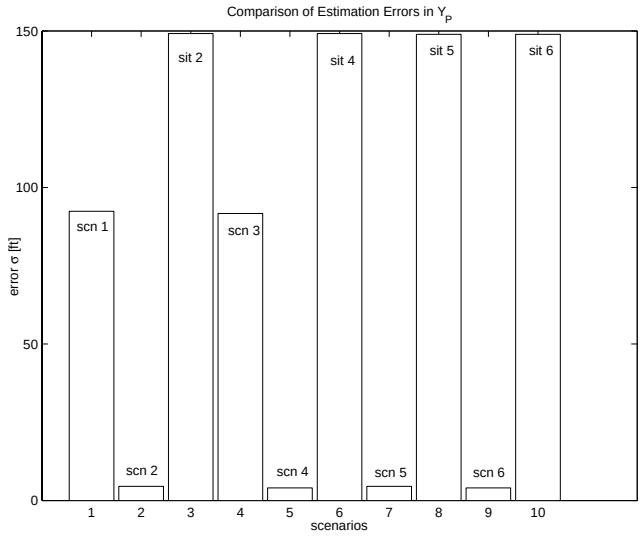


Figure 4.19 $Y_P$ - Geo-location - Case 1: Comparison of scenarios

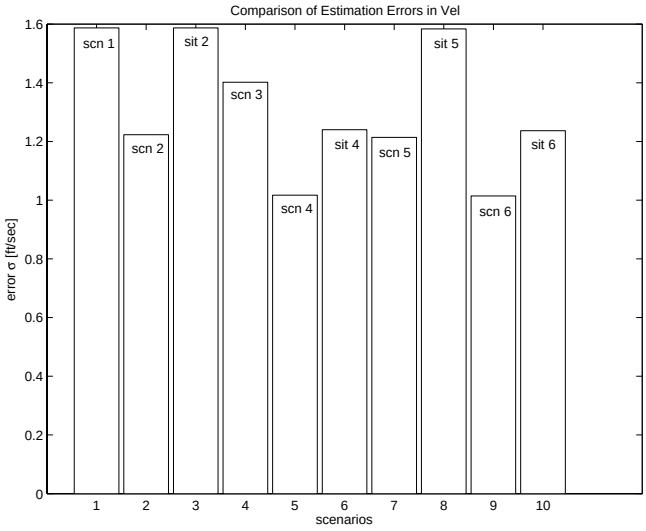


Figure 4.20 Velocity Estimation - Case 1: Comparison of Scenarios

***4.3.3.2 Case 2.*** In this case, we assume that the aircraft has flown an hour, and the INS provides own-ship position estimates as following

$$X_{0_{INS}} = X_{0_{true}} + 0.8 \ nm, \qquad Y_{0_{INS}} = Y_{0_{true}} + 75 \ \ feet, \qquad V_{INS} = V_{true} + 2.5 \ \ ft/sec$$

Randomly chosen prior information on the ground object, and the slant range measurement statistics are as in Case 1.

Fig 4.21 shows the comparison of the measurement scenarios for $\hat{X}_0^+$. The results are very obvious. The estimation performance in the scenarios with prior information on the ground object is superior to the performance in the scenarios where this additional information is not available. Indeed, in scenarios where $\hat{X}_P^-$ information is included (Scns 5, 6, measurement Sits 5 and 6 the estimation accuracy is highly correlated with $\hat{X}_P^-$ accuracy. The $\hat{X}_0^+$ accuracy in the other scenarios is about the same as the INS provided $X_0$ estimate, since the improvement is not significant. Fig 4.22 also shows the zoomed-in version of the estimation errors for Scns 5 and 6 and measurement Sits 5 and 6. In Scns 5 and 6 the estimation performance is slightly better than in Sits 5 and 6.

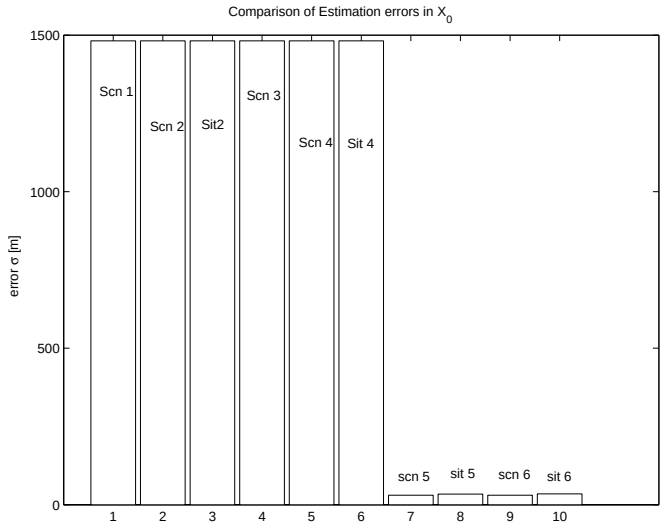


Figure 4.21 Own-ship $X$-Position Estimate - Case 2: Comparison of Scenarios

Geo-location on the $X$ axis performance for different measurement scenarios is shown in Fig 4.23. The results are almost the same as for $\hat{X}_0^+$ estimation.

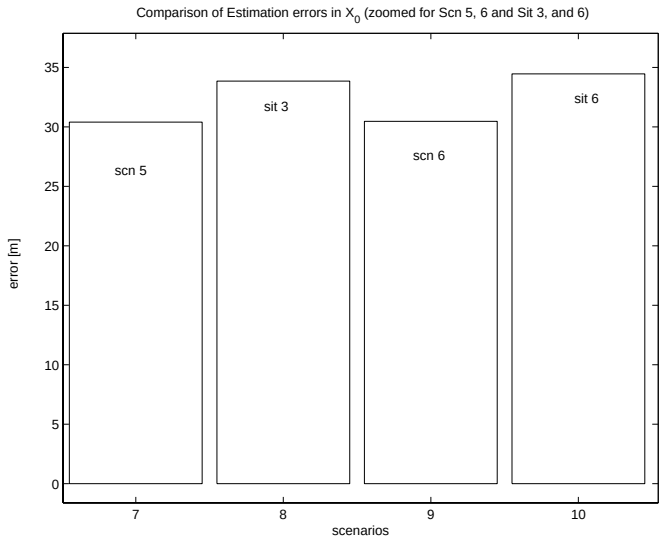


Figure 4.22 Own-ship $X$-Position Estimate, Zoomed - Case 2: Comparison of Scenarios

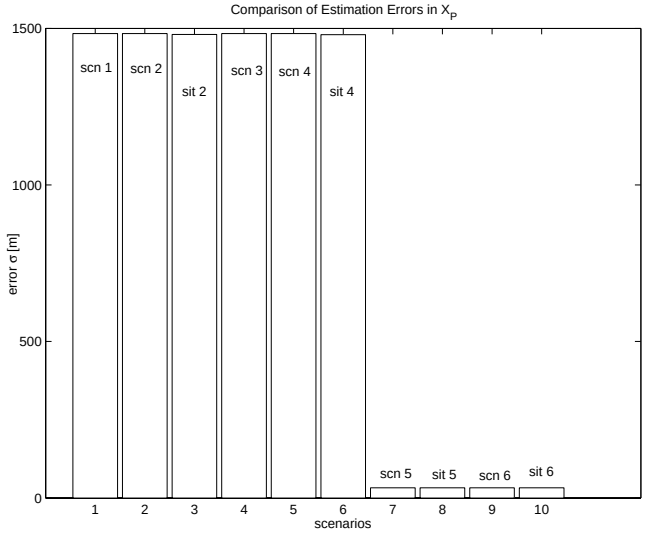


Figure 4.23 $X_P$ - Geo-location - Case 2: Comparison of Scenarios

Own-ship altitude estimates are compared in Fig 4.24. We observe that inclusion of $\hat{Y}_P^-$ information affects only estimates in various Scenarios; that is, the accuracy of the altitude estimates produced in the measurement Situations is driven by the INS provided altitude measurements and does not change with the inclusion of $\hat{Y}_P^-$ information. Furthermore, the accuracy of the estimates in various measurement Situations including $\hat{Y}_P^-$ information, is almost identical to the accuracy in the Scenarios that do not include $\hat{Y}_P^-$ information.

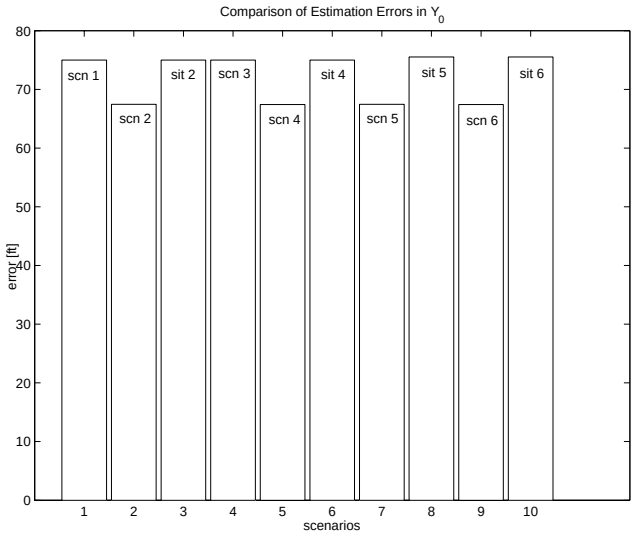


Figure 4.24 Own-ship $Y$-Position Estimate - Case 2: Comparison of Scenarios

Fig 4.25 shows the $Y$ geo-location error comparison. Contrary to expectations, we observe that the results in the various measurement Situations outperform the Scenarios' results. The error magnitudes in measurement Sits 2, 4, 5, and 6 are very close, however, in measurement Sit 5 the error is slightly less.

In Fig 4.26, the velocity estimate comparison is given. The estimation errors do not display a clear pattern. Probably, the inclusion of the slant range measurement makes some difference. Indeed, this is one of the rare occasions where the estimation results in the measurement Situations outperform the Scenarios' result.

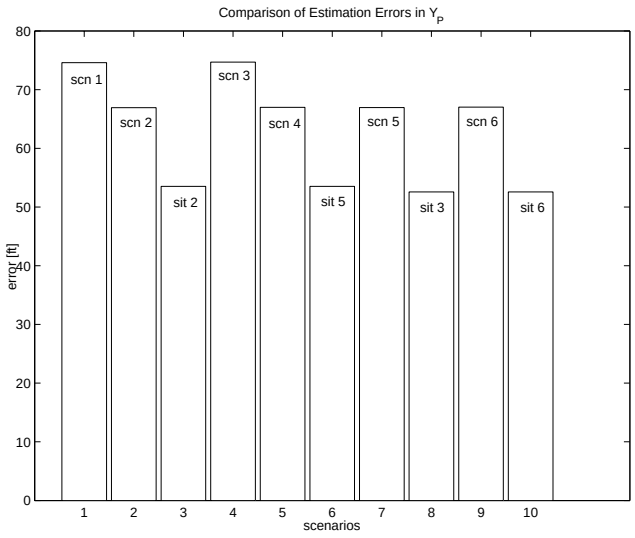


Figure 4.25 $Y_P$ - Geo-location - Case 2: Comparison of Scenarios

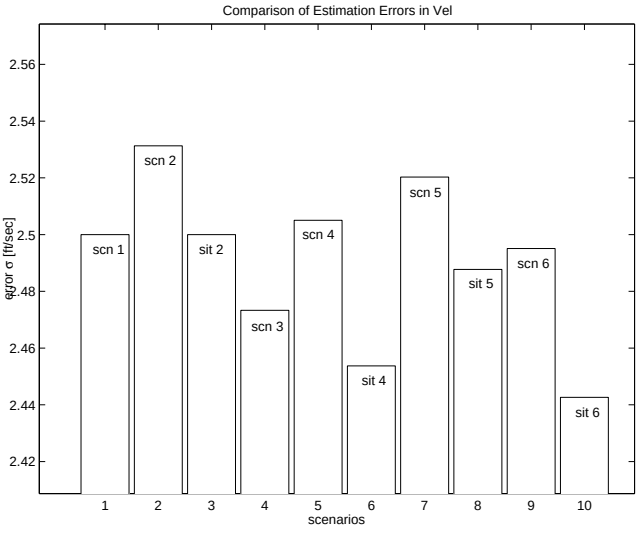


Figure 4.26 Velocity Estimation - Case 2: Comparison of Scenarios

***4.3.3.3 Case 3.*** In the Case 3, we use complete prior information on the location of P and we use a slant range measurement.

$$X_{0_{INS}} = X_{0_{true}} + 0.8 \ nm, \qquad Y_{0_{INS}} = Y_{0_{true}} + 75 \ \ feet, \qquad V_{INS} = V_{true} + 2.5 \ \ ft/sec$$

$$X_P = X_{P_{true}} + 100ft, \qquad Y_P = Y_{P_{true}} + 100ft, \qquad R = R_{true} + 200ft$$

First, in Fig 4.27 we compare the estimation results for own-ship position $\hat{X}_0^+$. The estimation error comparisons are similar to the the results in Cases 1 and 2. In Scns 5, and 6, and in measurement Sits 5 and 6, a very accurate estimates are obtained, but this time, there is a notable difference between Scns 5 and 6 and measurement Sits 5 and 6: The best results are obtained in Scn 6.

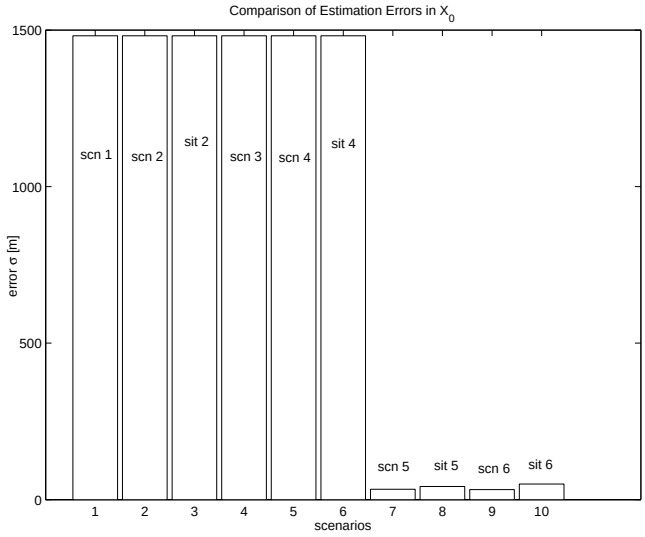


Figure 4.27 Own-ship $X$-Position Estimate - Case 3: Comparison of Scenarios

The comparison of geo-location performance for $X_P$ is given in Fig 4.28. The results reflect the $X_0$ estimation results.

Inclusion of $\hat{Y}_P^-$ information significantly affects own-ship altitude estimation performance. This is shown in Fig 4.29. The Scenarios including $\hat{Y}_P^-$ information yield better altitude accuracy and in the rest of the Scenarios and measurement Situations almost the same accuracy is obtained. We note that the inclusion of $\hat{Y}_P^-$ information does not affect the estimation accuracy in the various measurement Situations.

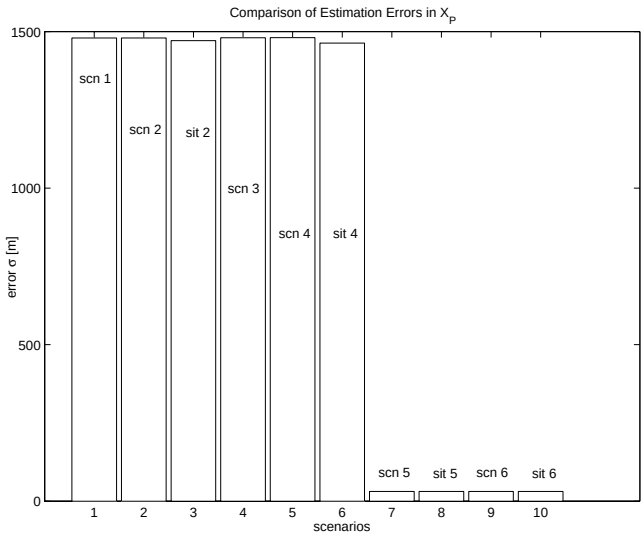


Figure 4.28 $X_P$ - Geo-location - Case 3: Comparison of Scenarios

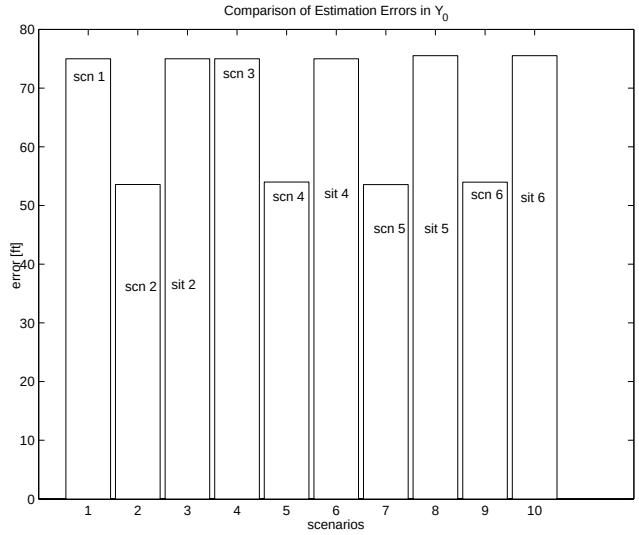


Figure 4.29 Own-ship $Y$-Position Estimate - Case 3: Comparison of Scenarios

Fig 4.30 shows the ground object altitude estimation performance for the various scenarios. As in Case 2, in the various measurement Situations the estimation performance is better than in the respective Scenarios. Two Scenarios (Scns 1 and Scn 3) do not include $\hat{Y}_P^-$ prior information, so they yield the poorest accuracies.

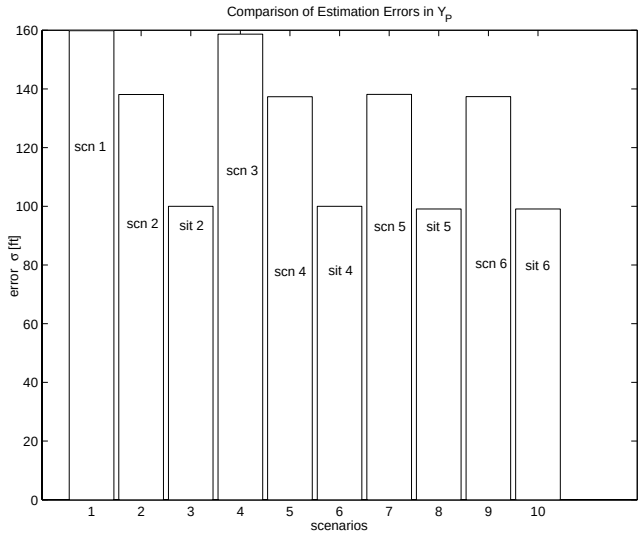


Figure 4.30 $Y_P$ - Geo-location - Case 3: Comparison of Scenarios

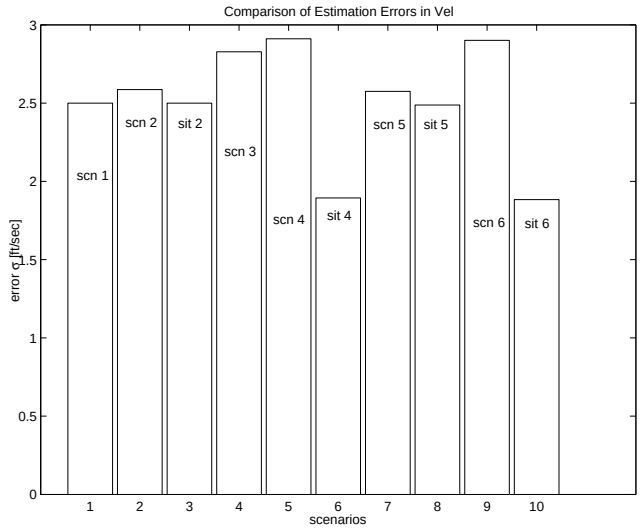


Figure 4.31 Velocity Estimation - Case 3: Comparison of Scenarios

The velocity estimation comparison is given in Fig 4.31. The slant range measurement contributes to accuracy enhancement. Thus, in measurement Sits 4 and 6 the mini-

mum estimation error. is recorded. In the scenarios equivalent to these two measurement Situations (Scns 4 and 6), the largest errors are recorded even though they include the same measurements realizations as in measurement Sits 5 and 6. The estimation performance in the remaining measurement situations is slightly better than in the Scenarios.

## *4.4 Summary*

In this section, we performed the analysis of the estimation performance based on the simulations. Initially, we investigated optimal measurement geometry to set up measurement scenarios used in simulations. We classified the simulations into two phases. In Phase 1, the estimation of A/C angular navigation variables were performed. The statistics of the estimation performance were given in Tables. In Phase 2, we used two different algorithm to perform the A/C positional navigation variables: standard linear regression and singular linear regression. Each algorithm were validated by simulations including six different measurement situations. The estimation performance statistics result from the simulation of each measurement situation were again documented in Tables. We thoroughly discussed the results of the statistics. Finally, we performed the comparison of two aforementioned algorithm based on the measurement scenarios simulated.

# V. Conclusions and Recommendations

## 5.1 Conclusions

INS-aiding by optically tracking a stationary ground object over time is investigated. It is assumed that the position of the ground object is not known and that passive, bearings-only, measurements are taken over time using an electro-optical tracker. The measurement situation is modelled and an estimation algorithm is developed.

A careful analysis of the proposed parsimonious optical measurement scheme reveals the following. The LOS measurements are conducive to a stand-alone estimate of the angles $\alpha'$ and $\beta'$ included between the aircraft's inertial velocity vector $\mathbf{V}$ and the aircraft body axes. Hence, assuming the absence of wind; that is, when the air mass is stationary and the ground speed $\equiv$ air speed, we obtain a stand-alone estimate of the aircraft's Angle of Attack $\alpha$ and side slip angle $\beta$. More importantly, the measured $\alpha'$ and $\beta'$ angles are related to the aircraft angular navigation variables, i.e., the aircraft's attitude, heading, and flight path angle. Thus, the $\alpha'$ and $\beta'$ angle measurements provided by the optical sensor can be used for INS aiding. Indeed, the proposed INS aiding concept is a modern mechanization of a $driftmeter$ [9].

The INS-aiding process entails two phases. We exclusively address the angular navigational variables in Phase 1 and update the INS-provided estimates of aircraft's pitch angle $\theta$ and aircraft's fight path angle $\gamma$ using the optically provided $\alpha'$ measurement. It is shown that the aircraft's attitude and flight path angles' estimates can be improved, thus achieving a degree of INS aiding. In a full three dimensional setting, the $\alpha'$ and $\beta'$ optical measurements afford improved roll, pitch, yaw angles, $\psi, \theta, \phi$, and flight path angle $\gamma$ and heading $H$ estimates. The attendant algorithm which uses bearings-only measurements is referred to as Phase 1 of the INS aiding process. Improving the aircraft's attitude estimate is important in modern sensor-rich platforms. However, the optical flow measurement, while helping to improve the angular navigational variables' estimates, has little impact on the estimation of the aircraft's positional navigation variables. Since the improved angular navigation variables will be used in the determination of orientation of accelerometers

(direction cosine matrix), we claim that any improvement in angular variables causes an improvement in positional accuracy.

The results of Phase 1 are used in Phase 2 to improve the INS-provided position estimates. Phase 2 includes two different estimation algorithms. None of the algorithms satisfies the objectives determined in the very beginning when the bearings-only measurements on an unknown ground object are used as a stand-alone aiding measurement. In order to improve the estimates of the positional navigation variables, information on the position of the ground object is required. The inclusion of information on altitude only, or the altitude and position coordinate of point P with or without the slant range measurement to the ground object, are investigated. Hence, the inclusion of information on the ground object's position in the linear regression is undertaken. Finally, the slant range measurement to the tracked point P is also augmented into the linear regression. In the scenarios we assume the ground object is unknown, the estimation performance is poor. The most accurate own-ship position estimate and the most accurate geo-location results are jointly obtained, using prior ground object position and altitude information, and the slant range measurement. Comparison of the algorithms shows that the second estimation algorithm (singular linear regression) yields better estimation performance, in general.

## *5.2 Recommendations*

To extend this study, the following recommendations are provided.

1. In Phase 1, the Minimum Error Variable (MV) estimation formulae are used to estimate the angular navigation variables. The equation error covariance R used is a diagonal matrix. This is tantamount to assuming that the INS-provided $\theta$ and $\gamma$ estimates are uncorrelated. The proper off-diagonal elements of the equation error matrix, if available, should be included. By so doing, the estimation accuracy will increase.

2. For each specified scenario, in Phase 1, we perform a MC experiment to obtain the statistics of the errors in $x$ and $y$. The latter would be required in the sequel. Thus, assuming $V$ is known, we estimated $\hat{x}_i$ and $\hat{y}_i$; since the true $x$ and $y$ in

the simulation are known, we experimentally obtain the $2 \times 2$ covariance matrix $P_{x,y}$ which renders the statistics of the $x$ and $y$ estimation errors. A more accurate covariance matrix estimate might be possible since the 1000 MC runs using MatLab's random number generator may not reflect an adequate statistics. Thus, while a highly optimistic statistic is obtained in one scenario, the next set of random numbers may produce lopsided results. The latter, especially in an estimation process in which very small numbers are handled, may yield misleading results. Moreover, the comparison between two scenarios may not be fair. Increasing the number of MC runs is the best solution, but it will increase the calculation time and memory requirements.

3. The optimal measurement geometry is developed in Section 4.1. In that section, we mention a constraint on the measurement geometry: the limitation for the LOS depression angle in front of a fighter aircraft. This constraint implies that track initialization is not chosen at will; the last point to initiate the track is determined by the Eq. (4.3). The $X_P$ and $Y_P$ used in this calculation is theoretically assumed unknown. We use these two synthetical variables to determine $X_0$; however, it shouldn't be conceived of as an aircraft position estimate at the beginning of ground object tracking. It "simulates" the point where the pilot manually initiates the track.

4. At the end of the Section 4.1, the measurement scenario using delayed tracking to get close enough to guarantee overflying the ground object is declared the optimal scenario. To realize this delayed tracking, we use $X_P$ and $Y_P$ information which is assumed unknown. This is not possible in real life. Simply put, the pilot must estimate his distance from the ground object, his altitude and his airspeed.

5. Aforementioned conclusions state that the tracking an unknown ground object by using optical measurement aids the INS angular navigation variable estimates but has little impact on the estimation of the aircraft's positional navigation variables. The basic reason for this is the weakness of observability of the aircraft's state which is provided by the the aircraft's aerodynamic angles. An automated passive ground object tracker, independent from the pilot, may take bearing measurements and may be applied to the proposed aiding algorithm. Continuously performing the estimation process may improve the situation little by little.

INS aiding algorithms suggested in this research aim to improve A/C navigation variables. After taking several LOS measurements, estimation calculation is performed for the initial point of the aircraft. In the simulation results, we analyze the statistics of the variables' estimation supported by the optical measurements. Actually, what can be done is that another simulation to aid the INS current measurements using these estimates. Furthermore, a successive aiding simulations may yield significant reduction of INS positioning error.

6. In the estimation algorithm, two look-up tables are used. The first look-up table is for providing the optimum values of the sampling interval for an acceptable geometry and statistics. The second is utilized for the statistics of the optical measurement of the angle between aircraft's flight path and initial LOS vector, $\gamma_D$. The error variance of this measurement changes for each flight condition; thus, a table is created including experimental error variances for the $\gamma_D$ measurements. These two tables are constructed by running MC runs and by analyzing the results. The MC experiments for sampling interval are usually performed at lower altitudes; experiments at higher altitudes are rare. The look-up table for $\sigma_{\gamma_D}$ is 10 by 48. Look-up tables can always be enlarged. This has the potential for improved estimation performance.

7. At higher altitudes, the significant deterioration of estimation performance and the requirement for increased tracking times are the the most notable disadvantages of the INS aiding method. These handicaps deserve to be further studied.

8. The parameter estimation algorithm using singular regression in Section 4.3.2 presents some singularity problems for various flight conditions. Flight conditions involving steep dive angles at altitudes above 15,000 feet cause estimation results which may not be accurate because of bad scaling. The diagonal matrix $D$ with positive elements is the output of the SVD of the $R$ matrix defined in Eq. (4.104). Matrix $D$ is used for parameter estimation as shown in Eqs. (4.138) - (4.141). Below is an example of a matrix $D$ obtain at a flight conditions 20,000 feet altitude and 20° dive

angle:

$$D = \begin{bmatrix} 2195138.56 & 0 & 0 & 0 & 0 & 0 & 0 \\ 0 & 928.93 & 0 & 0 & 0 & 0 & 0 \\ 0 & 0 & 928.93 & 0 & 0 & 0 & 0 \\ 0 & 0 & 0 & 522.52 & 0 & 0 & 0 \\ 0 & 0 & 0 & 0 & 3.286 & 0 & 0 \\ 0 & 0 & 0 & 0 & 0 & 0.58 & 0 \\ 0 & 0 & 0 & 0 & 0 & 0 & 0.0000042 \end{bmatrix}$$

$D_{1,1}$ increases with the slant range to the ground object, which increases with altitude and dive angle. So, in the example above, the scaling problem is unavoidable, and the numerical results may probably be inaccurate. Rescaling (nondimensionalization) is needed prior to the application of the SVD algorithm to preclude numerical problems and for a robust estimation algorithm.

9. During the derivation of the measurement equations for the aircraft's aerodynamic angles $\alpha$' and $\beta$', we assumed that the air mass is stationary, i.e., in the absence of wind, ground speed $\equiv$ air speed. This assumption simplifies the equation derivation. The measurement situation can be extended by including wind in the algorithm. Thus, use the additional airspeed and $\alpha$ and $\beta$ measurements provided by the ADC for wind estimation.

10. In this study, our estimation algorithm hinges on a 2-dimensional measurement scenario. In theory, it is not different from the 3-dimensional scenario; however, it is an issue needed to be worked out.

11. We use the MV estimation formulation in our work. Kalman Filtering techniques may be applied to the problem at hand. The most significant advantage of Kalman Filtering might be the "tuning" of the filters for optimum estimation. The measurement noise statistics we used in this study are chosen from the current applications' statistics. If the measurement noises are obtained from the empirical data, and the filter tuning is possible, the estimation performance might be improved.

12. In the estimation algorithm using singular linear regression, we perform linearization for slant range measurement inclusion into the linear regression formulation. The approximation used in this linearization causes some errors in the estimation results. While Scenario 6 includes the ground object's coordinates information and the slant range measurement to the ground object, Scenario 5 includes the ground object's coordinates information but not the slant range information. Theoretically, Scenario 6 should outperform Scenario 5. However, contrary to theory, in some flight conditions, Scenario 5 performs equally or even slightly better in practice. We think that the above mentioned approximation error is the culprit. Again, Extended or Non-Linear Kalman Filtering, or tuning of filters for the approximation errors, may improve the estimation accuracy.

13. Finally, we investigated INS aiding by tracking an unknown ground object by using optical measurement in detail and for first time. What we present in this thesis is a novel navigation concept supported by MC experiments using MatLab. For a realistic application, there is more work to do. Laboratory tests, performance evaluations, and flight tests are needed. Nevertheless, this work is an initial step for future research.

# *Appendix A. Optical Bearing Measurements By Tracking An Unknown Landmark*

The idea of INS aiding by using bearings measurements on unknown (lunar) landmarks was first suggested in [7] space navigation research of *Apollo Mission*. Different from the conventional means of obtaining inertial measurements, the navigational system is obliged to use the changes in the tracking angle as the vehicle passes over a landmark which has *unknown coordinates*.

Let's assume that the astronaut is able to lock onto an identifiable but unknown point on the earth's surface. Figure A.1 describes the measurement geometry.

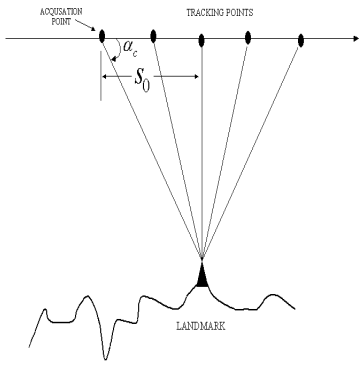


Figure A.1 Nominal tracking sequence.

Also assume that $H_0$ is the height of the velocity vector, $r_0$ is the distance travelled for some time $\tau$, and $\omega_0$ is the angular velocity of the vehicle. In this situation, the computed bearing measurements is given by:

$$\cot \alpha_c = \frac{S_0 - r_0 \omega_0 \tau}{H_0} \tag{A.1}$$

The problem here is to determine the errors: $r(t_1)$, $\dot{r}(t_1)$, $\theta(t_1)$, $r_0\omega(t_1)$, $\phi(t_1)$, and $\dot{\phi}(t_1)$ at the acquisition point. The time change of the computed $\alpha_c$ is compared with the actually

measured $\alpha_m$. The difference between them can help to determine the velocity error vector. Figure A.2 shows that the altitude error $r(t_1)$ cannot be distinguished from the lack of knowledge in the altitude of landmark. After time $\tau$, the actual bearing measurement is

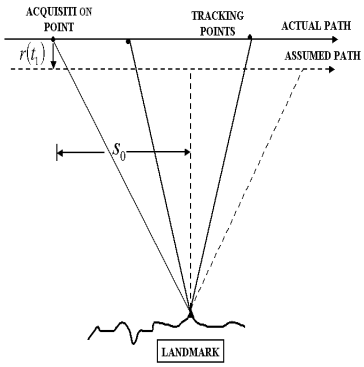


Figure A.2 Tracking with erroneous vehicle or landmark altitude.

$$\cot \alpha_a = \frac{S_0 - r_0 \omega_0 \tau}{H_0 + r(t_1) - \Delta H} + \frac{\cot \alpha(0)(r(t_1) - \Delta H)}{H_0 + r(t_1) - \Delta H} \tag{A.2}$$

where $\Delta H$ is the altitude uncertainty of the landmark.

After some time $\tau$ from the beginning of the track, there may be two possible velocity errors: Horizontal and vertical errors. Figures A.3 and A.4 show these situations, respectively.

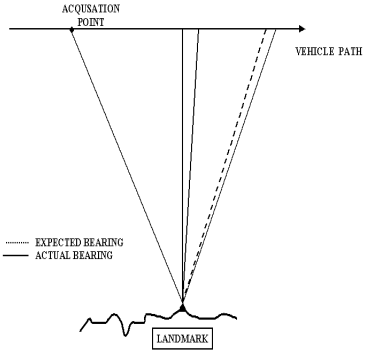


Figure A.3 Tracking with an erroneous horizontal velocity.

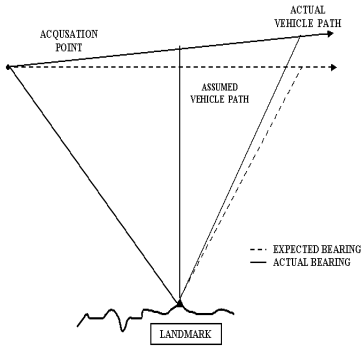


Figure A.4 Tracking with an erroneous vertical velocity.

The equation of bearing measurements in the case of tracking with erroneous horizontal velocity follows:

$$\cot \alpha_a = \frac{S_0 - \big(\omega_0 + \omega(t_1)\big) r_0 \tau}{H_0} \tag{A.3}$$

When the tracking is performed with erroneous vertical errors, bearing measurements are denoted as below:

$$\cot \alpha_a = \frac{S_0 - r_0 \omega_0 \tau}{H_0 + \dot{r}(t_1)\tau} \tag{A.4}$$

Another error source is the initial range error. Determination of the velocity errors by Eq. (A.4) cause an angle between vehicle's assumed and actual path as shown in Fig. A.5. But it is impossible to distinguish the range error from the velocity error. The bearing

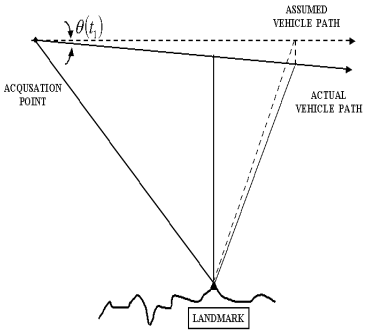


Figure A.5 Tracking with an erroneous vertical velocity.

measurements made along the actual path are calculated as:

$$\cot \alpha_a = \frac{S_0 - r_0\omega_0\tau}{H_0 - \theta(t_1)r_0\omega_0\tau} \tag{A.5}$$

Notice that all the error terms in Eq. (A.2) to Eq. (A.5) are generally small, so that linear approximation can be applied as:

$$\frac{1}{1+\delta} \approx 1 - \delta$$

By using this approximation, Eq. (A.2) can be re-written as:

$$\cot \alpha_a \approx \frac{S_0 - r_0\omega_0\tau}{H_0} + \frac{r_0\omega_0 t(r(t_1) - \Delta H)}{H_0^2} \tag{A.6}$$

Eq. (A.3) becomes:

$$\cot \alpha_a \approx \frac{S_0 - r_0\omega_0\tau}{H_0} - \frac{\omega(t_1)r_0}{H_0}\tau \tag{A.7}$$

Eq. (A.4) is approximated as:

$$\cot \alpha_a \approx \frac{S_0 - r_0\omega_0\tau}{H_0} - \frac{S_0\dot{r}(t_1)}{H_0^2}\tau + \frac{r_0\omega_0\dot{r}(t_1)}{H_0^2}\tau^2 \tag{A.8}$$

Approximation of Eq. (A.5) yields:

$$\cot \alpha_a = \frac{S_0 - r_0\omega_0\tau}{H_0} + \frac{S_0 r_0\omega_0\theta(t_1)}{H_0^2}\tau - \frac{r_0^2\omega_0^2\theta(t_1)}{H_0^2}\tau^2 \tag{A.9}$$

The first terms of Eq. (A.6) through Eq. (A.9) can be recognized as $\cot \alpha_c$; replacing them with $\cot \alpha_c$ and re-arranging yields

$$\begin{aligned} \cot \alpha_a - \cot \alpha_c \quad &\approx \quad \frac{1}{H_0^2}\big(r_0\omega_0[r(t_1) - \Delta H]r_0\omega(t_1)H_0 - S_0[r(t_1) - r_0\omega_0\theta(t_1)]\big)\tau \\ &\quad + \frac{r_0\omega_0}{H_0^2}[r(t_1) - r_0\omega_0\theta(t_1)]\tau^2 \end{aligned} \tag{A.10}$$

The negligible magnitude of $r_0\omega(t_1)H_0$ allows this expression to simplify to

$$\begin{aligned}\cot\alpha_a - \cot\alpha_c &\approx \frac{1}{H_0^2}\big(r_0\omega_0[r(t_1) - \Delta H] + S_0[r_0\omega_0\theta(t_1) - r(t_1)]\big)\tau \\ &\quad + \frac{r_0\omega_0}{H_0^2}[\dot{r}(t_1) - r_0\omega_0\theta(t_1)]\tau^2 \end{aligned} \tag{A.11}$$

The projection of Figure A.1 can be seen in a plane normal to the assumed velocity vector. By doing so, one can determine track errors in the vehicle trajectory. For this purpose, the unknown landmark should also be contained in this plane. Although this measurement provides no information about the *position error* $\phi$, Figure A.6 shows that it does provide information about the *track velocity* error. Two variables from the in plane component of

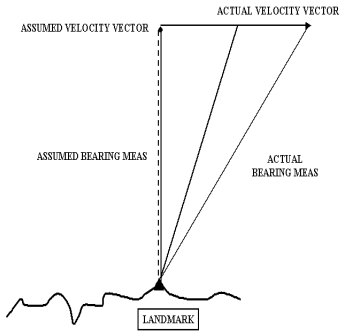


Figure A.6 Tracking with an erroneous track velocity.

this measurement has to be known to obtain $\phi$:

1. The distance between the landmark and the velocity vector (sum of them, not the individual components).
2. The sum of the vertical velocity and the range error.

These measurements can be obtained by Eq. (A.11), and the measurement geometry is shown in Fig. A.7. Considering the angle $\beta$ between the assumed bearing measurement and the actual bearing measurement, it can be written that

$$\sin\beta \approx \frac{\phi r_0\tau}{H_0 + r(t_1) - \Delta H + \big(\dot{r}(t_1) - r_0\omega_0\theta(t_1)\big)\tau} \tag{A.12}$$

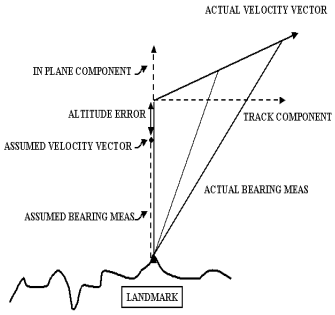


Figure A.7 Tracking with an erroneous track velocity, altitude, and horizontal-vertical velocity error.

$[\dot{r}(t_1) - r_0\omega_0\theta(t_1)]$ of the denominator, depending on the particular orbit, will be negligible. On the other hand, from small angle approximation, $\sin\beta = \beta$ will be valid. Hence,

$$\phi \approx \frac{\beta(\tau)\big(H_0 + r(t_1) - \Delta H\big)}{r_0 t} \tag{A.13}$$

Now, by using Eq. (A.11) and Eq. (A.13), one can solve for orbital parameters even if the unknown landmark measurements are used.

As explained, the unknown landmark measurements provide information about the vehicle's velocity vector. Since each measurement yields only one equation, it is obvious that the number of the landmarks to be tracked must be equal to the number of the unknown parameters [7].

# *Appendix B. "Gaussian" Distribution of Angles*

## *B.1 Univariate Gaussian Distribution of an Angle*

The 1-$\sigma$ probability $p$ is the probability that a random variable's realization is within 1-$\sigma$ of its expectation. The 1-$\sigma$ probability of a "Gaussian" angular random variable is calculated as follows

We use the definition of the error function

$$\frac{1}{\sqrt{2\pi}} \int_0^x e^{-\frac{1}{2}x^2} dx = \frac{1}{2} erf(\frac{x}{\sqrt{2}}) \tag{B.1}$$

Hence

$$\frac{1}{\sqrt{2\pi\sigma}} \int_0^x e^{-\frac{1}{2}\frac{x^2}{\sigma^2}} dx = \frac{1}{2} erf(\frac{x}{\sqrt{2}\sigma}) \tag{B.2}$$

Thus, the probability density function of a "Gaussian" angular variable $\theta$ is

$$f(\theta) = \frac{\frac{1}{\sqrt{2\pi}\sigma} e^{-\frac{1}{2}\frac{\theta^2}{\sigma^2}}}{erf(\frac{1}{\sqrt{2}}\frac{\pi}{\sigma})}, \qquad -\pi \leq \theta \leq \pi \tag{B.3}$$

Hence, the 1-$\sigma$ probability for a Gaussian angular variable is

$$p = \frac{erf(\frac{1}{\sqrt{2}})}{erf(\frac{1}{\sqrt{2}}\frac{\pi}{\sigma})} \tag{B.4}$$

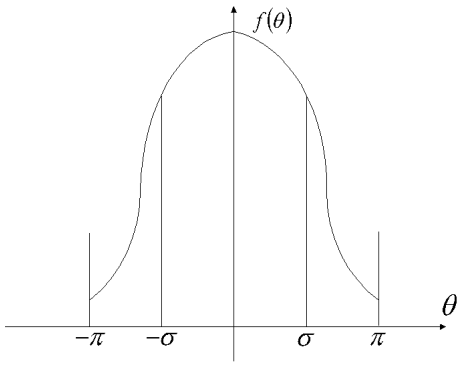


## *B.2 Bivariate Gaussian Distribution in Euclidian Space*

The 1-$\sigma$ probability of a Gaussian random variable in Euclidian space is

$$p = \frac{1}{2\pi|det(P)|^{\frac{1}{2}}} \iint_X e^{-\frac{1}{2}\vec{x}^T P^{-1}\vec{x}} d\vec{x}, \qquad \text{where } X = \{\vec{x}|\vec{x}^T P^{-1}\vec{x} \leq [\text{dimension of } \vec{x}]\} \tag{B.5}$$

The covariance P is a real symmetric positive definite matrix.

Let

$$P = T^T \begin{bmatrix} \lambda_1^2 & 0 \\ 0 & \lambda_2^2 \end{bmatrix} T \tag{B.6}$$

Hence

$$\begin{aligned} P^{-1} &= T^T \begin{bmatrix} \frac{1}{\lambda_1^2} & 0 \\ 0 & \frac{1}{\lambda_2^2} \end{bmatrix} T \\ &= \left[ \begin{bmatrix} \frac{1}{\lambda_1} & 0 \\ 0 & \frac{1}{\lambda_2} \end{bmatrix} T \right]^T \begin{bmatrix} \frac{1}{\lambda_1} & 0 \\ 0 & \frac{1}{\lambda_2} \end{bmatrix} T \end{aligned} \tag{B.7}$$

Use the linear transformation

$$\vec{y} = \begin{bmatrix} \frac{1}{\lambda_1} & 0 \\ 0 & \frac{1}{\lambda_2} \end{bmatrix} T\vec{x} \tag{B.8}$$

Then

$$\vec{x}^T P^{-1} \vec{x} = \vec{y}^T \vec{y} \tag{B.9}$$

The linear transformation $\mathcal{T} : \vec{y} \rightarrow \vec{x}$ is

$$\mathcal{T} = T^T \begin{bmatrix} \frac{1}{\lambda_1} & 0 \\ 0 & \frac{1}{\lambda_2} \end{bmatrix} \tag{B.10}$$

and

$$\begin{aligned} det(\mathcal{T}) &= \lambda_1 \lambda_2 & \text{(B.11)} \\ &= |det(P)|^{\frac{1}{2}} & \text{(B.12)} \end{aligned}$$

When polar coordinates are used, the non-linear transformation $\mathcal{T} : \begin{bmatrix} \rho \\ \theta \end{bmatrix} \rightarrow \begin{bmatrix} y_1 \\ y_2 \end{bmatrix}$ is specified by

$$\begin{aligned} y_1 &= \rho cos\theta \\ y_2 &= \rho sin\theta \end{aligned}, \tag{B.13}$$

$$\begin{aligned} det|\mathcal{T}| &= \begin{vmatrix} \frac{\delta y_1}{\delta \rho} & \frac{\delta y_1}{\delta \theta} \\ \frac{\delta y_2}{\delta \rho} & \frac{\delta y_2}{\delta \theta} \end{vmatrix} & \text{(B.14)} \\ & & \text{(B.15)} \end{aligned}$$

and we calculate

$$det|\mathcal{T}| = \begin{vmatrix} cos\theta & -\rho sin\theta \\ sin\theta & \rho cos\theta \end{vmatrix} = \rho \tag{B.16}$$

Since

$$p = \frac{1}{2\pi|det(P)|^{\frac{1}{2}}} \iint_X e^{-\frac{1}{2}\vec{x}^T P^{-1}\vec{x}} d\vec{x} \tag{B.17}$$

$$X = \{\vec{x}|\vec{x}^T P^{-1}\vec{x} \leq 1\}, \tag{B.18}$$

Using eq. (B.12), we obtain

$$p = \frac{1}{2\pi|det(P)|^{\frac{1}{2}}} \iint_Y e^{-\frac{1}{2}\vec{y}^T\vec{y}} d\vec{y}|det(P)|^{\frac{1}{2}} \tag{B.19}$$

$$Y = \{\vec{y}|\vec{y}^T\vec{y} \leq 1\} \tag{B.20}$$

Using eq. (B.16), we calculate

$$p = \frac{1}{2\pi}\int_{\varphi=0}^{2\pi} d\varphi \int_{\rho=0}^{1} \rho \ e^{-\frac{1}{2}\rho^2} d\rho \tag{B.21}$$

$$= \int_0^1 \rho \ e^{-\frac{1}{2}\rho^2} d\rho \tag{B.22}$$

$$= -e^{-\frac{1}{2}\rho^2}\Big|_0^1 \tag{B.23}$$

$$= 1 - \frac{1}{\sqrt{e}} = 0.3935 \tag{B.24}$$

## *B.3 Bivariate Angular "Gaussian" Distribution*

The probability density function

$$f(\vec{x}) = \frac{\frac{1}{2\pi|det(P)|^{\frac{1}{2}}} e^{-\frac{1}{2}\vec{x}^T P^{-1}\vec{x}}}{p_1} \tag{B.25}$$

where

$$p_1 = \frac{1}{2\pi|det(P)|^{\frac{1}{2}}} \int_{-\pi}^{\pi}\int_{-\pi}^{\pi} e^{-\frac{1}{2}\vec{x}^T P^{-1}\vec{x}} d\vec{x} \tag{B.26}$$

Using the linear transformation $\mathcal{T}$, we obtain

$$p_1 = \frac{1}{2\pi} \iint_Y e^{-\frac{1}{2}\vec{y}^T \vec{y}} d\vec{y} \tag{B.27}$$

where the (parallelogram) Y is the image under the transformation $\mathcal{T}$ of the square $\{(x_1, x_2)\} = \{-\pi \leq x_1 \leq \pi, -\pi \leq x_2 \leq \pi\}$. The vertices of the parallelogram Y are

$$\vec{Y}_{11} = \pi \begin{bmatrix} \frac{1}{\lambda_1} & 0 \\ 0 & \frac{1}{\lambda_2} \end{bmatrix} T \begin{bmatrix} 1 \\ 1 \end{bmatrix} \tag{B.28}$$

$$\vec{Y}_{12} = \pi \begin{bmatrix} \frac{1}{\lambda_1} & 0 \\ 0 & \frac{1}{\lambda_2} \end{bmatrix} T \begin{bmatrix} 1 \\ -1 \end{bmatrix} \tag{B.29}$$

$$\vec{Y}_{22} = -\vec{Y}_{11} \tag{B.30}$$

$$\vec{Y}_{21} = -\vec{Y}_{12} \tag{B.31}$$

and we calculate

$$|\vec{Y}_{11}|^2 = \pi^2 \begin{bmatrix} 1 & 1 \end{bmatrix} T^T \begin{bmatrix} \frac{1}{\lambda_1^2} & 0 \\ 0 & \frac{1}{\lambda_2^2} \end{bmatrix} T \begin{bmatrix} 1 \\ 1 \end{bmatrix} \tag{B.32}$$

$$= \pi^2 \begin{bmatrix} 1 & 1 \end{bmatrix} P^{-1} \begin{bmatrix} 1 \\ 1 \end{bmatrix} \tag{B.33}$$

Similarly

$$|\vec{Y}_{12}|^2 = \pi^2 \begin{bmatrix} 1 & -1 \end{bmatrix} P^{-1} \begin{bmatrix} 1 \\ -1 \end{bmatrix} \tag{B.34}$$

let

$$P^{-1} = \begin{bmatrix} a & c \\ c & b \end{bmatrix} \tag{B.35}$$

Then

$$|\vec{Y}_{11}| = \pi\sqrt{a+b+2c} \tag{B.36}$$

$$|\vec{Y}_{12}| = \pi\sqrt{a+b-2c} \tag{B.37}$$

Let $\rho = \pi\sqrt{a+b+2|c|}$.

Evidently,

$$p_1 < \frac{1}{2\pi}\iint_Y e^{-\frac{1}{2}\vec{y}^T\vec{y}}d\vec{y} < 1 \tag{B.38}$$

$$\{\vec{Y}|\vec{Y}^T\vec{Y} = \rho^2\} \tag{B.39}$$

Hence

$$p_1 < \frac{1}{2\pi}\iint_Y e^{-\frac{1}{2}\vec{y}^T\vec{y}}d\vec{y} = \int_0^\rho \rho e^{-\frac{1}{2}\rho^2}d\rho \tag{B.40}$$

$$= -e^{-\frac{1}{2}\rho^2}\Big|_0^\rho \tag{B.41}$$

$$= 1 - \frac{1}{e^{\frac{1}{2}\rho^2}} \tag{B.42}$$

Thus

$$p_1 < 1 - \frac{1}{e^{\frac{1}{2}(a+b+2|c|)\pi^2}} \tag{B.43}$$

Hence, the 1-$\sigma$ probability for a bivariate angular "Gaussian" variable satisfies

$$p > \frac{1-\frac{1}{\sqrt{e}}}{1-\frac{1}{e^{\frac{\pi^2}{2}(a+b+2|c|)}}} \tag{B.44}$$

where $a+b+2|c|$ is the sum of the absolute values of the elements of $P^{-1}$.

### *B.3.1 Example.*

$$P = \sigma^2 \begin{bmatrix} 1 & 0 \\ 0 & 1 \end{bmatrix} \tag{B.45}$$

Then

$$p > \frac{1 - \frac{1}{\sqrt{e}}}{1 - \frac{1}{e^{(\frac{\pi}{\sigma})^2}}} \tag{B.46}$$

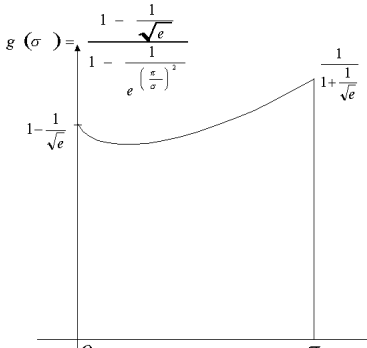


Figure B.1 The function $g(\sigma) = \frac{1-\frac{1}{\sqrt{e}}}{1-\frac{1}{e^{(\frac{\pi}{\sigma})^2}}}$

## *B.4 Probability of being in 1-$\sigma$ and $\Sigma_1/\Sigma_2$*

We have performed a MC simulation experiment, and obtained the estimation errors $\hat{\theta}_i^+ - \theta$ and $\hat{\gamma}_i^+ - \gamma$, $i = 1, 2, ..., N$; $N = 1000$, $\vec{x} = \begin{bmatrix} \hat{\theta}^+ - \theta \\ \hat{\gamma}^+ - \gamma \end{bmatrix}$. We calculate what percentage of these errors are in the predicted 1-$\sigma$ bound: The experimentally obtained $1-\sigma$ probability is the ratio of the number of times when $\vec{x}_i$ satisfies $\vec{x}_i^T P^{-1} \vec{x}_i \leq$ [dimension of $\vec{x}_i$] to the total numbers of runs, N. The "Experimental 1-$\sigma$ Prob." entry into the Table 4.2 gives these statistics for different measurement geometries.

# *Appendix C. Linearization of The Equality Constraint*

We have the non-linear equality constraint

$$f(\vec{X}) = 0$$

where

$$\vec{X} = (R, X_0, Y_0, X_P, Y_P)$$

and

$$f(R, X_0, Y_0, X_P, Y_P) = R - \sqrt{(X_0 - X_P)^2 + (Y_0 - Y_P)^2}$$

Now,

$$f(\vec{X}) \;\; \approx \;\; f(\vec{X}^-) + \nabla f|_{\vec{X}^-}(\vec{X} - \vec{X}^-)$$

so that

$$\nabla f|_{\vec{X}^-}\vec{X} \;\; \approx \;\; f(\vec{X}) + \nabla f|_{\vec{X}^-}\vec{X}^- - f(\vec{X}^-)$$

i.e.,

$$\nabla f|_{\vec{X}^-}\vec{X} \;\; \approx \;\; \nabla f|_{\vec{X}^-}\vec{X}^- - f(\vec{X}^-)$$

We calculate

$$\nabla f|_{\vec{X}^-} = \left[1, \frac{1}{\sqrt{(X_0^- - X_P^-)^2 + (Y_0^- - Y_P^-)^2}}\left(X_P^- - X_0^-,\;\; Y_P^- - Y_0^-,\;\; X_0^- - X_P^-,\;\; Y_0^- - Y_P^-\right)\right]$$

and

$$\nabla f|_{\vec{X}^-}\vec{X}^- - f(\vec{X}^-) = R^- + \frac{1}{R^-}\Big[(X_P^- - X_0^-)X_0^-,\ (Y_P^- - Y_0^-)Y_0^-,\ (X_0^- - X_P^-)X_P^-,\ (Y_0^- - Y_P^-)Y_P^-\Big]$$
$$-R^- + \sqrt{(X_0^- - X_P^-)^2 + (Y_0^- - Y_P^-)^2}$$

$$\begin{aligned} &= \frac{(X_0 - X_P)^2 + (Y_0 - Y_P)^2 + (X_P^- - X_0^-)(X_0^- - X_P^-) + (Y_P^- - Y_0^-)(Y_0^- - Y_P^-)}{\sqrt{(X_0 - X_P)^2 + (Y_0 - Y_P)^2}} \\ &= 0 \end{aligned}$$

Hence, we obtain the linearized equality constraint

$$0 = \Big(\sqrt{(X_0 - X_P)^2 + (Y_0 - Y_P)^2},\ (X_P^- - X_0^-),\ (Y_P^- - Y_0^-),\ (X_0^- - X_P^-),\ (Y_0^- - Y_P^-)\Big)\begin{bmatrix} R \\ X_0 \\ Y_0 \\ X_P \\ Y_P \end{bmatrix}$$

# *Bibliography*


1. Bronson Richard, *Matrix Operations*. The McGraw-Hill Companies, Inc., 1989.
2. George Siouris, *Aerospace Avionic Systems, A Modern Synthesis*. Academic Press, 1993.
3. Gonzalez, Rafael C. *Digital Image Processing* (2nd Edition). Massachusetts: Addison-Wesley Publishing Company Inc., 1987, [45-51].
4. Kayton, Myron and Walter R. Fried, *Avionics Navigation Systems* (2nd Edition). New York: John Willey and Sons, Inc., 1997, [10,69].
5. Maybeck, Peter S. *Stochastic Models, Estimation, and Control, Volume 1* New York: Academic Press, 1979. Republished, Arlington, Virginia: Navtech, 1994.
6. R. M. Rogers *Applied Mathematics in Integrated Navigation Systems*. AIAA Press, 2000.
7. *Space Navigation Guidance and Control, Report R-500*. MIT Instrumantation Laboratory, 1965. 5-3 to 5-21
8. Titterton, D.H and J. L. Weston, *Strapdown Inertial Navigation Technology*. England: The Lavenham Press Ltd., 1997, [364-365].
9. Van Sickle, N. D. *Modern Airmanship*. New Jersey: D. Van Nostrand Company, Inc., 1957, [579-583].
10. Widnall, William S. and Peter A. Grundy, *Inertial Navigation System Error Models*. Massachusetts: Intermetrics Inc., 1973, [21-22].
11. Young, Brian James. *An Integrated Synthetic Aperture Radar / Global Positioning System / Inertial Navigation System For target Geo-location Improvement*. MS Thesis, AFIT/GE ENG 98M-32. School of Engineering, Air Force Institude of Technology(AU), Wright-Patterson AFB OH, March 1999.

# REPORT DOCUMENTATION PAGE

Form Approved
OMB No. 074-0188



| 1. REPORT DATE *(DD-MM-YYYY)* | 2. REPORT TYPE | 3. DATES COVERED *(From – To)* |
|---|---|---|
| 04-03-2002 | **Master's Thesis** | Jun 2001 – Mar 2002 |

**4. TITLE AND SUBTITLE**

INS AIDING BY TRACKING AN ANKNOWN GROUND OBJECT

**5a. CONTRACT NUMBER**

**5b. GRANT NUMBER**

**5c. PROGRAM ELEMENT NUMBER**

**6. AUTHOR(S)**

Polat, Murat, Lieutenant, TUAF

**5d. PROJECT NUMBER**

**5e. TASK NUMBER**

**5f. WORK UNIT NUMBER**

**7. PERFORMING ORGANIZATION NAMES(S) AND ADDRESS(S)**
Air Force Institute of Technology
Graduate School of Engineering and Management (AFIT/EN)
2950 P Street, Building 640
WPAFB OH 45433-7765

**8. PERFORMING ORGANIZATION REPORT NUMBER**

AFIT/GE/ENG/02M-20

**9. SPONSORING/MONITORING AGENCY NAME(S) AND ADDRESS(ES)**
AFRL/SNAT
Attn: Dr. Devert Wicker
Bldg 621
WPAFB OH 45433-7765
DSN: 785-1115
e-mail: Devert.Wicker@wpafb.ab.mil

**10. SPONSOR/MONITOR'S ACRONYM(S)**

**11. SPONSOR/MONITOR'S REPORT NUMBER(S)**

**12. DISTRIBUTION/AVAILABILITY STATEMENT**

APPROVED FOR PUBLIC RELEASE; DISTRIBUTION UNLIMITED.

**13. SUPPLEMENTARY NOTES**

**14. ABSTRACT**

The reduction of the navigation error in an inertial navigation system by optically tracking a ground object is investigated. Multiple observations of the ground object are used. The location of the ground object is assumed unknown. A careful analysis of the measurement situation at hand reveals that by optically tracking an unknown ground object using passive, *bearings-only* measurements, the aircraft's angle of attack and sideslip angle can be measured. Thus, two new independent measurement equations featuring the aircraft's angular navigation variables are obtained. Hence, by optically tracking over time an unknown ground object, inertial navigation system aiding is in fact possible. Moreover, the estimation algorithm, which operates on the bearing measurements record, simultaneously, and in parallel, produces corrections required for both inertial navigation system aiding and geo-location of the ground object. Furthermore, the theory developed in this paper is easily adapted to accommodate additional measurements and/or prior information. The former entail range measurements; and prior information entails some, or all, position coordinates of the ground object. These enhancements reflect the current operational practice. Thus, the theory presented in this paper is sufficiently general to encompass the conventional methods of inertial navigation system updating where both bearing and range measurements are used and the coordinates of the ground object are known. In all cases where additional independent measurements and/or prior information are used, the accuracy of both the navigation solution and the geo-location are enhanced.

**15. SUBJECT TERMS**

Inertial Navigation Aiding, Passive Tracking, Estimation.

| 16. SECURITY CLASSIFICATION OF: | | | 17. LIMITATION OF ABSTRACT | 18. NUMBER OF PAGES | 19a. NAME OF RESPONSIBLE PERSON |
|---|---|---|---|---|---|
| a. REPORT | b. ABSTRACT | c. THIS PAGE | | | Dr. Pachter, Meir, Professor |
| U | U | U | UU | 162 | 19b. TELEPHONE NUMBER *(Include area code)* (937) 255-3636, ext 4593; e-mail: Meir.Pachter@afit.edu |